Dipl.-Ing. Lisa Marx, BSc

Partitioning and Structural Kinetics of Antimicrobial Peptides in Lipid Membrane Mimics of Varying Complexity

DOCTORAL THESIS

to achieve the university degree of

Doktorin der technischen Wissenschaften

submitted to

Graz University of Technology

Supervisor

Assoz. Prof. Dipl.-Ing. Dr.techn. Georg Pabst

Institute of Materials Physics

Graz University of Technology

in cooperation with

Institute of Molecular Biosciences

University of Graz

Graz, March 2021

EIDESSTATTLICHE ERKLÄRUNG

Ich erkläre an Eides statt, dass ich die vorliegende Arbeit selbstständig verfasst, andere als die angegebenen Quellen/Hilfsmittel nicht benutzt und die den benutzten Quellen wörtlich und inhaltlich entnommenen Stellen als solche kenntlich gemacht habe. Das in TUGRAZonline hochgeladene Textdokument ist mit der vorliegenden Dissertation identisch.

Datum, Unterschrift

Abstract

As a part of the innate immune response against pathogens, small proteins called antimicrobial peptides have been investigated for nearly four decades as promising agents to kill bacteria. Since bacterial cells are very complex organisms, membrane mimetic systems provide a valuable platform to study specific interactions of AMPs with cell membranes, but have to be regarded with care when extrapolating results to AMP activity in life bacteria. This poses the challenge to work with mimics that are accomplished enough to sufficiently represent the complex bacterial cell membranes and their interactions with AMPs, but simultaneously keep the studied systems experimentally tractable.
We demonstrated that the activity of the antimicrobial peptides L18W-PGLa, MG2a and their equimolar mixture from the magainin familily, as well as the lactoferricin derivatives LF11-215 and LF11-324, is strongly dependend on the lipid composition and transbilayer lipid distribution of the investigated membrane mimics. In peptide partitioning studies we exploited a common thermodynamic framework in vesicles composed of different phosphatidylethanolamine (PE), phosphatidylgylcerol (PG) and cardiolipin (CL) mixtures using tryptophan fluorescence and determined their membrane activity using a dye-leakage assay and small-angle X-ray scattering. In investigations of different lipid-to-peptide ratios for increasing lipid concentrations, partitioning data could be extrapolated to high lipid concentrations used in e.g. small angle scattering experiments, highlighting that the amount of peptide remaining in the solution needs to be considered when interpreting the effects induced by AMPs. Investigating the influence of membrane asymmetry on permeability studies us-

ing asymmetric vesicles consisting of $POPG_{in}$ and $POPE_{out}$, we observed distinctive leakage kinetics in asymmetric mimics compared to symmetric vesicles of the same overall lipid composition. Using time-resolved small-angle neutron scattering, we could connect the disparate peptide activity in aLUVs to lipid flip-flop induced by the AMP PGLa on similar timescales observed in leakage experiments, with a dependence on the investigated lipid-to-peptide ratios.

Kurzfassung

Antimikrobielle Peptide (AMPs) sind kleine Proteine und Teil des angeborenen Immunsystems. Sie werden bereits seit fast vier Jahrzehnten als erfolgsversprechende Wirkstoffe zur Abtötung von Bakterien erforscht. Da es sich bei Bakterienzellen um sehr komplexe Organismen handelt, bieten biomembranähnliche Modellsysteme ein wertvolle Plattform um spezifische Interaktionen von AMPs mit Zellmembranen zu untersuchen. Die Interpretation der Ergebnisse in diesen Modellsystemen und ihre Verbindung zur Wirkungsweise der Peptide in lebenden Bakterien stellt allerdings ein große Herausforderung dar. Dabei müssen Membranmodelle gewählt werden, die einerseits ausreichend ausgereift sind um die komplexen Membranen von Bakterienzellen und deren Wechselwirkung mit den Peptiden realitätsgetreu wiederzugeben, andererseits aber experimentell noch umsetzbar und regulierbar sind.

Wir konnten zeigen, dass die Aktivität der Peptide L18W-PGLa, MG2a von der Familie der Magainins und deren äquimolare Mischung, als auch die Aktivität der Lactoferricin-Abkömmlinge LF11-215 and LF11-324, stark von der Lipidzusammensetzung und der Lipidverteilung innerhalb der Lipid-Doppelschicht der Modellmembran abhängt.
In Partitionierungsstudien konnten wir einen thermodynamischen Ansatz ausnutzen um die Membranaffinität der Peptide in Lipidvesikeln bestehend aus unterschiedlichen Mischungen von Phosphatidylethanolamine (PE), Phosphatidylgylcerol (PG) and Cardiolipin (CL) mittels Tryptophan-Fluoreszenz Spektroskopie zu untersuchen. Des Weiteren konnten wir die Peptidaktivität in Lipidvesikeln mittels eines Membranpermeabilitätsassays und Kleinwinkelröntgenstreuexperi-

menten erforschen.
In Studien mit unterschiedlichen Lipid/Peptid Verhältnissen für zunehmende Lipidkonzentrationen, konnten Partitionierungsdaten zu sehr hohen Lipidkonzentrationen extrapoliert werden, wie sie zum Beispiel in Kleinwinkel-Streuexperimenten verwendet werden. Dies hat gezeigt, dass das Molverhältnis der Peptide die nicht in die Membran partitionieren und in Lösung bleiben unbedingt berücksichtigt werden muss, um die Wirkungsweise der Peptide auf molekularer Ebene richtig deuten zu können.
In einer weiteren Membranpermeabilitätsstudie wurde der Einfluss von transmembraner Asymmetrie in asymmetrischen Vesikeln bestehend aus $POPG_{in}$ und $POPE_{out}$ untersucht und charakteristische Leakage-Abläufe in symmetrischen und asymmetrischen Modellsystemen gegenübergestellt. Mittels zeitaufgelöster Kleinwinkelneutronenstreuung konnten wir die abweichende Peptidaktivität in asymmetrischen Vesikeln in Verbindung mit, durch das Peptid PGLa induziertem, Lipid Flip-Flop bringen. Lipid-Translokation konnte ähnlichen Zeitskalen zugeordnet werden wie sie auch durch Permeabilitätsstudien aufgezeigt wurden, in Abhängigkeit von den untersuchten Lipid/Peptid Verhältnissen.

Acknowledgment

During the time of my PhD I learned countless lessons, some of them are indefinitely burned into my memory. The general (but very true) lesson constantly repeated by my supervisor regarding laboratory work and generally performing any tasks: "Slowly, slowly, slowly" can safe a lot of time and repetitions if followed (especially in hindsight). Together with my colleagues I learned (many times over) that: "Not every beam time makes you happy" but we kept going nevertheless. The constant cycle of failures (or challenges on a more positive note) and small successes, definitively taught me to continue even when the goal seems out of reach. I would first and foremost like to thank my supervisor Georg, for his support and guidance over the last years and being an exceedingly approachable group leader. He provided a great working environment and an atmosphere of teamwork that made coming to work an enjoyable activity. A big thank you also to Charlie, for the continuous financial and professional support over the last years and for showing me that even when moving up the career ladder it is possible to stay down to earth and still meet everyone with positive energy and at eye level. I would also like to thank my colleagues Enrico and Moritz who taught me so much over the years and turned even the hardest beam times and the longest conferences into golden memories of sleep deprivation and laughing fits until my stomach hurt. Also a thank you for the notorious "bullshitting" sessions: the many extremely productive coffee breaks, reinventing the world and coming up with an endless stream of useful and (mostly) useless ideas, brightening up even the most unsuccessful day in the lab. Thank you to the whole Biophysics group, for the great working environment and easy going atmosphere. Also a great thank you to

Babsi and Michi, who were there at the beginning when I was still a half-baked PhD-student and who showed me the lay of the land. Also a huge thank you to the Laura^2, who simultaneously went through the PhD-experience and were my most valuable outlets and discussion partners over the last years and made this whole Odyssey so much easier. All of my gratitude also to my boyfriend Toni, who was the most supportive and understanding partner throughout all of this and never complained about late night or early morning lab days and backed me up through every pre-conference or pre-deadline craziness. Last but not least I want to thank my parents for always supporting us unconditionally and believing in us throughout our studies and life in general, this journey would not have been possible without them.

Contents

List of Abbreviations

aLUV - asymmetric large unilamellar vesicles

AMP - antimicrobial peptide

CD - cyclodextrin

CL / TOCL - 1,3-bis1,2-dioleoyl-sn-glycero-3-phospho-glycerol

DLS - dynamic light scattering

DSC - differential scanning calorimetry

E. coli - *Escherichia coli*

DPPC - 1,2-dipalmitoyl-sn- glycero-3-phosphocholine

DMPC - 1,2-dimyristoyl-sn-glycero-3-phosphocholine

GUV - giant unilamellar vesicles

HBS - HEPES-buffered saline

LPS - lipopolysaccharide

IM - inner (cytoplasmic) membrane

LUV - large unilamellar vesicle

MLV - multilamellar vesicle

NMR - nuclear magnetic resonance

List of Abbreviations

OM - outer membrane

POPC - palmitoyl-2-oleoylglycero-3-phosphocholine

PE / POPE - 1-palmitoyl-2-oleoyl-sn-glycero-3-phosphoethanolamine

PG / POPG - 1-palmitoyl-2-oleoyl-sn-glycero-3-phospho-(1′-rac-glycerol)

POPC - 1-palmitoyl-2-oleoyl-sn-glycero-3-phosphocholine

SANS - Small Angle Neutron Scattering

SAXS - Small Angle X-ray Scattering

Trp - tryptophan

List of Figures

1 Introduction and Motivation

In 2014, the World Health Organization declared the development of novel antimicrobial compounds a high priority, in response to the global emergence of antibiotic resistance [1] and further, in 2017 published a list of antibiotic-resistant pathogens to spur research efforts for medical developments against multi-resistant bacterial strains. Antimicrobial peptides (AMPs) have been considered as promising agents in this regard, to combat infectious diseases due their ability to discriminate the lipid architecture of cell envelopes, and evade classical resistance mechanisms based on direct molecular (keylock) interactions, which is a major disadvantage in conventional antibiotics, see, e.g., review: [2]. Although AMPs have also been shown to target intracellular compartments [3], the majority of AMPs act on the microbial cytoplasmic membrane [4]. The peptides amphipathic character and overall positive charge, structural flexibility and H-bonding capacity make them highly membrane active and specific [5]. Most AMPs develop their secondary structure only when coming into contact with microbial membranes and insertion of the peptides is driven by their hydrophobic residues while electrostatic interactions are responsible for the initial binding to bilayer surfaces of the pathogens and lead to a strong discrimination between mammalian (overall neutral surface charge) and bacterial (negative surface charge) membranes. Their effect on bacterial membranes is dependend on peptide physicochemical properties such as length, structure and hydrophobicity, but also on the effective AMP concentration on the target membrane (peptide partitioning).

Since bacterial cells are very complex and metabolically active or-

ganisms it is difficult to delineate the peptides' mode of action on a molecular level. To study specific interactions of AMPs with cell membranes, different membrane mimetic systems provide a valuable platform for such investigations, but have to be regarded with care when extrapolating results to AMP activity in life bacteria. In this regard, the challenge is to work with mimics that are accomplished enough to sufficiently represent the complex bacterial cell membranes and their interactions with AMPs but simultaneously keep the studied systems experimentally tractable. Reported effects of AMPs on lipid-only membrane mimics differ strongly and at relatively low peptide concentrations include induced lipid flip/flop [6], [7] and at higher peptide concentrations the formation of various types of membrane pores [8] and overall topological changes [9] and finally complete micellization for sufficiently high amounts of AMPs. These effects do not only depend on the properties of the investigated peptide but are also highly dependend on the lipid composition of the used membrane mimic, depending on lipid molecular shapes (intrinsic lipid curvature), charge and chemistry, see e.g([10], [11] and [12]).

The membrane composition of bacteria is highly conserved also for different bacterial strains, with their cytoplasmic membrane composed of a mixture of different phospholipid species, specificically the anionic phosphatidylglycerol (PG) and cardiolipin (CL) and zwitterionic phosphatidylethanolamine (PE) [13]. Gram-negative bacteria such as *Escherichia coli* exhibit a molecular ratio of charged and zwitterionic phospholipids of approximately 3:1. Gram-negative bacteria additionally consist of a highly asymmetric outer membrane, with an outer leaflet composed of lipopolysaccharide (LPS) and an inner leaflet containing phospholipids. Membrane asymmetry is a membrane property that has been observed for almost all biological membranes and has also been described for bacterial cytoplasmic membranes, of e.g. *Bacillus megaterium* which was shown to have an outer leaflet enriched in PG [14].

This thesis focuses on the interaction of antimicrobial peptides from the magainin and lactoferricin family with membrane mimics of Gram-negative bacteria. The investigated magainin peptides, L18W-PGLa and MG2a, are of particular interest due to their synergistic effect when applied as an equimolar mixture, significantly boosting the peptides activity, as observed in bacteria and lipid only mimics thereof and have been studied extensively in the past. Nevertheless, the peptides mode of action of these PGLa:MG2a mixtures has not been completely understood and has even led to controversies due to the use of different measurement techniques and model systems [9], [15]–[21]. In contrast, in the course of this thesis we additionally focused on two very short AMPs LF11-215 and LF11-324, two of the most promising lactoferricin-derivatives against a broad range of Gram-positive and Gram-negative bacterial strains [22], [23]. These peptides were shown to bind well to bacterial and model membranes but their efficacy, however, was demonstrated to stem from specific interactions with cytosolic components [24].

We used a common thermodynamic framework for antimicrobial peptide partitioning to compare the activity of these AMPs in different lipid-only vesicular mimics of the cytoplasmic membrane of Gram-negative bacteria, using tryptophan fluorescence experiments and determined their membrane activity using a dye leakage assay, dynamic light scattering (DLS) and small-angle X-ray scattering (SAXS). For finite peptide partitioning coefficients, the number of membrane bound peptides depends on the lipid and peptide concentrations of the investigated system [25]. Every experimental technique operates in a specific lipid concentration range and bridging results from different methods therefore has to be well-considered. At the same time, partitioning does not give any information about the peptides' structural effects on the investigated membrane or the kinetics of these interactions. This is illustrated in Figure 1.1, showing exemplary dye-leakage experiments in LUVs (see Section 3.1.1, displaying the peptide concentrations $[P]$ needed to induce a specific percentage of leakage

at a given lipid concentration $[L]$.
Data extrapolations show lipid and peptide concentration up to ranges

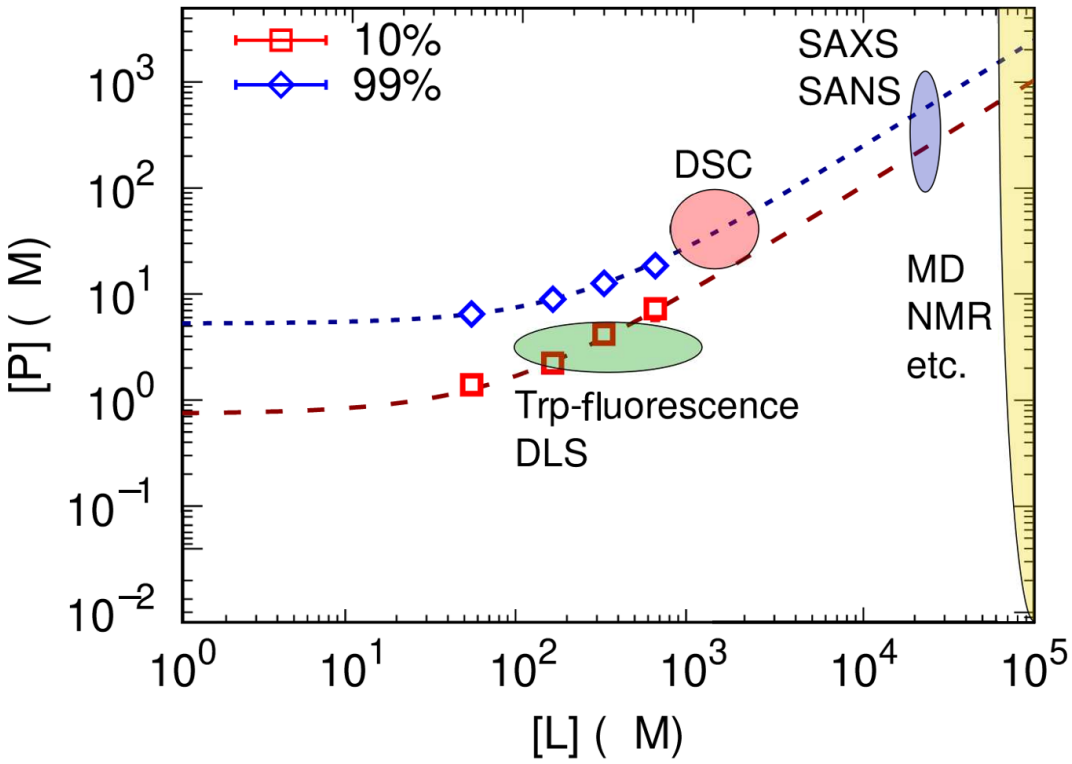

Figure 1.1: ANTS/DPX dye-leakage data of L18W-PGLa induced permeabilization in PE/PG (3:1) vesicles at different degrees of leakage bridging lipid and peptide concentration regimes of different experimental techniques. Data fits were extrapolated to low and high lipid/peptide concentrations (manuscript in preparation).

typically used in small angel scattering experiments ($[L]$ ~20 mM, $[P]$ ~0.8 mM). This extrapolation indicates that 99% of leakage would be reached at elevated lipid concentrations and peptide-to-lipid ratios of 1:25 as used in SAXS measurements conducted in the course of this thesis, see Section 3.1.4. $[L]/[P]$ ratios probed in Trp-fluorescence measurements shown in Section 3.1.1 ($[L]$ =100-1000 μM, $[P]$ =1-6 μM PGLa) are depicted in a green circle, as well as performed DLS ex-

periments, DSC measurements performed in e.g. [9], [21] are shown in red, while the yellow region represents all techniques that assume that all added peptides are partitioned into the membrane (e.g. Moleculuar dynamic simulations) or systems at very low hydration, like nuclear magnetic resonance. Using the equi-activity approach as previously described in [26], [27] ultimately allowed us to determine effective peptide partitioning of the investigated antimicrobial peptides and to quantify how much of an antimicrobial peptide leads to a specific effect or membrane activity (e.g. leakage, structural changes) in respect to the investigated lipid concentration and in dependence on membrane lipid composition.

To illustrate the influence of transbilayer asymmetry on membrane-peptide interactions we performed kinetic dye-leakage experiments in asymmetric vesicles consisting of the phospholipids PE and PG found in plasma membranes of Gram-negative bacteria and symmetric systems of the same lipid composition. We further investigated peptide-induced lipid flip-flop using time-resolved small angle neutron scattering (SANS) to correlate leakage kinetics with flip-flop rates at different peptide concentrations.

When combining insights gained from the different experiments performed in the course of this thesis, considering the effective number of bound peptides in membrane mimics of varying composition and under different experimental conditions has proven imperative to draw meaningful conclusions about the mode of action of antimicrobial peptides.

2 Materials and Methods

In this section general information about used materials, sample preparation, applied methods and data analysis tools are presented, clearly arranging and justifying used membrane mimics and investigation methods.

2.1 Bacterial membranes

The view of biological membranes as a mere shell for cell contents has long been proven to be obsolete. This remarkable organelle simultaneously functions as a cellular barrier and selective gateway, which demands for it to be robust enough to protect against influences from the external environment, but to still enable processes like cell division, motility and allow specific permeability of water and nutrients. This is achieved through a membrane barrier with a highly dynamic fluid structure, consisting of a double layer composed of different lipids as well as embedded proteins, and carbohydrates. This thesis focuses on cell membranes of Gram-negative bacteria, to study antimicrobial peptide interactions with the cellular barriers of these prokaryotic microorganisms. Therefore, it is imperative to posses a detailed level of understanding of the architecture and lipid composition of the bacterial membranes and to be able to establish viable, simplified membrane mimics that still represent crucial properties of membranes of Gram-negative bacteria like *Escherichia coli* (*E. coli*) schematically depicted in Figure 2.1. Characteristic for the Gram-negative bacterial cell envelope is the presence of an inner or plasma membrane (IM) that encloses the cytoplasm and an outer membrane (OM) that acts as

the outermost barrier to the cells surroundings. In between these two membranes is the gel-like matrix called the periplasmic space, which is firmly bound to the rigid peptidoglycan layer.

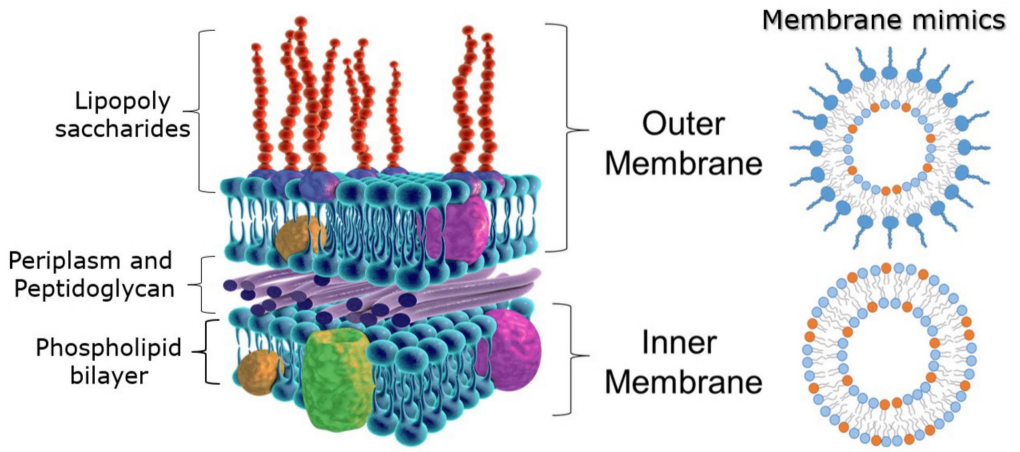

Figure 2.1: Schematic representation of the *E. coli* cell wall. Shown are the phospholipid bilayer of the inner membrane, peptidoglycan, periplasm and the highly asymmetric outer membrane including the characteristic lipopolysaccharides. On the right side of the figures corresponding vesicular membrane mimics of the IM and OM are depicted.

Due to the complexity of bacterial cells it is extremely difficult to translate experimentally measured effects of AMPs to the molecular level of membrane interactions. Therefore, significantly simplified lipid-only membrane mimics are widely used systems to delineate these mechanisms. One main objective in this regard is to avoid oversimplification and to master the extrapolating of results obtained for membrane mimics to the cellular level. Nevertheless, even though mimetic systems need to consider the complexity of the lipid composition in bacterial cell membranes, it is necessary to still keep the studied systems experimentally tractable.
A wide variety of different model systems has been developed and is continuously advancing in complexity regarding their architecture,

size, and composition. This includes vesicles of various sizes, or planar membranes, like supported lipid bilayers, all of which offer advantages and disadvantages depending on the used investigation method and investigated membrane property [28]. This thesis focuses on the investigation of lipid vesicles or liposomes of varying complexity, which have proven to be a very well suited system to investigate the modes of action of AMPs. Large unilamellar vesicles or LUVs consist of a double layer of lipids containing a single lipid species or a mixture of two or more different types of lipids, enclosing an aqueous compartment as shown in Figure 2.1. Although these simplified mimics are not perfect representations of the very complex bacterial cell, they provide the huge advantage of enabling biophysical studies in highly controlled chemical and experimental environments.

2.2 Inner Membrane Mimics of Gram-negative bacteria

Focusing first on the composition of the bacterial inner membrane, the lipid constituents of this versatile barrier are small amphiphilic molecules consisting of a hydrophilic headgroup (polar, attracted to aqueous phases) and hydrophobic tails (non polar, repelled by aqueous phases). For *E. coli* this membrane is known to consist of the phospholipids, phosphatidylethanolamine (PE), cardiolipin (CL) and phosphatidylglycerol (PG) in a 82:12:6 mol/mol/mol ratio, respectively [29], [30]. For our model membranes we therefore used a mixture of 1-palmitoyl-2-oleoyl-sn-glycero-3-phosphoethanolamine (POPE), 1',3'-bis[1,2-dioleoyl-sn-glycero-3-phospho]-glycerol (TOCL) and 1-palmitoyl-2-oleoyl-sn-glycero-3-phospho-(1'-rac-glycerol) (POPG).

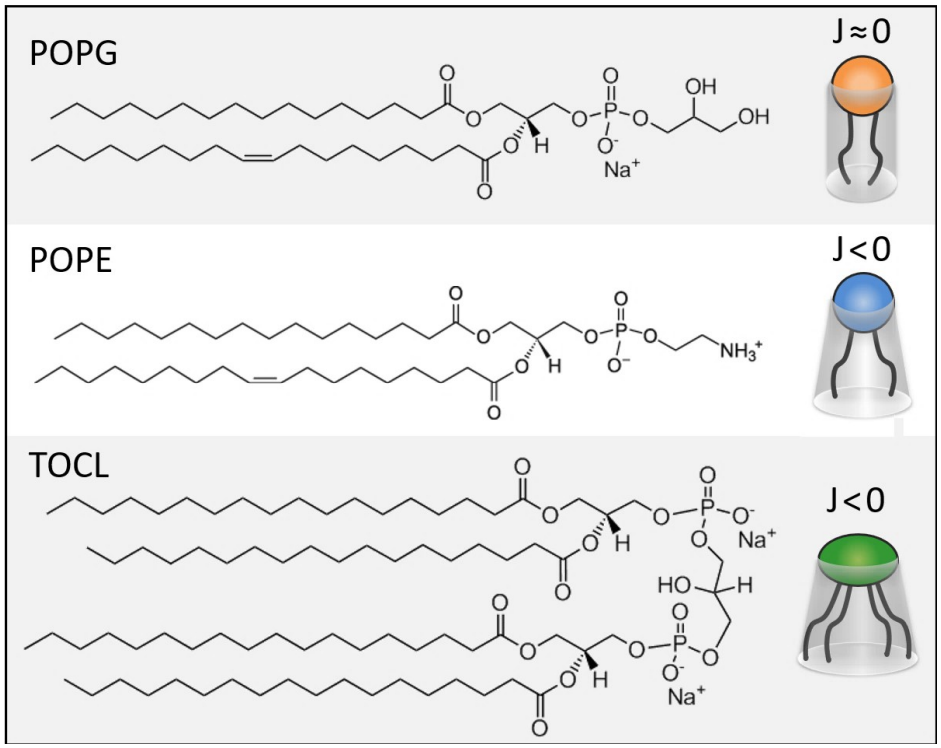

Figure 2.2: Chemical representation of POPG, POPE and TOCL lipids as well as their schematically depicted molecular shapes and corresponding intrinsic curvature J. (Source of chemical structures: avantilipids.com)

The used lipids differ in charge as well as in their molecular shape that the lipids adopt at certain conditions, determined by the intrinsic curvature J_0, defined as the negative inverse radius of the neutral plane of a stress-free monolayer [31]. Characteristics of the used lipid constituents are presented in Figure 2.2. The negatively charged POPG possesses a $J_0 \approx 0$, resulting in a cylindrical shape. POPE has zero charge and shows inverse conical shape with $J_0 < 0$ [12]. The larger molecule TOCL consists of four fatty acid chains and a larger headgroup containing two negative charges and also exhibits an inverse conical shape with $J_0 < 0$ [32]. Membranes with a more positive curvature exhibit lower lateral stress at the bilayers' polar-apolar interface

which leads to looser lipid packing at the first site of interaction with AMPs. This makes the right choice of lipids and mixing ratios crucial for realistic membrane mimics, especially when studying their interactions with antimicrobial peptides discussed in Section 2.4.

2.2.1 Preparation of Lipid vesicles

All used lipids were purchased from Avanti Polar Lipids (Alabaster, AL) as powder (purity >99%), namely POPE, POPG, TOCL and deuterated 16:0-d31-18:1 PG (1-palmitoyl-d31-2-oleoyl-sn-glycero-3-phospho-rac-(1-glycerol)), further referred to as PE, PG, CL and d31-PG respectively. Lipids were dissolved in organic solvent chloroform/methanol (9:1, vol/vol) and phosphate assayed for exact quantification of lipid content [33]. Thin lipid films were prepared at the bottom of round glass vials by mixing appropriate amounts of lipid stock solutions to obtain membrane mimics of different complexity composed of pure PG, pure d31-PG, PE/PG (3:1, mol/mol) and PE/PG/CL(82:6:12, mol/mol), followed by solvent evaporation under a nitrogen stream and overnight storage in a vacuum chamber to remove remaining organic solvent. Dried lipid films were hydrated in HEPES-buffered saline (HBS) solution (10 mM HEPES, 140 mM NaCl, pH 7.4), which is known to be well suited for maintaining physiological pH. After the addition of HBS, samples were vortexed every 15 min for a duration of 1 min and equilibrated in between at 35 °C. This process was followed by 5 freeze-and-thaw cycles plunging samples into liquid N_2 with intermittent heating to 35 °C and vortex-mixing. Large unilamellar vesicles (LUVs) were created through extrution, using a hand held mini-extruder (Avanti Polar Lipids, Alabaster, AL) by pushing the sample 31 times through polycarbonate filter with a pore diameter of 100 nm. After extrusion, vesicle size distribution and polydispersity were checked through dynamic light scattering (DLS), see Section 2.5.5. The final sample was again phosphate assayed to determine sample concentrations and to ensure measurements with precisely controlled amounts of lipids and subsequent mixing of well-controlled ratios of

lipid systems and antimicrobial peptides.

2.2.2 Asymmetric Membrane Mimics

It is the general consensus that almost all biological membranes exhibit an asymmetric distribution of lipids between the inner and outer leaflet of the lipid bilayer [34]. This also applies for bacteria, in membranes of Gram-positive bacteria for example PG is mainly found in the outer membrane leaflet and PE and phosphatidylinositol (PI) mostly on the inner leaflet, whereas cardiolipin has been shown to be evenly distributed between the two [35]. This asymmetrical lipid distribution impacts various membrane properties like lipid packing [36], lateral organization [37] and has been shown to influence membrane-peptide interactions [6], [7], [38].
To investigate the impact of asymmetry on the mode of action of antimicrobial peptides, asymmetric unilamellar vesicles (aLUVs) were produced, using a protocol established at our lab, based on methyl--cyclodextrin-catalyzed exchange. With this method, lipids from the outer leaflet of acceptor LUVs consisiting of pure PE (produced as described in Section 2.2.1) in HBS buffer, were exchanged for lipids provided by heavy-donor multilamellar vesicles (MLVs) made of PE, hydrated in HBS with 20 w/w % sucrose (0.632 M), to obtain donor vesicles containing a dense sucrose core. Donor lipids are transferred into the extruded unilamellar acceptor vesicles lacking the heavy sucrose core (donor/acceptor mol/mol ratio = 2), which makes it possible to separate donor and acceptor pools after the exchange by centrifugation according to their different vesicle sizes and densities. After an initial concentration step, residual CD and sucrose were removed with a centrifugal ultrafiltration device, the preparation method is described in detail in [39]. The overall lipid composition was then determined by gas chromatography–mass spectrometry, additionally performing a concentration series to obtain absolute concentration values (PE/PG mol/mol ratios between 1:0, 3:1, 1:1, 1:2, 1:4, 1:6, 1:8, 1:10 with 160 μM of 1-palmitoyl-2-oleoyl-glycero-3-phosphocholine (POPC)

added as a standard in every sample), revealing a PG/PE mol/mol ratio of 2.05. Assuming all of the exchanged PE is located on the outer leaflet of aLUVs this amounts to an inner leaflet composed of PG, while the outer leaflet is composed of 67,2% PE and 32,8% PG. Vesicle size was checked using DLS, affirming the integrity of produced aLUVs and absence of large donor MLVs. Methyl-β-cyclodextrin and sucrose were purchased from Sigma-Aldrich (Vienna, Austria) in powdered form. Asymmetric vesicles produced for measurements of time-resolved lipid flip-flop using SANS with chain deuterated, d31-PG on the inner leaflet and buffer washes were performed with 100% D_2O HBS.

2.2.3 Samples for Dye Leakage Experiments

For membrane permeability measurements, lipid films were produced from lipid stock solutions of one or more lipids species and then hydrated in presence of the dye/quencher pair 8-aminonaphthalene-1,3,6-trisulfonic acid/p-xylene-bis-pyridinium bromide (ANTS/DPX) assay (ANTS/DPX) and extruded as described in Section 2.2.1. The fluorophore filled LUVs were further separated from free ANTS/DPX by exclusion chromatography using a column filled with SephadexTM G-75 (Amersham Biosciences, Little Chalfont, UK) fine gel swollen in iso-osmotic HBS, as previously described by [22]. Phospholipid concentrations were again determined through the Bartlett phosphate assay. For leakage experiments using aLUVs, acceptor vesicles filled with ANTS/DPX were produced as described above and the preparation of asymmetric liposomes was performed in the conventional way described in Section 2.2.2. Vesicle integrity was checked using DLS and inclusion of the dye/quencher pair was measured by comparing fluorescence measurements of intact vesicles and dissolved vesicles after the addition of a 1 vol% solution of Triton X-100 to obtain 100% fluorescence. Inclusion fluorescence values were comparable to the values measured for acceptor vesicles before the asymmetry preparation, proving the feasibility of performing leakage assays using asymmetric,

ANTS/DPX-filled liposomes.

2.3 Outer Membrane Mimics of Gram-negative bacteria

The outer membrane of Gram-negative bacteria, is well-known for its asymmetric placement of lipopolysaccharide (LPS) and phospholipids, with LPS in the outer bilayer leaflet and phospholipid on the inner leaflet, in *Escherichia coli* K12 amounting to 75 wt% PE, 19 wt% PE and 6 wt% CL [30]. The minimal realistic model for E.coli outer membrane mimics involves LPS and PE/PG containing asymmetric membranes. Most recently, Paulowski et al. [40] successfully prepared giant unilamellar vesicles (GUVs) by the phase transfer method [41], with LPS on the outer and phospholipids on the inner leaflet, to compare their properties with those of planar lipid bilayers and solid supported membranes. Thereby they could characterize lipid phase behavior and the interaction with the antimicrobial peptide LL-32.
To compare results obtained in the course of this thesis, investigating interactions of AMPs with cytoplasmic membrane mimics in the form of LUVs, it would be highly instructive to perform similar measurements with LUVs mimicking the outer membrane of Gram-negative bacteria. Therefore we attempted to engineer asymmetric LUVs with LPS on the outer leaflet through cyclodextrin-mediated lipid exchange following the protocol described in Section 2.2.2, which to the best of our knowledge has not been done before.
In brief, the protocol in this case involves acceptor vesicles composed of the inner leaflet lipids (PE and PE) and donor vesicles composed of lipids of the outer membrane leaflet (here LPS). Specifically we used Ra-LPS from Salmonella minnesota in the donor system and PE/PG (3/1 mol/mol) in acceptor vesicles as well as a second system with donor vesicles consisting of Ra-LPS from *Escherichia coli* and acceptors composed of PE/PG (4/1 mol/mol).

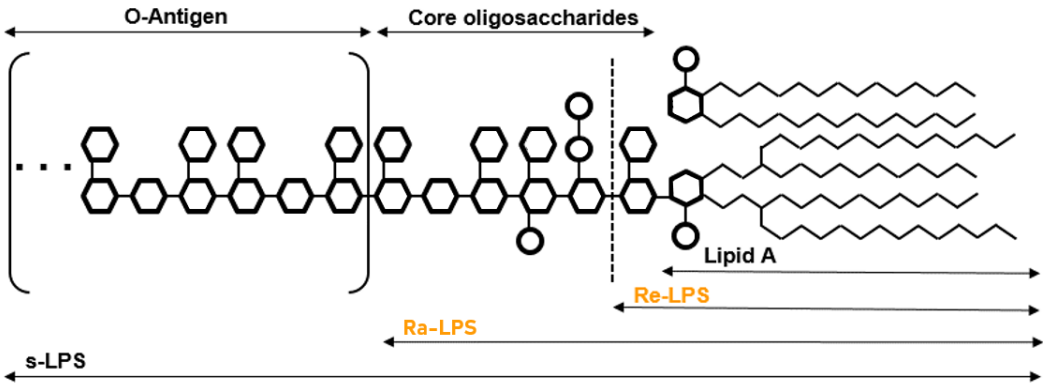

Figure 2.3: General structure of *E. coli* LPS. The sugar moieties of core oligosaccharides and the composition of lipid A are conserved for different *E. coli* strains, while the O-antigen region shows strong variations. Ra-LPS and Re-LPS denote the different rough chemotypes of LPS (used in this thesis in S. Minnesota and *E. coli*, respectively). Native, complete LPS is called smooth-LPS (s-LPS). Figure adapted from [42].

Lipopolysaccharides are large molecules that are only found in the outer membrane of Gram-negative bacteria and consists of a lipid component called lipid A and a polysaccharide component composed of the inner and outer core oligosaccharides and a repetitive glycan polymer called the O-antigen as sketched in Figure 2.3. If the full-length O-antigen is present, the LPS is considered smooth, while LPS without O-antigen is considered rough. Since the O-chains can vary significantly in length, for the purpose of creating homogeneous membrane mimics containing LPS in this work, we decided to use rough derivatives with only the inner core (Re-LPS) or the inner as well as the outer core oligosaccharides (Ra-LPS) present. Lipid A is a hydrophobic molecule with multiple fatty acid chains that anchor the LPS into the bacterial membrane. LPS in salt solutions, e.g. 1 mM $MgCl_2$, self-assembles into multilamellar vesicles (MLVs) [43]. This aggregated form is needed for centrifugal separation at the later steps of the preparation. MLVs were again incubated with cyclodextrin and mixed with the acceptor vesicles. Separation of aLUVs from MLVs and

cyclodextrin were achieved by several centrifugation steps and washes using filters as detailed in Section 2.2.2. Vesicle sizes and polydispersity index were shown to slightly increase in DLS measurements for produced aLUVs, successful LPS exchange and proved the absence of larger LPS structures in the aLUV sample. Corresponding results are presented in Section 3.3.

2.4 Antimicrobial Peptides

The effect of AMPs on the target membranes depends on the peptides' physicochemical properties such as the overall structure, hydrophobicity, length and charge and on peptide concentrations in connection with membrane partitioning. Investigations of peptide interactions with bacterial membrane mimics revealed membrane thinning or thickening [44], induced lipid flip-flop [6], [7], [38], pore-formation or changes in overall membrane structure, down to complete micellization at high concetrations, for reviews see e.g. [2], [30]. Figure 2.4 shows a schematic representation of different AMP modes action.

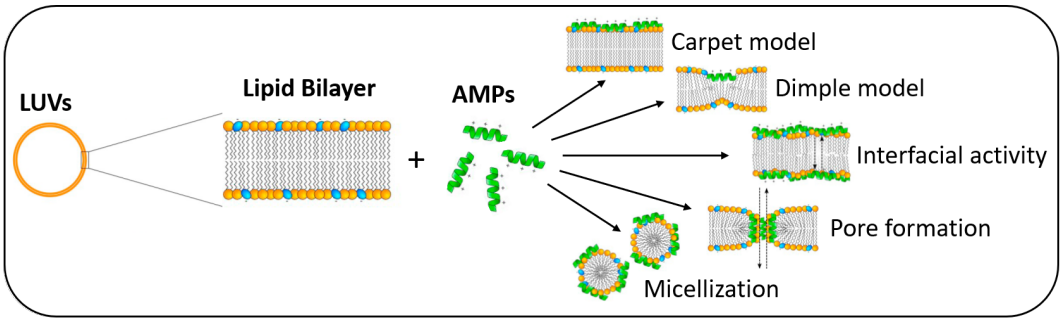

Figure 2.4: Schematic representation of possible modes of action of antimicrobial peptides with lipid membrane mimics. Figure adapted from [30].

The observed effects on the membranes do not solely depend on the properties of the peptides but are also strongly related to the

membrane composition, with significantly diverging interactions for different lipid compositions [12]. Using appropriate lipid-only mimics of bacterial membranes to study peptide- membrane interaction is therefore crucial to obtain physiologically relevant results and the choice of membrane mimics should be taken with care. In the course of this work, five different antimicrobial peptides from two different peptide families were investigated, including AMPs from the magainin family L18W-PGLa, MG2a and a heterodimer chemically linking L18W-PGLa and MG2a through a GGC-linker, denoted in the following as hybrid peptide as well as LF11-215 and LF11-324 derived from human lactoferricin. Freeze-dried peptides (purity >95%) were obtained in lyophilized form from PolyPeptide Laboratories (San Diego, CA).

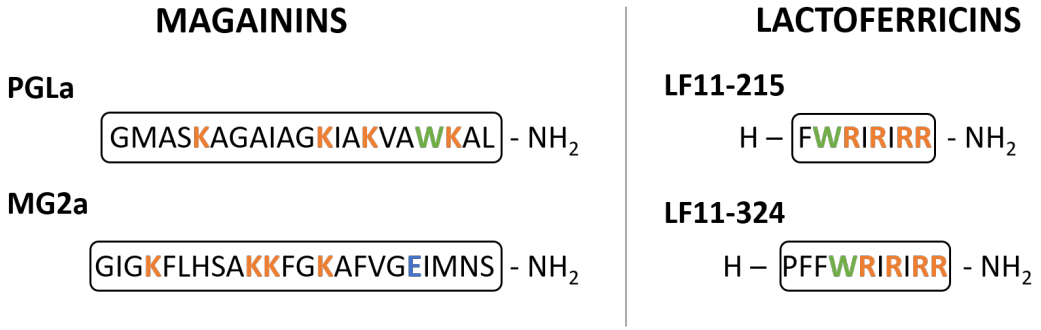

Figure 2.5: Primary sequences for peptides from magainin and lactoferricin families. Positively charged amino acid residues are coloured in orange, negative charges are marked blue. Fluorescent tryptophan residues are marked in green.

Magainins

Peptides from the magainin family have been studied extensively in the past [9], [12], [16]–[21]. MG2a and PGLa occur naturally in the skin of the African clawed frog *Xenopus laevis* [15], [45] and have been shown to act synergistically regarding their antimicrobial activities in

bacteria and model membranes. L18W-PGLa and MG2a are short, linear and cationic peptides, consisting of 21 and 23 residues respectively, their primary sequences are shown in Figure 2.5 including the distribution of charged residues. They are unfolded in solution and only adopt their amphipathic α-helical conformation when coming into contact with lipid membranes. When in their secondary conformation, L18W-PGLa exhibits a larger hydrophobic region compared to MG2a, leading PGLa to insert deeper into lipid membranes. Solid-state NMR experiments performed in multibilayer systems, revealed, besides a strong dependence on lipid composition, that PGLa as well MG2a stay aligned with the membrane surface [46], [47]. The peptides are known to be particularly membrane active, inducing strong negative intrinsic-curvatures at high peptide concentrations. In PE:PG membranes the two magainin AMPs were shown to induce topological changes in LUVs in connection with peptide aggregation, membrane adhesion and fusion events, leading to the formation of multilamellar vesicles an additional sponge phase in case of the synergistic mixture and the hybrid peptide [9], [21].

Lactoferricins

LF11 is an 11 amino-acid long fragment of lactoferricin, a peptide derived from human lactoferricin found e.g. in breast milk, saliva and tears [48]. LF11-215 and LF11-324 were proven to be two of the most promising LF11 derivatives regarding their antimicrobial activity against Gram-positive as well as Gram-negative strains [22], [23], [49]. LF11-324 exhibits increased hydrophobicity compared to LF11-215 was linked and could be linked to a higher activity, but led to lower cell specificity [23]. Both lactoferricin derived peptides were shown to preferentially interact with the negatively charged cardiolipin (CL) included in model membranes and led to peptide-enriched and peptide-poor lipid domain [23]. In vesicle leakage studies the peptides induced only moderate membrane permeabilization in mimics consisting of *E. coli* total lipid extracts even at high peptide-to-lipid

ratios. Structural effects of LF11-215 and LF11-324 on lipid bilayers, like thinning or stored curvature stress, were only marginal [22].

Preparation of AMP Stock Solutions

Peptide stock solutions of all peptides were prepared in HBS solution for the addition to lipid vesicles. Due to the weak solubility of LF11-324 in buffer, AMP stock solutions were prepared by adding 0.01% acetic acid and 0.1% vol/vol DMSO (final pH 7.2), to remove influences on the membrane structure [50]. AMP concentrations of the stock solutions were determined using a spectrophotometer NanoDrop ND-1000 (Thermo Fisher Scientific, Waltham, MA) for Trp containing peptides (L18W-PGLa, the PGLa-MG2a hybrid and LF11-215 as well as LF11-324) measuring absorption at λ=280 nm for corresponding extinction coefficients.

2.5 Methods

2.5.1 Small Angle Scattering

Small-angle X-ray scattering (SAXS) and small-angle neutron scattering (SANS) are non-invasive tools used to interrogate structural properties of increasingly complex biological membrane model systems and even life cells under physiologically relevant conditions [51]. While X-rays are scattered by the electrons of the atoms in the sample, neutrons are scattered by the atomic nuclei. As a result, SANS and SAXS show different dependencies regarding their scattering cross-sections. The X-ray scattering cross section increases proportionally to the atomic number and corresponding increasing number of present electrons, resulting in a greater electron density. The neutron scattering cross-section on the other hand is not proportional to the atomic number and isotopes of the same element can have completely different cross-sections. X-rays are more sensitive to heavier elements and

interact with hydrogen and deuterium identically, for neutrons some light elements like deuterium show similar scattering cross sections as heavy elements like lead (Pb), while scattering from hydrogen and deuterium varies significantly.
This was exploited in the course of this thesis using SANS measurements to investigate lipid flip-flop. When investigating lipid bilayers with X–rays, most of the contrast, stems from the phosphate group located in the lipid's headgroup with high net electron density, while for neutrons the contrast stems from the glycerol backbone of the lipid constituents. Accessible length scales range from the molecular to cellular level depending on the experimental settings such as the wavelength of the scattered beam ($\lambda \sim 0.1$ nm for X-rays, $\lambda \sim 0.5$ nm for neutrons) and accessible scattering angles, the smaller the recorded angle, the larger the object dimensions that are probed. SAS techniques exclusively exploit elastic scattering, characterized by zero energy transfer. The obtained scattering patterns are typically plotted with the measured scattering intensity over the modulus of the scattering vector q, defined as:

$$q = |\overrightarrow{k} - \overrightarrow{k_0}| = \frac{4\pi sin(\theta)}{\lambda} \tag{2.1}$$

where the norm of the incident wavevector (k) is equal to the norm of the scattered wavevector (k_0) and with θ corresponding to the scattering angle and λ giving the incident wavelength.

X-rays

SAXS is capable of delivering structural information of different dimensions depending on the angular range in which a clear scattering signal can be recorded. SAXS provides the ideal platform to study structures in the nanometer range like lipid bilayers with a membrane thickness of approximately 5 nm. Wide angle scattering (WAXS) and ultra-small angle scattering (USAXS) additionally give information

about the Angstrom-range and up to the micron-range, respectively. For unilamellar vesicles in solution, the lipid membranes are not positionally correlated, and therefore only display diffuse maxima in the recorded scattered X-ray signal. The signal stems from a contrast in electron density between LUVs and the solvent where the scattering angle of the first diffuse maximum depends on the head-group to head-group distance within the bilayer. To obtain structural information about the investigated membrane, elaborate bilayer models relying on well-based knowledge of the studied system are crucial to be able to analyze scattering data. In previous publications it was shown that peptides from the magainin family transform large unilamellar vesicles into multilamellar vesicles with collapsed layer spacing between the individual bilayers [9].This peptide induced aggregation of initially unilamellar vesicles leads to the formation of Bragg peaks, which permits data analysis based on Bragg peak positions and intensities only, see e.g. [52]. In MLVs, bilayers are arranged in onion-like concentric vesicles, resulting in a stack with a limited number of equally spaced lamellae, causing additional Bragg peaks in the recorded X-ray scattering pattern, where the scattering vector is given by

$$q(h) = \frac{2\pi h}{d} \tag{2.2}$$

with h giving the diffraction order and d denoting the lamellar spacing. The number of visible Bragg peaks depends on sample homogeneity, concentration and background noise levels dictated by experimental conditions. SAXS also offers the possibility to perform time-resolved measurements, enabling the investigation of lipid-peptide interaction kinetics.

Within the scope of this thesis, SAXS experiments were performed at the highflux Austrian beamline at Elettra Synchrotron in Trieste, Italy [53]. SAXS patterns were recorded using a Pilatus 1 M detector (Dectris, Baden-Daettwil, Switzerland) at a photon energy of 8 keV and in the q-range from 0.1 nm^{-1} to 5 nm^{-1}. Recorded data

were further processed with FIT2D [54]. Samples were measured in a customized cell, called the 'nanodrop', which enabled precise measurements using very small sample volumes (10μl) [55], at a lipid concentration of 20 mg/ml (24.5−27.9 mM depending on the used lipid species and mixtures) at a physiological temperature of 37°C. The built-in automatic sample changer was used to mix lipid samples with well-defined amounts of the different peptides and injecting a drop of the mixture into the nanodrop cell. Measurements of peptide kinetics were recorded starting 30 s after lipid-peptide mixing with an acquisition time of 1 s and a rest time of 10 s to avoid radiation damage of the sample. Additionally, preliminary end-states were measured after lipids were incubated with peptides at 37 °C for at least 4 h. End-state measurements consist of averages over 12 frames of 10 s exposure each and a rest time of 12 s between each shot. Data were analyzed based on first order Bragg peak positions only, extracting information such as time-dependend changes in the lamellar spacing d, domain size ζ and number of lamellae n_L in peptide-induced MLVs. Lamellar-spacing values of the first order lamellar peak were extracted by fitting the peak with a Lorentzian function and determining the respective q-value of the peak position. The domain size ζ is inversely proportional to the full-width-at-half-maximum of the first order lamellar peak, the average number of lamellar layers in the investigated system n_L can then be determined through the fraction of domain size and d-spacing values.

$$d = \frac{2\pi}{q}; \quad \zeta = \frac{2\pi}{FWHM}; \quad n_L = \frac{\zeta}{d} \tag{2.3}$$

Time-resolved SAXS data of different membrane mimics mixed with peptides from the magainin and lactoferricin family are shown in Section 3.1.4.

Neutrons

A number of different techniques have been used to measure lipid flip-flop in the past [56], but small angle neutron scattering has the advantage of doing so in a time-resolved, probe-free and non-headgroup specific manner [6], [7]. SANS offers the possibility of contrast enhancement by selectively labelling the sample with deuterium, as first demonstrated by [57], [58]. This makes it possible to distinguish between the two leaflets of asymmetric LUVs, by placing chain deuterated lipids in one of the two monolayers.

In this thesis 16:0-d31-18:1 PG was used on the inner leaflet of aLUVs and protiated PE on the outer leaflet, produced through cyclodextrin mediated exchange in 100% D_2O HEPES buffer solution to enhance contrast. SANS measurements were used to demonstrate compositional asymmetry directly through a lift-off of the first minimum in the SANS pattern, as presented in Figure 2.6. It shows SANS data of 16:0-d31-18:1PG_{in}/PE_{out} aLUVs in the q-range of the first minimum (0.1-0.25 $Å^{-1}$) as well as the scrambled LUVs, produced by dehydrating the asymmetric sample, rehydrating and extruding the vesicles, thus achieving a symmetric sample with the same lipid composition of the investigated aLUVs. Data were plotted as $I*q^3$ over q to make changes in the region of the first minimum more easily visible.

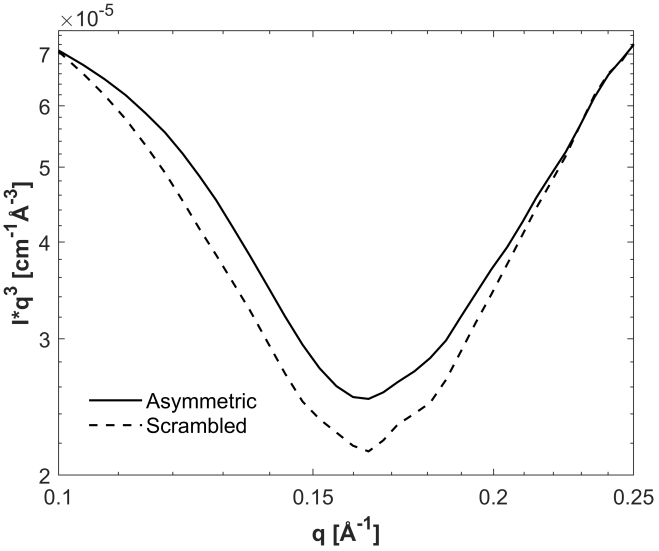

Figure 2.6: I*q^3(q) neutron scattering data from asymmetric LUVs (16:0-d31-18:1PG_{in}/PE_{out}) and scrambled, symmetric LUVs with the same lipid composition, measurements were conducted at 37 °C. Data were plotted as I*q^3 over q to highlight changes in the region of the first minimum.

We then tracked the influence of the AMPs PGLa, MG2a, their equimolar mixture and LF11-215 on lipid asymmetry through a change of the detected scattering signal over time, demonstrating lipid flip-flop and ultimately the transition into a symmetric, scrambled bilayer as previously shown by e.g. [6], [7]. SANS measurements [59] were performed at the D22 - Large dynamic range small-angle diffractometer, located at the Institute Laue-Langevin in Grenoble, France, with a two-^{3}He-detector setup at a wavelength of 6 Å ($\lambda/\Delta\ \lambda$ = 10 %), resulting in a q-range of 0.016-0.6 Å^{-1}. The high neutron flux and the flexibility of its setup make D22 an instrument that is particularly suited for real-time experiments and weakly scattering samples. Kinetics were measured with sample-to-detector distances of 1.3 and 5.6 m and a 5.6 m collimation; low-q measurements of reference and endstates were conducted distances of at 1.3 and 17.8 m, with a 17.8 m collimation. Samples were filled in Hellma 120-QS cuvettes of 1

mm pathway and heated to 37 °C using a bath circulator. Data were reduced using the GRASP-software, performing flat field, solid angle, dead time and transmission correction, normalizing by incident flux and subtracting contributions from empty cell and solvent. Asymmetric vesicles with and without peptides were studied using SANS to determine lipid flip-flop rates at lipid sample concentrations of 7 mg/mL in measurement cells of 280 μl sample volume at 37 °C for 2 min and averaging 5 or 10 data sets for sufficient counting statistics. Time-resolved lipid measurements are presented in Sektion 3.2. Data were analyzed regarding their intensity decrease when transitioning from an asymmetric to a symmetric system after lipid-peptide mixing in the q-range of the first form factor minimum (0.1-0.25 Å) and fitted via a log-level regression of the intensity decay described by the decay parameter Γ, defined as

$$\Gamma = \int_{0.1}^{0.25} Iq^3 dq \tag{2.4}$$

and normalized according to the intensity differences between symmetric (Γ_s) and asymmetric sample (Γ_a):

$$\Gamma = (\Gamma - \Gamma_s)/(\Gamma_a - \Gamma_s) \tag{2.5}$$

Best data fits of intensity decays stem from peptide-enhanced lipid flip-flop over time (t) allow the calculation of the the flip-flop rate k_f and $t_{1/2}$ flip-flop half-time according to equations

$$ln(\Gamma) = -2k_f t \tag{2.6a}$$

$$t_{1/2} = \frac{ln(2)}{2k_f} \tag{2.6b}$$

as described in [56]. Measured SANS data and derived decay parameters are presented in Section 3.2.

2.5.2 Membrane Permeability Assay

Antimicrobial peptides can permeabilize membrane vesicles to cause leakage of entrapped contents, which can then be quantified using a fluorescence-based method. Vesicles filled with ANTS (8-aminonaphthalene-1,3,6-trisulfonic acid, disodium salt) and DPX (p-xylene-bis-pyridinium bromide) were produced as described in Section 2.2.3.

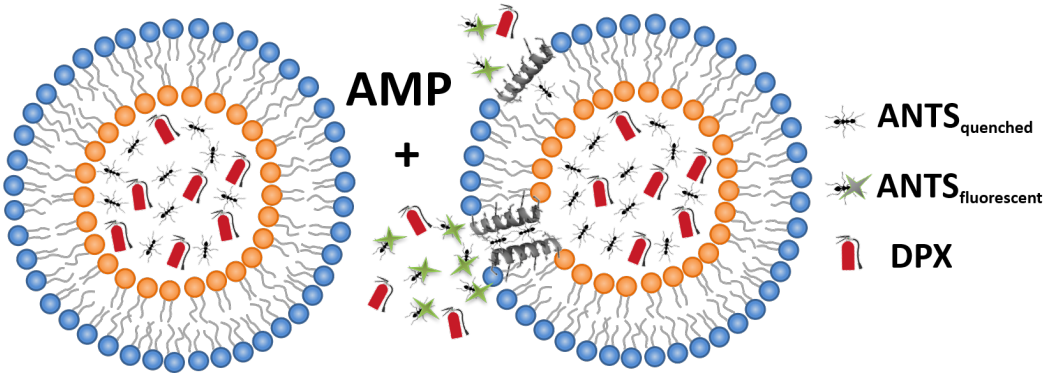

Figure 2.7: Mode of operation for performed membrane permeability assays: LUVs filled with ANTS/DPX, depicted here as an ant and fire-extinguisher, respectively. The fluorescent dye and quencher pair can be fully or partially released depending on the manner of membrane-peptide interaction, peptides (e.g from the magainin family) are shown in there α-helical conformation when coming into contact with the lipid bilayer. Upon dilution into the surrounding medium, ANTS fluorescence increases as quenching by DPX is diminished.

In assays of vesicle leakage, schematically shown in Figure 2.7, the fluorescent dye ANTS and quencher DPX are co-encapsulated into liposomes and upon release and dilution into surrounding medium, ANTS fluorescence will increase because quenching by DPX will decrease. The amount of released dye depends on peptide partitioning as well as the peptides' mode of action [22].

Fluorescence intensities were measured corresponding to specific percentages of ANTS/DPX leakage after peptide addition, determined

according to Equation

$$L_{\%} = \frac{I_P - I_0}{I_T - I_0}, \tag{2.7}$$

where I_P is the measured fluorescence intensity after peptide addition, I_0 is the baseline-intensity measured for vesicles before peptide addition, and I_T is the fluorescence corresponding complete dye release after adding a 1 vol% solution of the detergent Triton X-100.

Following a protocol of the Heerklotz-group as shown in [26], LUV samples with lipid concentrations of $[L] = 1$, 4, 10 and 20 mM were incubated with peptides at concentrations of $[P] = (0.025 - 2)$ mM at 37°C for 1 h, during the incubation time samples were continuously shaken (Eppendorf Thermomixer C Hamburg, Germany). Appropriate amounts of incubated samples were subsequently mixed with HBS and diluted to a final lipid concentration of 50 μM, averaging over at least two measurements. ANTS fluorophores were excited at a wavelength $\lambda = 360$ nm, and the intensity of the fluorescence emission peak was recorded at a wavelegth of $\lambda = 530$ nm, setting excitation and emission monochromators to 10 nm. Measurements were performed with a total sample volume of 2 ml in quartz cuvettes on a Cary Eclipse Fluorescence Spectrophotometer (Varian/Agilent Technologies, Palo Alto, CA).

The concentration dependend leakage study presented in Section 3.1.1 showed complex behaviour but shared an initial, monotonic increase of Leakage$_{\%}$, which was fitted with a sigmoidal function. Combinations of different peptide and lipid concentrations corresponding to specific Leakage$_{\%}$ values, could then be exploited to obtain partitioning parameters (see, Section 2.5.4), combing insights gained through leakage and tryptophan fluorescence measurements described in Section 2.5.3.

2.5.3 Tryptophan fluorescence

The amino acid tryptophan (Trp) is well known for its fluorescent properties, making it a convenient tool in fluorometric assays [60]. Solutions of Trp-containing peptides can be probed regarding their concentration using a spectrophotometer where the absorption at λ = 280 nm is measured and the peptide concentration in mg/ml is then given by a product of the measured absorbance, the molecular weight of the peptide and the molar extinction coefficient of Tryptophan at 280 nm. Tryptophan fluorescence is also remarkably sensitive to the polarity of its environment, which can be exploited to gain information about the interaction of tryptophan-containing peptides with phospholipid vesicles. When the peptide inserts into the membrane, Trp is situated in the hydrophobic environment of the lipid chains where the intrinsic Trp-fluorescence emission shows a decrease in quantum yield and a blue shift of the maximal emission wavelength compared to the pure peptide in solution. Tryptophan fluorescence can therefore be used to determine time-resolved peptide partitioning into membrane mimics of various compositions. Trp is found in both lactoferricin peptides LF11-215 and LF11-324 as well as L18W-PGLa from the magainin family but not in MG2a, amino-acid sequences are shown in Figure 2.5, tryptophan (W) is highlighted in green. Fluorescence emission was measured with the Cary Eclipse Fluorescence Spectrophotometer (Varian/Agilent Technologies, Palo Alto, CA), at an excitation wavelength of $\lambda = 280$ nm, which is the maximum intensity of the Trp-excitation/absorption band.

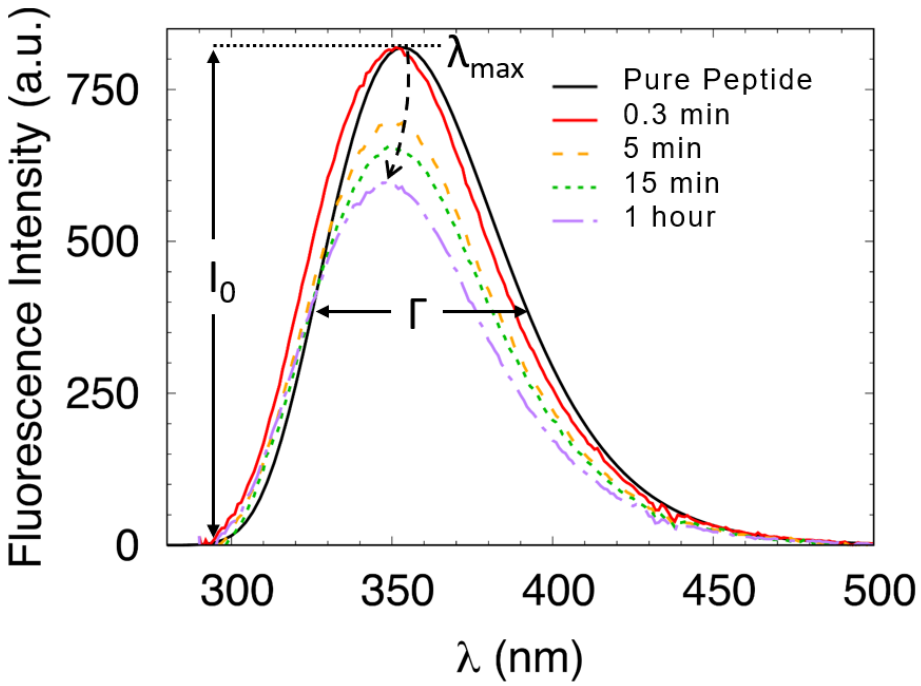

Figure 2.8: Example of time-resolved blue-shift and intensity decrease, observed in tryptophan fluorescence measurements of 4 μM LF11-215 before and after mixing with 100 μM PE/PG 3:1 between 0.3 - 60 min with corresponding tryptophan fluorescence parameters with the concentration dependend intensity I_0, emission wavelength λ_{max} and full-width-at-half-maximum of the emission peak Γ (Adapted from [24]).

By setting the slit width of the incident and outgoing beam to 5 or 10 nm, intensities of exciting and emitting light were adjusted to optimize the signal-to-noise ratio. Contributions from scattered light from vesicles and the instrumental baseline were subtracted from recorded fluorescence spectra. Lipid vesicles were prepared in HBS as described in Section 2.2.1 placed in quartz cuvettes and magnetically stirred to avoid sample sedimentation in aggregated samples. Measurements were performed at 37 °C, for various lipid and peptide concentrations and recorded at different time intervals after lipid-peptide mixing in the time-span between 0.3-60 min. Mag-

ainin peptides were added to PE/PG 3:1 mimics, lactoferricins were investigated in combination with pure PE, PE/PG 3:1 mol/mol and PE/PG/CL 82:6:12 mol/mol/mol. Peptide calibration curves were recorded for all peptides in HBS at concentrations between 2-6 μM. The fluorescence emission band of the peptides in solution was fitted with a log-normal-like function see Figure 2.8 [60].

$$\begin{aligned} &\lambda > (\lambda_{\max} - y\Gamma)\,, \quad I(I_0, \lambda, \Gamma) = I_0 \exp\left[-\frac{\ln 2}{\ln^2 \alpha} \ln^2\left(1 + \frac{(\lambda - \lambda_{\max})}{y\Gamma}\right)\right] \\ &\lambda \leq (\lambda_{\max} - y\Gamma)\,, \quad I(I_0, \lambda, \Gamma) = 0 \end{aligned} \tag{2.8}$$

where $\lambda_{\max}$ is the emission wavelength and I_0 the corresponding intensity ; Γ is the full-width-at-half-maximum (FWHM), α is a skewness parameter (optimized and fixed to 1.36), with $y = \alpha/(\alpha^2 - 1)$. Measurements from lipid-peptide mixtures were analyzed using a combination of two seperate bands, I^S for AMPs in solution and I^P, referring to partitioned AMPs into the membrane shown in Figure 2.9.

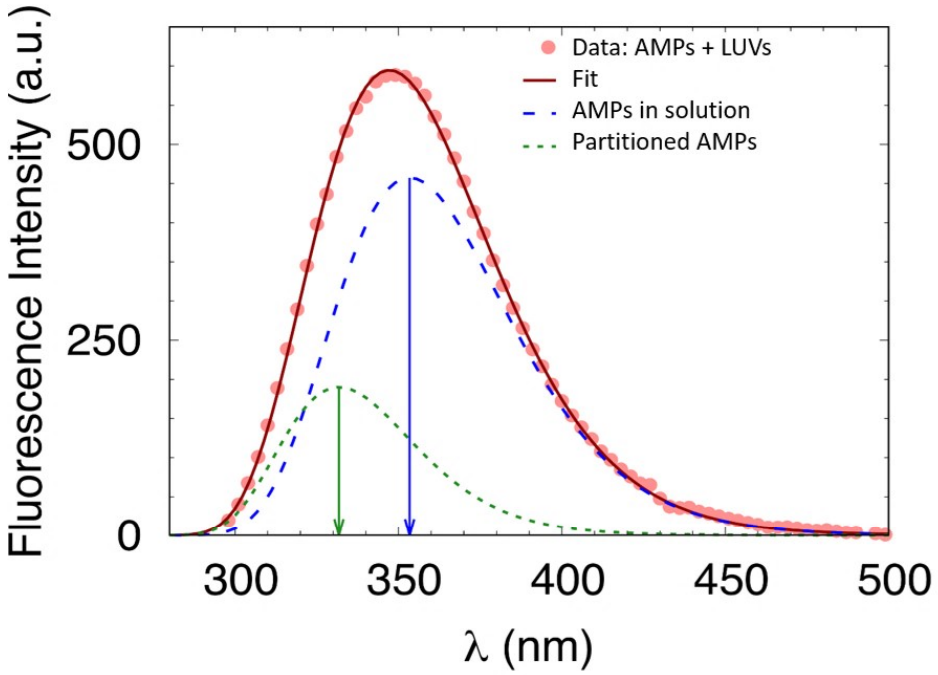

Figure 2.9: Exemplary spectral analysis of 4 μM LF11-215 mixed with 100 μM PE/PG. Recorded data is presented in red dots, the obtained fit is is presented as a red line. Emission fraction from AMPs in suspension is presented by dashed blue line, emission fraction from AMPs partitioned into the membrane is shown as a dotted green line. λ_{max} values are indicated by arrows. Figure adapted from [24]

Parameters of peptides in solution λ^S and Γ^S were fixed to the reference values obtained by analyzing spectra of pure AMPs. Intensity values of peptides in solution and partitioned into the membrane (I_0^S and I_0^P, respectively) and λ^P and Γ^P of partitioned peptides were free fit parameters. Obtained I_0^S values were then used to determine concentrations of the non-partitioned peptides $[P]_W$ and partitioned peptides described in Section 2.5.4.

2.5.4 Calculation of Partitioning Coefficients

In the course of this thesis, peptide partitioning was determined from dye leakage and tryptophan fluorescence measurements. A crucial aspect of membrane-peptide interaction is the peptide membrane affinity which does not only depend on peptide characteristics but also on the properties of the investigated membrane given by the used lipid mixtures. As discussed by White an co-workers in 1998 [61] (based the work of [62] investigating free energies of Octanol-to-water solvation of molecules), the association of AMPs with lipid vesicles has often been treated as a simple chemical equilibrium between peptide and lipid molecules or vesicles while the fluid nature of membranes and hydrophobic and electrostatic interactions responsible for almost all peptide–membrane interactions depend on collective properties of the lipids in the bilayer. This work therefore concentrates on a thermodynamic formalism for the partitioning between two initially separate fluid phases, membrane and solution as published in [24]. The mole fraction partitioning coefficient, K, is defined as

$$K = \frac{[P]_B/([P]_B + [L])}{[P]_W/([P]_W + [W])} \tag{2.9}$$

with $[P]_B$, $[P]_W$ the molar concentration of peptides partitioned into the lipid phase and the peptide concentration in the solvent, respectively. $[L]$ gives the molar concentration of lipids and $[W]$ the molar concentration of bulk water (55.3 M at 37 °C). The ions in the used HBS solvent can be neglected due to the comparably much lower concentration of ions as opposed to the molar water concentration $[W]$. Considering that the molar concentration of water $[W]$ is much greater than the molar concentration of peptides $[P_W]$ and the molar concentration of lipids in the system $[L]$ is much greater than the molar concentration of partitioned peptides $[P_B]$. Equation 2.9 for K can therefore be approximated by

$$K \simeq \frac{[P]_B[W]}{[P]_W[L]}, \tag{2.10}$$

The total peptide concentration $[P]$ is given by the sum of peptides in solution $[P]_W$ and partitioned peptides $[P]_B$,

$$[P] = \underbrace{\frac{R_B[W]}{K}}_{[P]_W} + \underbrace{R_B[L]}_{[P]_B} = R_B\left(\frac{[W]}{K} + [L]\right), \tag{2.11}$$

where R_B is the number of bound peptides per lipid molecule $R_B = [P]_B/[L]$.

The chemical potential per single petide for lipid bound or free AMPs is given by

$$\mu = \mu^0 + k_B T \ln(a) = \mu^0 + k_B T \ln(\gamma R_B) \tag{2.12}$$

with μ^0 giving the chemical potential in the standard state, k_B the Boltzmann's constant, T the temperature, and a the peptide activity [25]. The activity is given by the product of R_B and the activity coefficient γ. In equilibrium the chemical potential of peptides in bulk and in solution is equal, $\mu_B = \mu_W$, the free energy of transfer of a single peptide from solution into the membrane is given by,

$$\begin{aligned} \Delta G_0 = \mu_B^0 - \mu_W^0 \simeq -k_B T \ln\left(\frac{\gamma_B R_B}{R_W}\right) = \\ = -k_B T \ln(K) - k_B T \ln(\gamma_B) \end{aligned} \tag{2.13}$$

since $[P]_B \ll [P]_W$, $\gamma_w \simeq 1$ can be used as an approximation. Only in the regime of infinite dilution of partitioned peptides ($\gamma_B \approx 1$), which in this case defines the standard state, an R_B-independent ΔG_0 could be directly obtained from K values alone [61]. In general, however, the peptide activity cannot be neglected.

To compare peptide interactions with membrane mimics and bacterial cells, an analogous approach was used to determine partitioning in bacterial cells, where bacteria were treated as a homogeneous medium accessible to the peptides as described in [24].

2.5.5 Dynamic Light Scattering

Dynamic light scattering (DLS) is a noninvasive technique frequently used for the determination of size distribution of small particles in solution. In the course of this thesis, structural changes in initially unilamellar vesicles were monitored using DLS. With this method average values of particle sizes (Z-average) can be determined as well as their polydispersity index (PDI), defined as the squared ratio of the size distribution peak width and particle size. For large unilamellar vesicles of sufficient homogeneity a measured size of $\sim$ 100 nm and a PDI 0.1 were set as quality guideline. Monochromatic laser light is directed at the sample, the incident laser light gets elastically scattered in all directions and the scattered light is then detected at a specific angle. The measured signal shows random changes due to the randomly changing relative position of the investigated particles, caused by Brownian motion, where smaller particles are known to move at higher speeds than larger particles. The signal is interpreted in terms of an autocorrelation function, who's decay is proportional to particle size: the faster the decay, the smaller the particle size. The relationship between the speed of the moving particles and their size is described by the Stokes-Einstein equation, in which the diffusion coefficient D depends on the hydrodynamic radius of the investigated particles, viscosity of the solvent and temperature. It should be noted that the Stokes-Einstein equation is only applicable if Brownian motion is the only factor influencing particle motion. Other non-random sources for particle movement like sedimentation can falsify results [63]. In the course of this work, measurements were conducted using a Zetasizer Nano ZSP (Malvern Instruments, Herrenberg, Germany) equipped with 10 mW laser with a wavelength = 632.8 nm to obtain size distribution profiles of LUVs. Samples were diluted with HBS to a concentration of 50 or 100 μM. Scattering was detected at an angle of 173°C (backscatter detection), reducing multiple scattering.

2.5.6 Differential Scanning Calorimetry

To check for presence of LPS after performing the asymmetry assay for outer membrane mimicking aLUVs as described in Section 2.3 and as a first indicator of asymmetry, differential scanning calorimetry (DSC) measurements were conducted. DSC is an experimental method in which the difference in required heat to increase the temperature of a sample and respective reference sample is measured over a gradual increase or decrease in temperature. Using this technique it is possible to study the phase transitions in lipids and other biological systems, see e.g. [64]. The sample cell contains the respective lipid sample while the reference cell is filled with pure HBS buffer. By comparing the power consumption needed to keep the sample/reference cell at the same temperature during heating/cooling cycles, a DSC thermogram is obtained where the specific heat capacity is plotted over the range of scanned temperatures. This can be exploited to investigate physical transformations such as lipid phase transitions specific for the examined lipid type. During a transition from the ordered gel phase, with fully extended hydrocarbon chains and tight packing, to the disordered fluid lamellar phase, with randomly oriented hydrocarbon chains, more heat needs to flow into the sample cell than into the reference cell to keep both at the same temperature. This is due to the absorption of heat by the sample as it undergoes the endothermic phase transition from gel to liquid. This leads to maxima in heat capacity at temperatures specific to the investigated lipids or lipid mixtures. Calorimetric experiments were performed on a MicroCal VP-DSC high sensitivity differential scanning calorimeter (MicroCal, Inc., Northhampton, MA, USA). Heating and cooling scans were conducted with a scan rate of 0.5 °C per min between 2-50 °C at a sample concentration of $\sim$ 2 mg/mL. Investigated samples were acceptor vesicles consisting of PE/PG 3:1 mol/mol and PE/PG 4:1 mol/mol, donor vesicles made of Ra-LPS from *Salmonella minnesota*, as well as Re-LPS from *Escherichia coli*, respective asymmetric LUVs (PE/PG 3:1)$_{in}$/ Ra-LPS$_{out}$ and (PE/PG 4:1)$_{in}$/ Ra-LPS$_{out}$ with corresponding

scrambled vesicles. DSC measurements of symmetric and asymmetric systems of outer membrane mimics are presented in Section 2.3.

3 Results and Discussion

This chapter presents selected data from the attached publications as well as other unpublished results obtained by the author during the course of this thesis, summarizing and relating findings to each other in a wider context. The published manuscript can be found in the Appendix 4.

In the course of this thesis the influence of the lipid composition and overall sample concentration of cytoplasmic membrane mimics of Gram-negative bacteria on interactions with antimicrobial peptides was investigated using different biophysical and biochemical techniques. In this context, we exploited a common thermodynamic framework for the partitioning of antimicrobial peptides from the magainin and lactoferricin families as previously applied in [26], [27]. We focused on the effect of the magainins L18W-PGLa, MG2a and their synergistic ensemble (manuscript in preparation) as well as the two lactoferricins LF11-215 and LF11-324, on model membranes, as published in [24]. Partitioning was investigated using Trp-fluorescence measurements as well as dye leakage experiments. While Trp-fluorescence measurements offer information about the actual number of partitioned peptides per lipid molecule - results from ANTS/DPX leakage experiments provide the number of partitioned peptides that cause a specific dye-efflux. Determined partitioning values from either technique as well as other peptide induced effects on the investigated membrane mimics were shown to not simply depend on the used AMP. Instead, a strong dependence on the lipid species and their ratios making up the model membranes as well as their distribution within the bilayer in a non-trivial manner was shown, additionally to

a dependency on overall lipid and peptide concentrations.

3.1 Peptide Partitioning

Peptide partitioning behavior of the magainins L18W-PGLa, MG2a and their equimolar mixture, as well the lactoferricins LF11-215 and LF11-324 was investigated using tryptophan fluorescence and dye leakage measurements, methods are described in Sections 2.5.3 and 2.5.2, respectively. The calculation of partitioning coefficients is described in Section 2.5.4.

3.1.1 Dependence of L18W-PGLa Partitioning on Lipid Concentration

Using tryptophan fluorescence measurements, we first focused on the dependence of peptide partitioning on the overall lipid concentration within the studied systems (manuscript in preparation). We therefore investigated the membrane affinity of the L18W-PGLa peptide in PE/PG (3:1 mol/mol) mimics at a fixed peptide concentration of $[P] = 4\ \mu$M. As described in more detail in Section 2.5.3 the fluorescence signal from the Trp-containing peptide L18W-PGLa exhibits a blue-shift when inserted into lipid membranes, with values of $\lambda^B \simeq (330 - 333)$ nm and $\Gamma^B \simeq (50 - 53)$ nm, compared to pure peptides in solution with a $\lambda^W \simeq 354$ nm and $\Gamma^W \simeq 64$ nm.

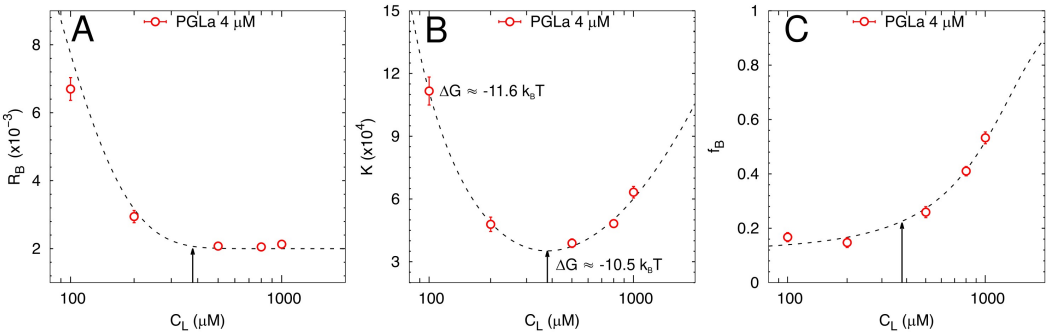

Figure 3.1: Peptide partitioning from Trp-fluorescence experiments in PE/PG 3:1 LUVs ($[L] = 100 - 1000$ μM). The dependence of **A)** the number of bound L18W-PGLa peptides per lipid molecule R_B, **B)** the partitioning coefficient K and **C)** the fraction of bound peptides f_B, on the overall lipid concentration $[L]$ inside the system for a fixed L18W-PGLa concentration ($[P]$ =4 μM). Exact values are presented in table in Table 3.1. The arrows mark the lipid concentration $[L] \sim 380$ μM of the minimum in K, additionally, selected $k_BT \ln(K_x) = -[\Delta G_x^0 + k_BT \ln(\gamma_B)]$ values are displayed (manuscript in preparation).

Figure 3.1 shows partitioning parameters for increasing lipid concentration, with A) R_B, the number of partitioned peptides per lipid molecule, B) K, the molar partitioning coefficient and C) f_B, the fraction of peptide bound to the membrane in relation to the total peptide concentration within the system. Parameters were determined using the analytical tools described in Section 2.5.4 and values derived from measurements after 60 min of lipid peptide incubation are presented in Table 3.1.

In Figure 3.1 A) the number of bound peptides per lipid shows an initial rapid decrease for higher lipid concentrations but reaches a plateau at $[L] \leq 380$ μM, while the fraction of bound L18W-PGLa increases monotonously with increasing $[L]$ (Figure 3.1 C)). The partitioning coefficient exhibits a minimum at a lipid concentration of $[L] \sim 380$ μM, see Figure 3.1 B), corresponding to the beginning of the plateau of R_B. This implies that partitioning of L18W-PGLa at a $[L] \sim 380$ μM is energetically the least favorable and partitioning

Table 3.1: Partitioning results from Trp-fluorescence spectroscopy measurements of L18W-PGLa $[P] = 4$ μM into PE/PG 3:1 vesicles of varying concentration $[L] = 100 - 1000$ μM after one hour of lipid-peptide incubation: R_B gives the number of bound peptides per lipid molecule, K the partitioning coefficient and f_B the fraction of membrane bound L18W-PGLa (Manuscript in preparation).

PE/PG 3:1	100 μM	200 μM	500 μM	800 μM	1000 μM
$R_B \times 10^{-3}$	6.7±0.2	2.9±0.2	2.1±0.1	2.1±0.1	2.1±0.1
$K \times 10^4$	11.1±0.8	4.8±0.3	3.9±0.2	4.8±0.2	6.3±0.3
f_B [%]	17.8±0.9	14.7±0.9	25.9±1.0	41.0±0.9	53.3±1.1

does not simply increase for higher lipid concentrations but shows more complex behaviour. Although K increases again for lipid concentrations $[L] > 380$ μM, the number of membrane bound peptides per lipid does not show a corresponding increase. This can be explained through the rather small difference in free energy or activity $[\Delta G_x^0 + k_B T \ln(\gamma_B)]$ even for substantial changes in K by a factor of three, for the two most strongly diverging values displayed in Figure 3.1 B).
Corresponding Trp-fluorescence kinetics of L18W-PGLa, recorded over the course of 60 min after lipid-peptide mixing with an initial dead-time of 30 sec, are presented in Figure 3.2 A-C), showing the temporal evolution of the partitioning parameters R_B, K and f_B for different lipid concentrations ($[L]$ =100-1000 μM). Partitioning kinetics also appear to be $[L]$-dependend: All partitioning parameters determined from mixtures of different lipid concentrations are shown to reach a plateau in less than 10 min, and then stay constant over the course of one hour, except for the lowest lipid concentration of $[L]$ =100 μM, where partitioning parameters reach constant values in the course of 60 min. For the highest investigated lipid concentration $[L]$ =1000 μM, values already appear to be rather constant from the first measurement conducted 30 sec after mixing.

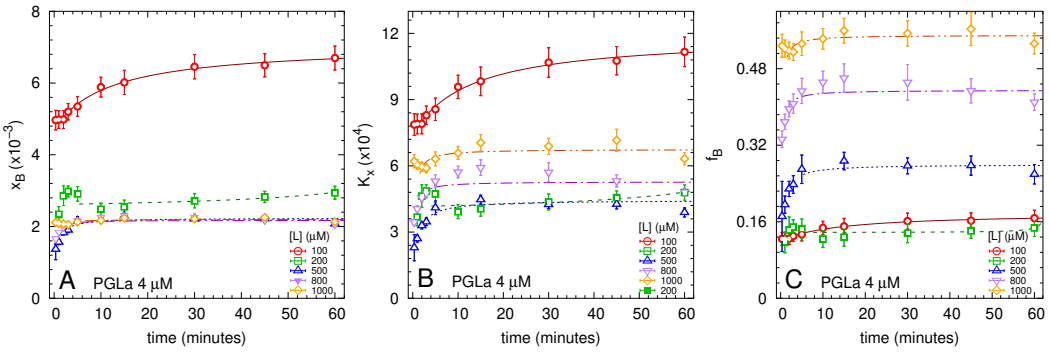

Figure 3.2: Partitioning parameters derived from time-resolved Trp-fluorescence measurements of $[P] = 4$ μM for L18W-PGLa at different PE/PG 3:1 concentrations, **A-C)** showing R_B, K and f_B, respectively. Lines are guides for the eye (manuscript in preparation).

To correlate the partitioning of L18W-PGLa with its activity, we additionally performed leakage experiments, investigating membrane permeability by measuring dye-efflux from PE/PG 3:1 vesicles after incubation with L18W-PGLa at various $[L]/[P]$ ratios. We used the equi-activity approach as previously shown in [26], [27] to quantify how much of the peptide is actually needed to induce the same effect or membrane activity (in this case leakage) in regard to the investigated lipid concentration and membrane lipid composition. We studied the effect of L18W-PGLa at physiological temperature in the lipid fluid phase, up to much higher lipid concentrations than typically used in dye leakage experiments ($[L]$=50-600 μM). Recorded leakage data are presented in Figure 3.3 A) and were interpolated with a sigmoidal function which made it possible to perform peptide partitioning analysis analogously to Trp-fluorescence data analysis for well-defined dye-leakage percentages shown in Figure 3.3 B, fitted linearly.

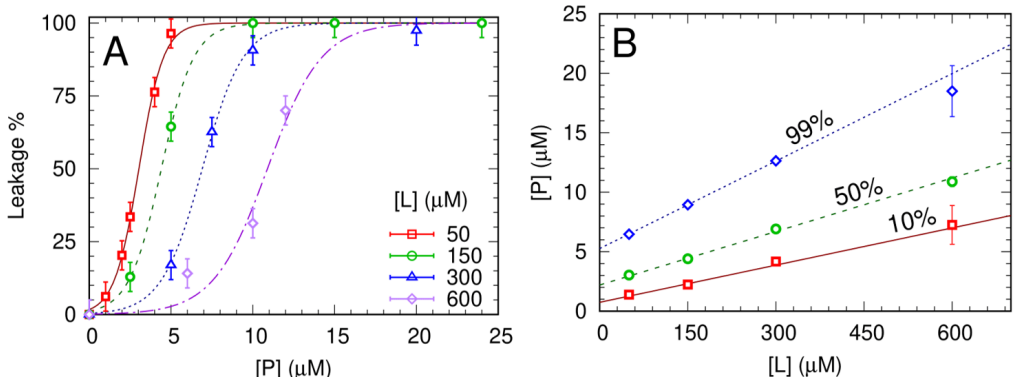

Figure 3.3: Data from membrane permeability assays induced by L18W-PGLa with the dye-quencher pair ANTS/DPX from PE/PG 3:1 lipid vesicles. **A)** Leakage percentages as a function of peptide concentration concentration [P] at different total lipid concentrations [L]. Data were fitted with a sigmoidal function by fixing a final plateau at 100%. **B)** Lipid and peptide concentrations corresponding to 10% (red squares), 50% (green circles) and 99% (blue diamonds) leakage. Data were fitted linearly to extract partitioning parameters (manuscript in preparation).

The obtained partitioning parameters R_B and K, are presented in Figure 3.4 as a function of leakage percentage. While R_B shows an increase up to a maximum value of $R_B \sim 0.025$ at 100% leakage, the partitioning coefficient K shows a monotonous decrease for increasing leakage percentages, which corresponds to an increase in peptide concentration, independent of the regarded lipid concentration. This means that dye-leakage experiments should be regarded as an indirect method to study peptide partitioning.

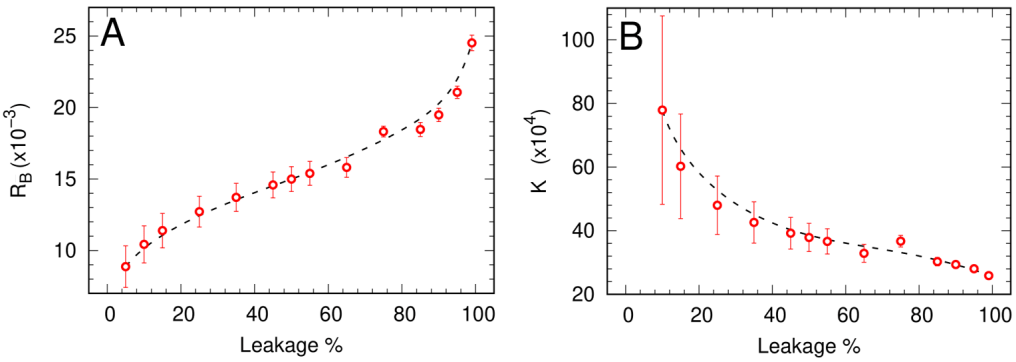

Figure 3.4: Partitioning parameters of L18W-PGLa extracted from leakage data presented in Figure 3.3, with **A)** the number of bound peptides per lipid R_B and **B)** the partitioning coefficient K for L18W-PGla, at increasing dye leakage percentages. Dashed lines are guides for the eyes.

3.1.2 Synergistic Effect of Magainins Connected to Partitioning

In a next step, we performed Trp-fluorescence measurements at a fixed lipid concentration of $[L] = 100$ μM and varying peptide concentration ($[P_{PGLa}] = 1 - 6$ μM) and investigated the partitioning of L18W-PGla in the absence and presence of the non-Trp containing MG2a, shown in Figure 3.5 A-C). The two magainins are well known for their synergistic mode of action. Increased peptide partitioning of one peptide in the presence of the other, is one of the possible explanations for their enhanced effect when applied in an equimolar mixture [19]. For both investigated systems similar trends were observed for R_B, K and f_B with increasing peptide concentrations, although obtained values were almost quadrupled for L18W-PGLa in presence of MG2a (equimolar mixture). R_B shows a monotonous increase that presents much stronger for the equimolar mixture, while K features a subtle maximum, which is also more apparent for the peptide mixture. The generally higher values of the partitioning coef-

ficient observed in the presence of MG2a, which postulates that the transfer of L18W-PGLa from solution into the membrane under the synergistic conditions of the peptide mixture, is either energetically more favorable or signifies and enhanced peptide activity or both. The difference in $[\Delta G_x^0 + k_B T \ln(\gamma_B)]$ values in absence and presence of MG2a, is however again rather small. When taking into account the total peptide concentration (PGLa + MG2a) in case of the equimolar mixture ($[P] \sim [P] * 2$), the maxima of K in both data sets coincide. The fraction of bound L18W-PGLa in reference to the total L18W-PGLa concentration (f_B) is approximately doubled under synergistic conditions and reaches up to 40% of bound peptide.

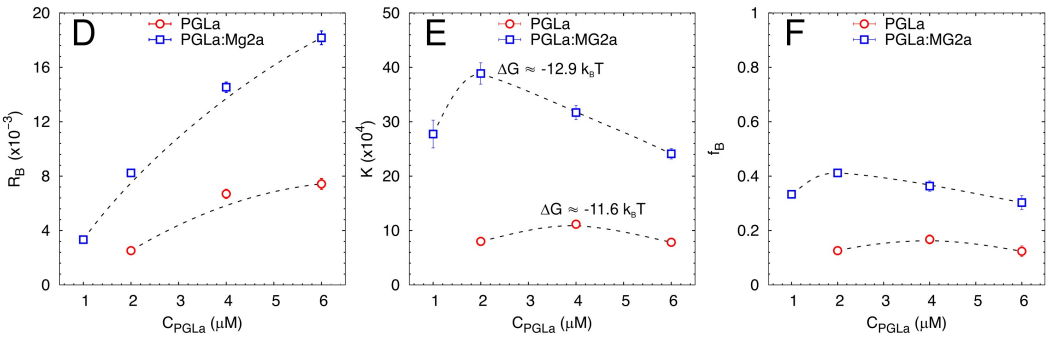

Figure 3.5: Peptide partitioning from Trp-fluorescence experiments in PE/PG 3:1 LUVs ($[L] = 100$ μM), showing **A)** the number of bound L18W-PGLa peptides per lipid molecule R_B, **B)** the partitioning coefficient K and **C)** the fraction of bound peptides f_B, plotted as a function of L18W-PGLa concentration for L18W-PGLa-only systems and L18W-PGLa:MG2a 1:1 mixtures ($[P]$ =1-6μM L18W-PGLa). Corresponding $k_B T \ln(K_x) = -[\Delta G_x^0 + k_B T \ln(\gamma_B)]$ values are displayed for two selected $[L]/[P]$ ratios. Dashed lines serve as a guide for the eye. Extracted partitioning values after one hour of lipid-peptide incubation are presented in Table 3.2 (manuscript in preparation).

To probe for potential structural changes induced by the peptides, we performed dynamic light scattering measurements after each Trp-experiment. Additionally we measured MG2a-LUV mixtures at

Table 3.2: Partitioning results from Trp-fluorescence spectroscopy measurements of L18W-PGLa in the presence and absence of MG2a peptides (L18W-PGLa $[P] = 2 - 8$ μM) into PE/PG 3:1 vesicles at $[L] = 100$ μM after one hour of lipid-peptide incubation, with R_B the number of bound L18W-PGLa peptides per lipid molecule and K the partitioning coefficient (manuscript in preparation).

L18W-PGLa	2 μM	4 μM	6 μM
$R_B \times 10^{-3}$	2.5±0.2	6.7±0.3	7.4±0.4
$K \times 10^4$	8±0.8	11.1±0.8	7.8±0.5
f_B [%]	12.6±1.1	17.8±0.9	12.4±0.7
L18W-PGLa [+MG2a]	2 μM*	4 μM*	6 μM*
$R_B \times 10^{-3}$	8.2±0.2	14.5±0.4	18.2±0.5
$K \times 10^4$	39.0±2	31.7±1.3	24.1±1
f_B [%]	41.2±1.2	36.3±0.98	30.3±0.8

* Sample aggregation

$[L]$ =100 μM and $[P]$ =2, 4 and 8 μM after an incubation period of 60 min at 37°C. Figure 3.6 shows corresponding DLS data. No significant changes in size distribution were detected for separate addition of L18W-PGLa or MG2a. The equimolar mixture of both peptides revealed significant structural changes even at the lowest investigated peptide concentration ($[P]$ =2 μM), leading to a broadened size distribution (increased polydispersity index), and increased hydrodynamic radii. This can be explained through the formation of large aggregates after mixing PE/PG/CL mimics with AMPs, as observed in SAXS measurements described in Section 3.1.4.

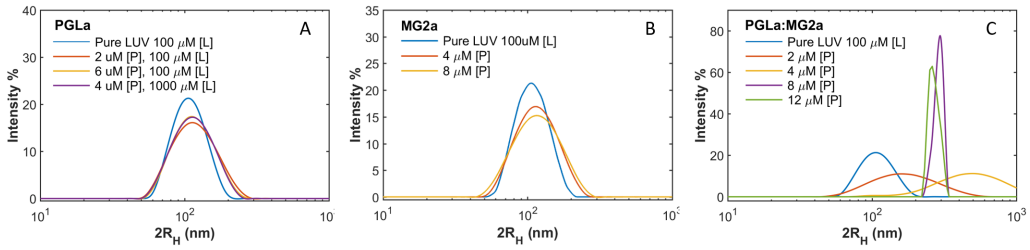

Figure 3.6: Intensity-weighted size distribution functions from DLS measurements of PE/PG 3:1 membrane mimics after incubation with peptides for 60 min at 37 °C. **A)** LUVs at $[L]$= 100/1000 μM after incubation with solely L18W-PGLa ($[P]$=2-6 μM). **B)** $[L]$=100 μM vesicles with solely MG2a ($[P]$=4-8 μM) and **C)** $[L]$=100 μM LUVs with the equimolar mixture ($[P]$=2-12 μM), (manuscript in preparation).

3.1.3 Dependence of Partitioning on Lipid Composition for Lactoferricin Derived Peptides

In a related study, we investigated peptide partitioning in dependence of lipid composition of the used membrane mimics for lactoferricin-derived peptides [24].
Therefore, we performed Trp-fluorescence measurements in three different vesicular membrane mimics composed of: pure PG, PE/PG 3:1 mol/mol and PE/PG/CL 82:6:12 mol/mol/mol, to determine partitioning parameters of the peptides L11-215 and L11-324. Both peptides are known to contain Trp and exhibited emission spectra of $\lambda^W \simeq 354$ nm and $\Gamma^W \simeq 65$ nm in HBS buffer, indicating that all Trp residues are exposed to a polar environment [65]. As reported for L18W-PGLa in PE/PG mimics, the Trp emission bands exhibited a blue-shift regardless of lipid composition and peptide type. We could thereby determine partitioning kinetics for both lactoferricin derived peptides into the three different lipid bilayers.
The fluorescence signal from the partitioned Lactoferricins in different membrane mimics exhibited values of $\lambda^B \simeq (331 - 335)$ nm and $\Gamma^B \simeq (49 - 54)$ nm, indicating an average location of the Trp residues

within the hydrophobic region of the membrane [65]. Figure 3.7 A)/C) and B)/D) shows time-dependend R_B and K values for $[P] = 4$ μM of LF11-215 and LF11-324, respectively, in the three investigated membrane mimics at a lipid concentration of $[L] = 100$ μM. Different kinetics and absolute partitioning values were observed with varying membrane lipid composition, partitioning kinetics also varied for the two investigated peptides. Interestingly, in pure PG-LUVs, LF11-215 exhibited the highest R_B and K values, while partitioning proved to be the lowest in this membrane mimic for the LF11-324 peptide and only reached a third of the values observed for LF11-215. Both peptides in PG mimics reach stationary values within 30 s after mixing and showed no further significant change during the measurement time of 60 min. Both peptides behaved similarly in PE-containing mimics, exhibiting significantly increased partitioning for systems including CL, while in both PE lipid systems similar kinetics were recorded. R_B and K show an increase within roughly 20 min after mixing, before reaching a plateau. Strikingly, the first values recorded after mixing for all three membrane mimics diverge for LF11-215 according to their final values, in case of the LF11-324 peptide, the initial value after mixing of R_B as well as K coincides in all three mimics.

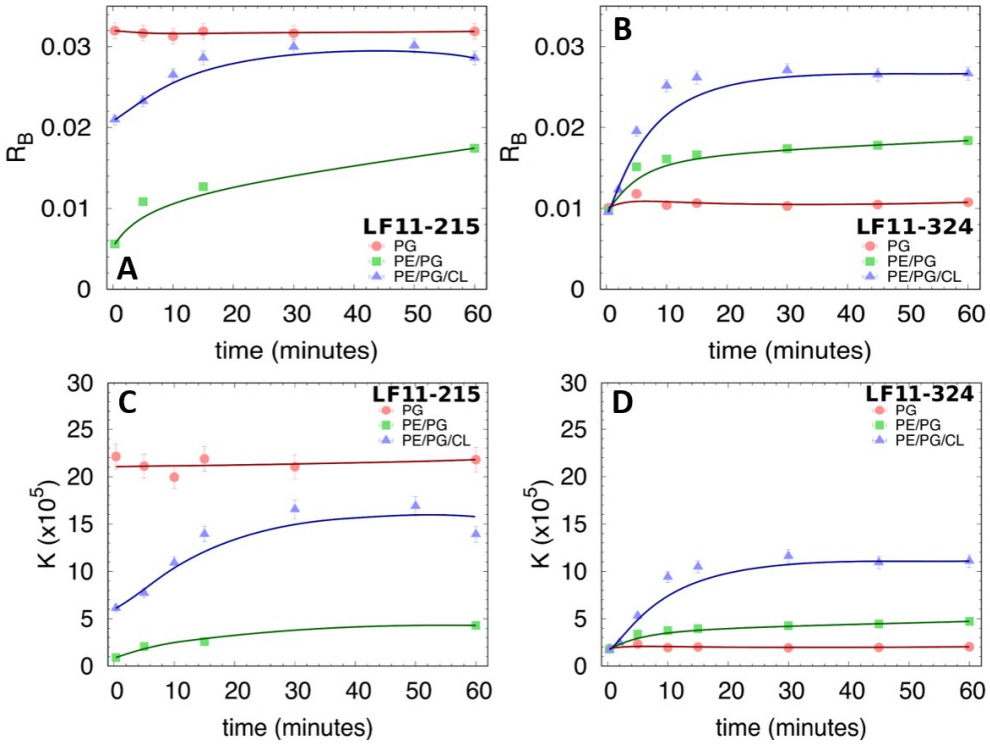

Figure 3.7: Partitioning of LF11-215 and LF11-324 determined from Trp-fluorescence experiments in three different membrane mimics (PG, PE/PG and PE/PG/CL). Changes in R_B, the number of bound peptides per lipid over time after mixing with three membrane mimics for **A)** LF11-215 and **B)** LF11-324 as well as **C-D)** kinetics of the partitioning coefficient K for LF11-215 and LF11-324, respectively. Figure taken from [24]

Calculated partitioning parameters (R_B the number of bound peptides per lipid, K the partitioning coefficient) after lipid-peptide incubation and magnetic stirring for 60 min at 37°C are presented in Table 3.3. The increased affinity of AMPs to CL-containing membranes compared to PE/PG mimics was only observed for the higher peptide concentration. At $[P] = 2$ μM partitioning was approximately equal for both PE-containing membrane mimics. The great difference between partitioning of both lactoferricins in PG membranes was also only observed at the increased peptide concentration ($[P] = 4$ μM).

Table 3.3: Partitioning results from Trp-fluorescence spectroscopy measurements of LF11-215 and LF11-324 peptides ($[P] = 2/4$ μM) into three different membrane mimics of $[L] = 100$ μM after one hour of lipid-peptide incubation. Table taken from [24]

LF11-215 (2 μM / 4 μM)	R_B $\times 10^{-3}$	K $\times 10^4$
PG	14.9±0.3 / 31.9±0.4	161±6 / 217±8
PE/PG	11.2±0.3 / 17.5±0.7	70±4 / 43±3
PE/PG/CL*	11.9±0.2 / 28.6±0.3	82±4 / 139±6
LF11-324 (2 μM / 4 μM)	R_B $\times 10^{-3}$	K $\times 10^4$
PG	10.5±0.3 / 10.7±0.9	61±4 / 20±20
PE/PG*	11.0±0.3 / 18.4±0.6	67±4 / 47±3
PE/PG/CL**	10.6±0.3 / 26.7±0.4	63±4 / 111±5

* Sample aggregation at $[P] = 4$ μM
** Sample aggregation at $[P] = 2$ and 4 μM.

The corresponding, intensity-weighted size distribution functions from DLS measurements after incubation with either peptide for one hour at 37 °C are shown in Figure 3.8. Structural changes were investigated for all three membrane mimics in combination with LF11-215 ($[P] = 4$ μM) shown in Figure 3.8 A), revealing no changes induced in PG mimics when compared to measurements of extruded LUVs without peptide addition, while PE/PG membranes exhibited a two component system with both LUVs and bigger structures present and in CL-containing mimics no LUVs remained. Figure 3.8 B) shows DLS investigations of structural changes induced by elevated concentrations of LF11-324 ($[P] = 100 - 1500$ μM) in PG mimics. Structural changes were only observed at peptide concentrations ($[P] \geq 1000$ μM).

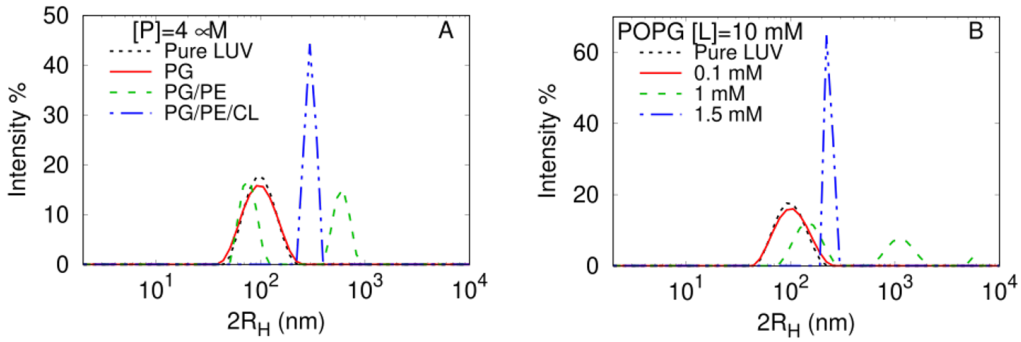

Figure 3.8: DLS measurements of different membrane mimics after incubation with peptides for one hour at 37 °C. The dotted black line represents measurements of extruded PE/PG and pure PG LUVs prior to peptide activity in A) and B), respectively. **A)** Different lipid systems ($[L] = 100$ μM) after incubation with LF11-215 ($[P] = 4$ μM). **B)** Varying concentrations of LF11-324 concentrations mixed with pure PG mimics ($[L] = 10$ mM). Figure taken from [24]

As conducted for L18W-PGLa, we correlated the partitioning of the lactoferricin-derived peptides with their activity through leakage experiments, investigating membrane permeability by measuring dye-efflux from LUVs after sample incubation for 60 min at physiological temperatures of 37°C with LF11-215 at different $[L]/[P]$ ratios. This enabled us to investigate membrane-peptide interactions up to highly elevated lipid concentrations typically used in small angle scattering experiments ($[L]$ ∼20 mM).

Recorded leakage percentages are presented in Figure 3.9 as a function of peptide concentration mixed with A) PG, B) PE/PG and C) PE/PG/CL mimics. As revealed by DLS measurements shown in Figure 3.8, substantial amounts of leakage ($>$ 15%) could always be related to the formation of larger structures, represented in Figure 3.9 A-C) by gray shaded regions, which are shown to depend on overall lipid-peptide ratios as well as membrane composition. Leakage-inducing peptide concentrations were shown to be significantly increased in pure PG mimics $[P] \leq 1000$ μM compared to $[P] \leq 250$ μM

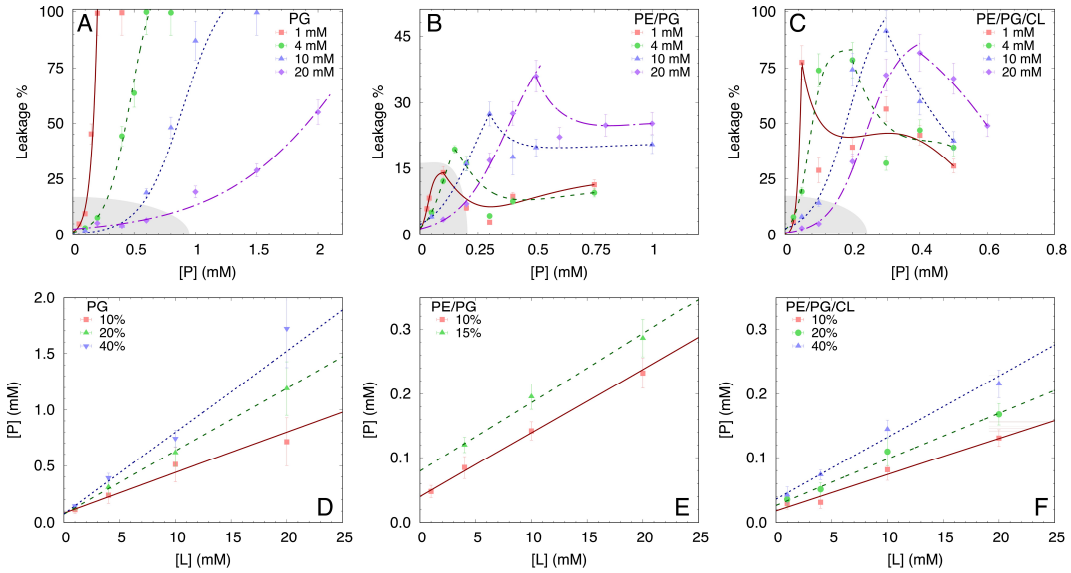

Figure 3.9: LF11-215 induced leakage in vesicles composed of PG **A)**, PE/PG **B)**, and PE/PG/CL **C)** for varying lipid concentrations. Initial leakage increases were fitted using a sigmoidal function, lines in PE-containing systems, following the subsequent decrease are guides to the eye. Grey-shaded areas mark the unilamellar regime without significant lipid aggregation. **D)-F)** shows leakage data analysis to determine partitioning parameters (Table 3.4) according to Equation 2.11 from straight line fits for the three different membrane mimics. Figure taken from [24]

in PE-containing membranes. For PG mimics a sigmoidal increase in leakage with increasing peptide concentrations was observed for all investigated lipid concentrations between ($[L] = 1 - 20$ mM), while systems with PE presented more complex behaviour with increasing peptide concentration. In this case, for all investigated lipid concentrations with increasing peptide concentration, a leakage maximum at a certain $[L]/[P]$ ratio was observed and followed by a leakage decrease down to a specific value. Comparing mimics of PE/PG and PE/PG/CL, CL-containing membranes proved to be the more permeable for the dye in presence of LF11-215, with PE/PG vesicles exhibiting particularly low dye efflux, never exceeding 40% even at high lipid concentrations, while CL mimics almost reached full leakage quota at specific $[L]/[P]$ ratios. Data were further analyzed to obtain partitioning parameters as described in Section 2.5.4. The initial increases in leakage percentage plotted over peptide concentration for different lipid concentrations presented in Figure 3.9 were fitted with a sigmoidal function to be able to extract and compare specific leakage percentages corresponding to specific $[L]/[P]$ ratios, independent of the systems overall structure. Respective partitioning parameters are presented in Table 3.4. R_B and K values are shown to increase for higher leakage percentages in all three membrane mimics, systems containing PE generally showed significantly lower values compared to PG mimics. This indicates that a higher number of peptides per lipid is required to induce leakage in PG vesicles, since at high lipid concentrations almost all peptides are partitioned into the membrane. To induce leakage in PE-containing mimics a lower percentage of peptides per lipid is required.

3.1.4 Investigations of Structural Kinetics using Time-Resolved SAXS

Taking a closer look at the peptides' structural effects on the model membranes as suggested by leakage and DLS experiments described

Table 3.4: Partitioning parameters for LF11-215 ($[P] = 0.05 - 2$ mM), derived from dye-leakage measurements of membrane mimics with different composition ($[L] = 1 - 20$ mM). Table taken from [24]

Leakage	$R_B \times 10^{-3}$	$K \times 10^4$
PG 10%	36±4	2.4±0.7
PG 20%	55.9±1.6	4.2±0.4
PG 40%	72±6	5.4±1.4
PE/PG 10%	9.8±0.4	1.37±0.16
PE/PG 15%	10.7±1.0	0.75±0.15
PE/PG/CL 10%	5.6±0.7	1.7±0.8
PE/PG/CL 20%	7.2±0.5	1.5±0.3
PE/PG/CL 40%	9.6±0.9	1.5±0.4

above, we performed time-resolved small angle X-ray scattering experiments, introduced in Section 2.5.1, to investigate the kinetics of structural changes induced by the AMPs from the magainin and lactoferricin family in different membrane mimics. SAXS data was analyzed based on Bragg peak positions only, to gain more insight into the observed structures, elaborate data modelling would be required, as demonstrated in [21] in combination with investigations using complementary techniques like contrast-variation SANS or transmission electron spectroscopy, which proved to be beyond the scope of this thesis.

In a comparison of the activity of L18W-PGLa, MG2a, L18W-PGLa:MG2a 1:1 mol/mol mixture and an additional chemically linked heterodimer of L18W-PGLa and MG2a referred to as the hybrid peptide, we first studied their time-resolved effect on LUVs with a PE/PG 3:1 mol/mol composition.

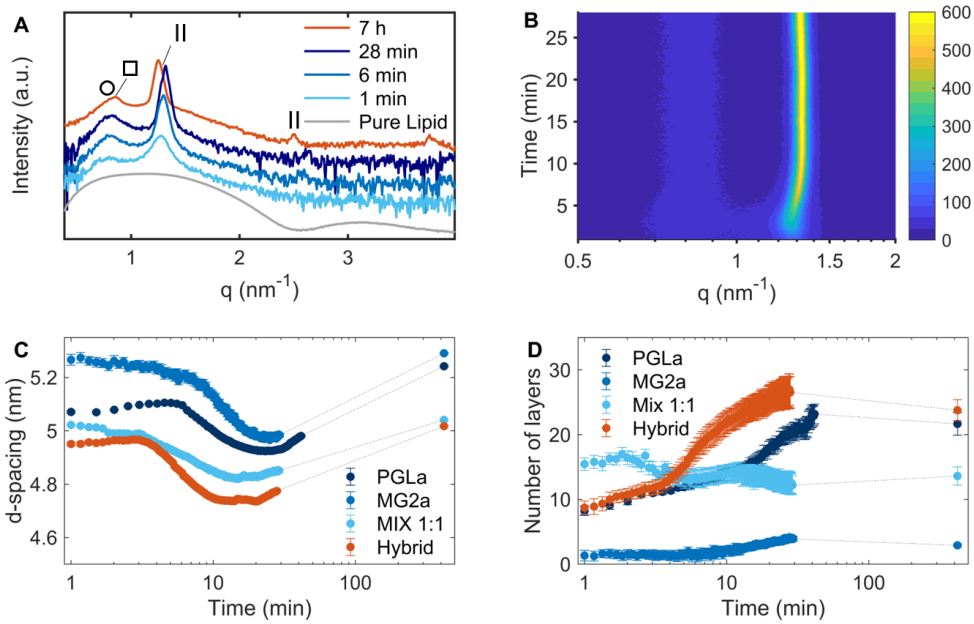

Figure 3.10: Time-resolved SAXS data of PE/PG 3:1 LUVs mixed with **A)** the hybrid peptide showing SAXS patterns of pure vesicles and changes over time at a $[P]/[L] = 1{:}25$ (**o** indicates the sponge phase, **□** the cubic phase and **II** the collapsed lamellar phase). **B)** shows the corresponding surface plot showing changes in the first order lamellar peak. Panel **D)** presents the changes in lamellar d-spacing and **E)** number of lamellae in the investigated membrane mimics over time induced by L18W-PGLa, MG2a, their equimolar mixture and the hybrid at a $[P]/[L] = 1{:}25$.

SAXS patterns of phospholipid LUVs have been previously shown to exhibit a purely diffuse scattering pattern that stems from positionally uncorrelated lipid bilayers. Diffuse scattering was observed in vesicle reference systems of all investigated compositions, depicted for PE/PG 3:1 LUVs in Figure 3.10 A) (bottom, grey curve). It was demonstrated in a previous study [9] that L18W-PGLa and MG2a induce the formation of multilamellar aggregates with collapsed layer spacings after equilibrating lipid-peptide mixtures for three days. In further endstate measurements the equimolar mixture and the hybrid

peptide were revealed to additionally induce a molten cubic phase (sponge phase), and in the case of the hybrid also a cubic phase was observed. In the time-resolved measurements conducted in the course of this thesis, PGLa, the equimolar mixture, as well as the hybrid, were shown to induce rapid (within 30 s) formation of a lamellar phase with collapsed interbilayer spacing, at a ratio of $[P]/[L] = 1 : 25$ for PE containing systems. MG2a and the lactoferricin-derived peptides presented slower kinetics. Figure 3.10 A) and B) and Figure 3.11) presents scattering curves obtained between 1-30 min after peptide addition to PE/PG 3:1 mimics and preliminary endstate measurements obtained after 7 h. Scattering patterns of the L18W-PGLa:MG2a mix and the hybrid exhibited an additional peak at $q \sim 0.8$ nm^{-1}, indicating a sponge phase, already visible in the first kinetic measurement recorded 1 min after mixing. In case of the hybrid peptide, the peak corresponding to the sponge phase did not change significantly within the kinetic measurement. Distinctive kinetics were observed in case of the lamellar phase, with the Bragg peaks becoming more pronounced and the peak position changing over time. In the case of the hybrid peptide additionally to the lamellar and sponge phase, a coexisting cubic Pn3m phase, as indicated by an additional, slightly sharper peak at $q \sim 0.9$ nm^{-1}, which was visible in the endstate measurement, but not during the 30 min time-span of the kinetic measurements, see Figure 3.10 A). This could be due to the cubic phase forming later on, or because the peak disappears in the increased noise level of the time-resolved measurements. The equimolar mixture as well as the hybrid, induced rapid precipitation of the sample, leading to a decrease in measured intensity since a reduced amount of the sample is illuminated by the X-ray beam. This explains the increased noise of scattering data at longer times.

Figure 3.10 C) shows the change of the lamellar-spacing d over time, corresponding to the temporal evolution of the first order Bragg peak, see Equation 2.3. Non-monotonic behaviour for d was observed, with an initial decrease between 10 - 20 min after mixing, and subsequent slow increase. At the beginning of the kinetic measurement the LUVs

have already been transformed into a multilamellar system with essentially no water between the individual bilayers. Observed d-values were greater for lipid-peptide mixtures containing MG2a than for mixtures with L18W-PGLa, signifying more condensed layer spacings for L18W-PGLa. d-values were even lower for the equimolar mixture and the hybrid ($d(\text{MG2a}) > d(\text{L18W-PGLa}) > d(\text{L18W-PGLa:MG2a}) > d(\text{hybrid})$). The estimated number of positionally correlated layers (n_l), determined according to Equation 2.3, increased for all peptides but the equimolar mixture, the highest number of layers were observed for the hybrid peptide, followed by L18W-PGLa and MG2a. ($n(\text{hybrid}) > n(\text{L18W-PGLa}) > n(\text{L18W-PGLa:MG2a}) > n(\text{MG2a})$). n_l was initially highest for the equimolar mixture, but remained fairly constant during the time-span of the measurement.

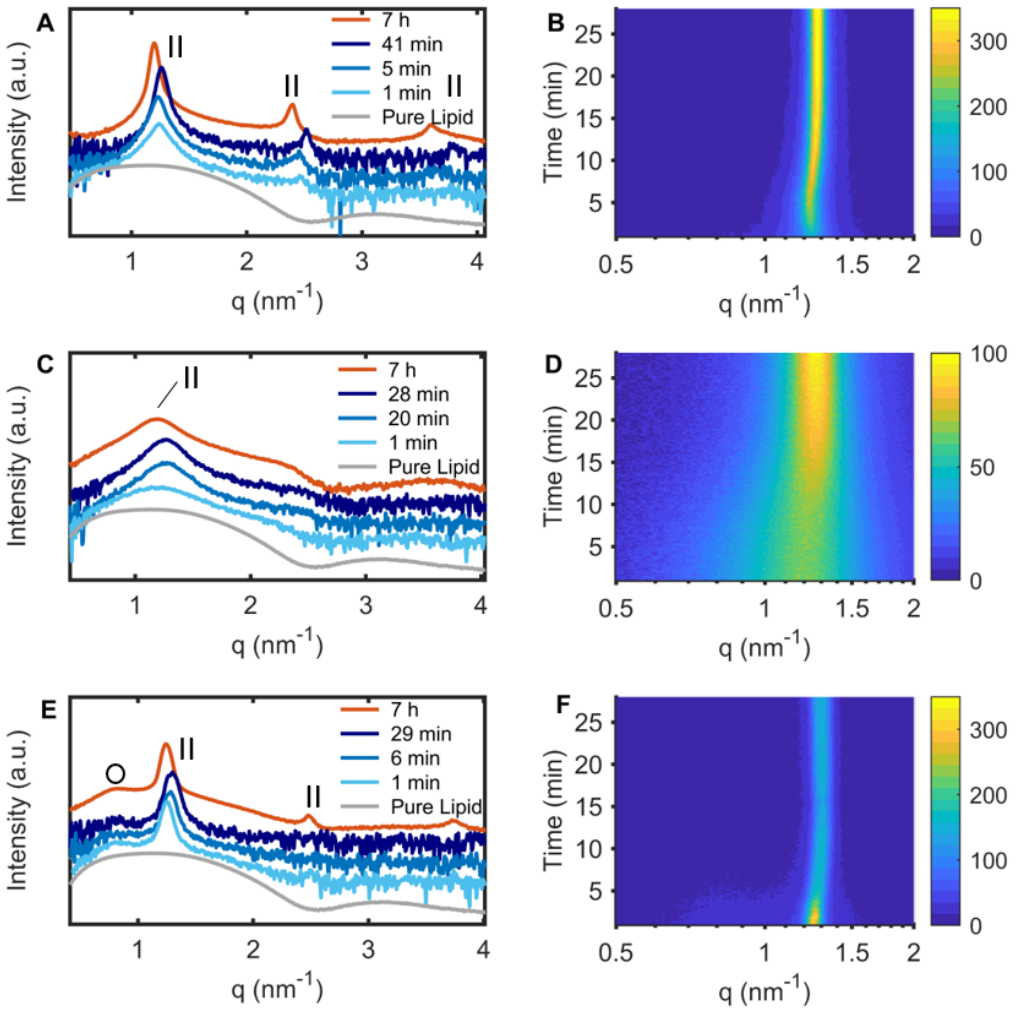

Figure 3.11: Structural kinetics observed with SAXS in PE/PG-LUVs induced by **A)** L18W-PGLa and **A)** MG2a and **E)** MG2a+L18W-PGLa at a $[P]/[L] = 1 : 25$ as well as corresponding surface plots **B)**, **D)** and **E)** (**o** indicates the sponge phase, and **II** the collapsed lamellar phase).

For further investigations of peptide kinetics, we compared the processes observed for L18W-PGLa in two membrane mimics with different membrane composition. Additionally to the simple PE/PG (3:1 mol/mol) mixture examined above, we also investigated a membrane mimic composed of PE/PG/CL (82:6:12 mol/mol/mol). Figure 3.12 A) shows a comparison of the d-value for the two membrane mimics mixed with L18W-PGLa. d is already lower in the first measurements obtained for CL containing membranes and the observed decrease during the first 10 min and subsequent increase is significantly more pronounced for this mimic. This holds also true for the estimated number of correlated layers presented in 3.12 B) with a considerably larger increase in number of layers over time for the PE/PG/CL membrane mimic. The shift of the first order lamellar peak is clearly visible in the recorded SAXS data shown Figure 3.12 C) and corresponding surface plot D).

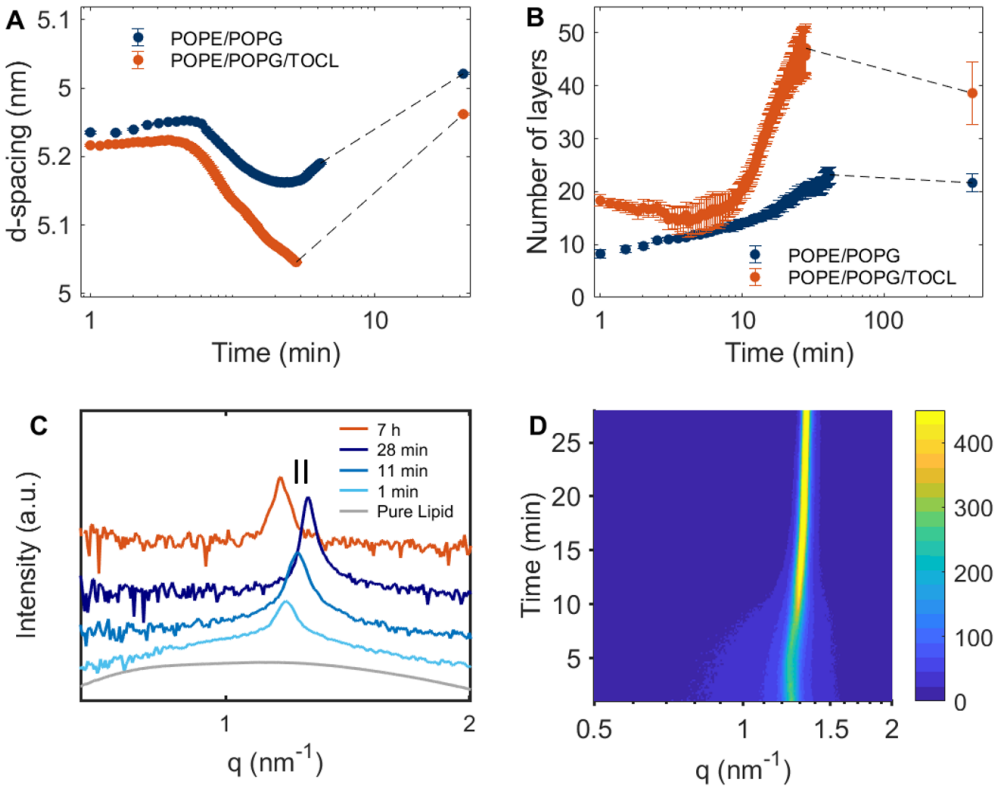

Figure 3.12: Comparison of L18W-PGLa kinetics in PE/PG and PE/PG/CL containing samples, showing changes in **A)** *d*-spacing and **B)** number of lamellae, in both membrane mimics over time after peptide addition. **C)** presents the SAXS curves of CL-containing LUVs and 1-28 min after mixing with theL18W-PGLa, as well as the preliminary endstate measured 7 h after mixing (**II** indicates the collapsed lamellar phase) and **D)** the corresponding surface plot.

A comparison of the structural effect of MG2a, the equimolar mixture and hybrid on the CL-containing mimic is presented in Figure 3.13. While for L18W-PGLa only the first order lamellar peak is visible (Figure 3.12 C)) as observed for PE/PG mimics, mixtures with MG2a show more elaborate kinetics presented in Figure 3.13 A). An addi-

tional peak can be observed, corresponding to $d \sim 10.5$ nm arising approximately 10 min after mixing and disappearing simultaneously with a splitting of the first order lamellar peak after roughly 20 min corresponding to a change in d-spacing from $d \sim 5.7$ nm down to 4.8 nm. This could be explained through vesicle fusion processes of approaching membranes leading to a swollen lamellar phase (related to the peaks with $d \sim 10.6$ nm) and then gradually changing into a system of fully collapsed bilayers with $d \sim 4.8$ nm. This could explain how the collapsed lamellar structures also observed for the other AMPs are formed, where these kinetics were possibly to fast to be recorded.

Structural changes induced by the equimolar mixture and the hybrid presented in Figure 3.13 C) and E), respectively, show similar kinetics in CL containing membranes as observed in the simpler PE/PG mixtures. The hybrids endstate shows a double peak, corresponding to $d \sim 6.3$ nm and $d \sim 4.8$ nm, with the latter clearly stemming from a collapsed lamellar phase. In a previous study [9], a value of $d_{(1,1,0)} \sim 7.3$ nm was determined for the Pn3m cubic phase induced by the hybrid in PE/PG mimics. The additional peak observed here for mixtures of the hybrid and CL-containing mimics corresponding to $d \sim 6.3$ nm might therefore be connected to a more curved non-lamellar phase or a somewhat more swollen lamellar phase. However, due to large noise levels in the discussed SAXS data, no further Bragg-peaks could be evaluated in this case and therefore a definitive identification is not possible. No endstates could be measured for MG2a and the equimolar mixture, after the 7 h incubation period with CL at 37°C containing mimics, the highly aggregated samples were stuck to the bottom of the micro well-plate they were incubated in and could therefore not be injected into the sample cell by the auto-sampler.

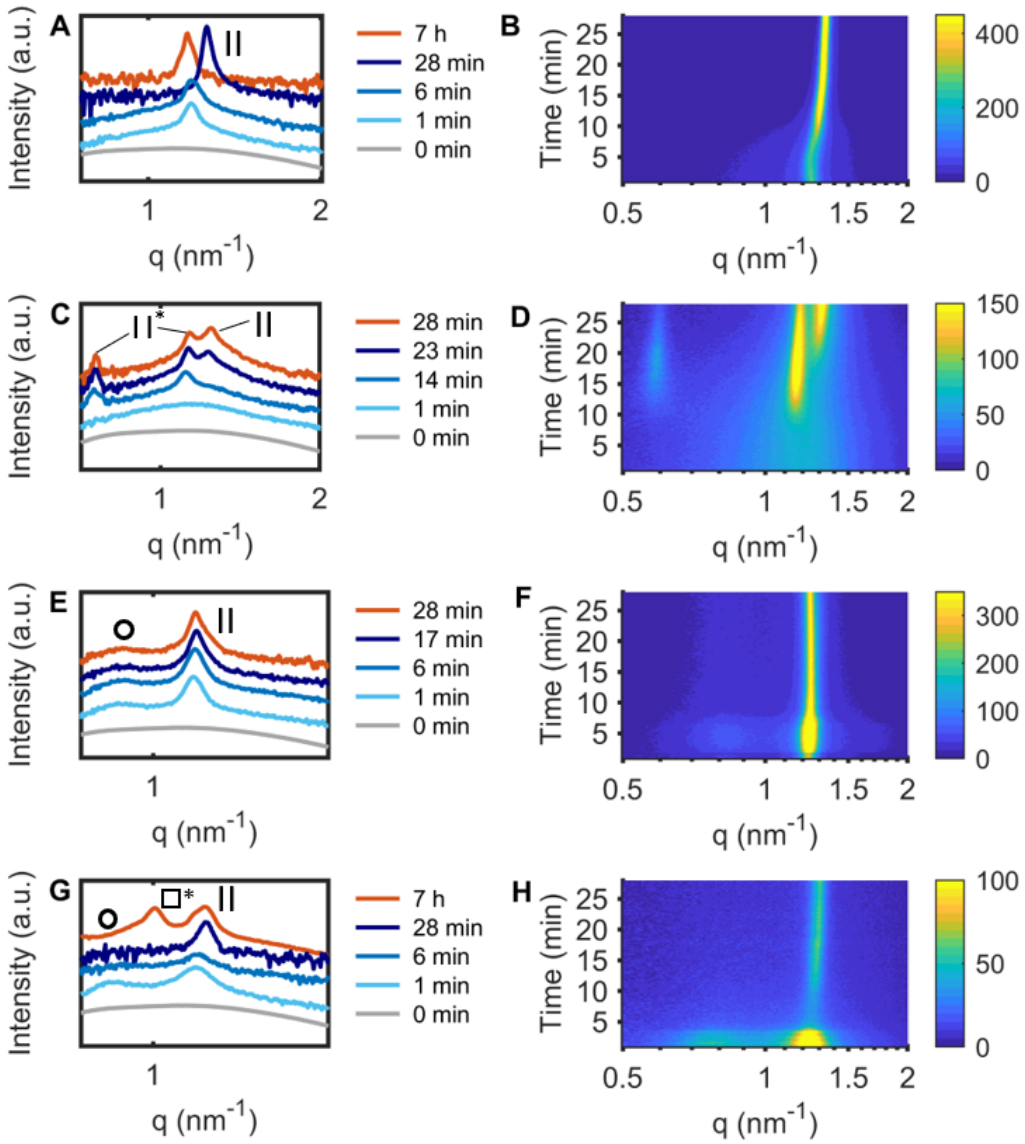

Figure 3.13: Time-resolved SAXS patterns showing structural changes in PE/PG/CL LUVs induced by **A)** MG2a **C)** L18W-PGLa:MG2a and **E)** the hybrid at a [P]/[L] = 1:25 with **B)**, **D)** and **F)** showing the corresponding surface plots, respectively. **A)** and **G)** also include preliminary endstates measured 7 h after mixing. No end-states could be measured for MG2a and the equimolar mixture in this case. (**II** indicates the collapsed lamellar phase, **II*** the swollen lamellar phase, **o** the sponge phase and □* a possible condensed cubic phase).

The kinetics of peptide-induced structural changes were also investigated for the lactoferricins LF11-215 and LF11-324 in PE/PG (3:1 mol/mol) and PE/PG/CL (82:6:12 mol/mol/mol) mimics, and additionally in pure PG vesicles [24]. For endstate measurements, LUVs mixed with the AMPs at $[L]/[P]$ ratio of 1:25 were incubated at 37°C for 4 h, recorded SAXS patterns are presented in Figures 3.14 A) and B) for LF11-215 and LF11-324, respectively. Reference systems are depicted by dashed lines and all exhibit purely diffuse scattering patterns. Both peptides induced structural changes in all membrane mimics, although changes were much less pronounced compared to effects of peptides from the magainin family. The least pronounced changes were observed in PG membranes. Mixtures of PG liposomes with LF11-324, still showed a purely diffuse scattering pattern and solely indicated a slight shift of the first minimum at $q \sim$2.8 nm^{-1} to higher q, which could stem from a thinning of the membrane. For PG LUVs with LF11-215 additionally an indistinctive positional correlation peak at q $\sim$ 1.2 nm^{-1} was observed, corresponding to a d-spacing of 5.24 nm. In both PE-containing mimics mixed with either AMP, measured endstates showed a small, but clearly discernible positional correlation peak at $q \sim$ 1.2 nm^{-1} but additionally, still exhibit a much more pronounced diffuse scattering pattern when compared to scattering patterns observed for structures induced by the magainins. PE containing systems mixed with either one of the investigated lactoferricins showed an additional modulation at $q \sim$ 2.0 nm^{-1}, which could stem from an unequal distribution of peptides throughout the system by either preferentially locating in one leaflet of the lipid bilayer or through the formation of peptide-enriched domains. In accordance with measurements conducted for magainins, we performed time-resolved SAXS measurements for all three membrane mimics in combination with LF11-215 presented in Figure 3.15. No structural kinetics were observed for LUVs consisting of pure PG, where only the endstate presented a weak feature of a positional correlation peak. As observed for Magainins, the kinetics in PE-containing membranes appeared faster and more pronounced in PE/PG/CL-mixtures. In the

first recorded frame 30 s after mixing a weak correlation peak was already visible see Figure 3.15 C). In PE/PG vesicle, induced changes were comparably less pronounced and slower, with the first onset of a peak visible approximately 5 min after lipid-peptide mixing. In PE/PG and PE/PG/CL membranes, again, a time-dependend non-monotonic behaviour of d was observed (Figure 3.15 D). Diverging from observed evolution of d-spacing values shown in Figure 3.12 A) an immediate decrease was observed before a slow increase over several minutes after peptide addition. In agreement with measurements presented above for mixtures with L18W-PGLa, the derived d-values of PE/PG were always larger than those of PE/PG/CL mixtures ($\Delta d \sim 0.1$ nm) in recorded end-states, where more pronounced changes were observed for the simpler PE/PG mimic during the time-span of this measurement. This could be attributed the the faster kinetics observed for CL containing mimics and significant decrease in d already happening before the first frame of the measurement ($<$30 s). Figure 3.15 D) also shows d-spacing values for endstates of LF11-324 with PE/PG and PE/PG/CL, which exhibited significantly lower d-values in the presence of LF11-324, $d = 5.12$ nm and $d = 5.07$ nm, respectively.

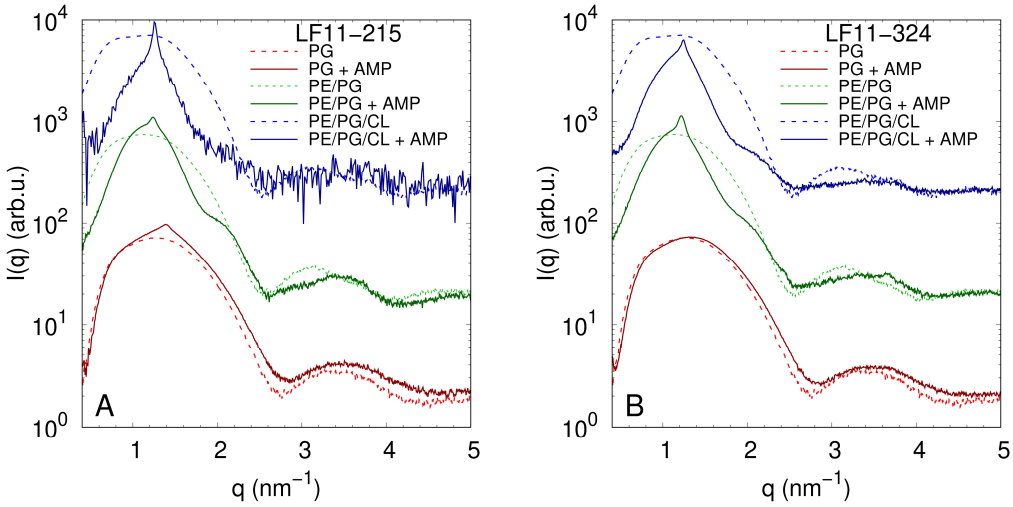

Figure 3.14: SAXS patterns of PG, PE/PG and PE/PG/CL before and after 4 h of incubation with **A)** LF11-215 and **B)** LF11-324 at $[P]/[L] = 1 : 25$, corresponding to $[L] = (24.5-27.9$ mM) and $[P] \sim 1.1$ mM. Figure taken from [24]

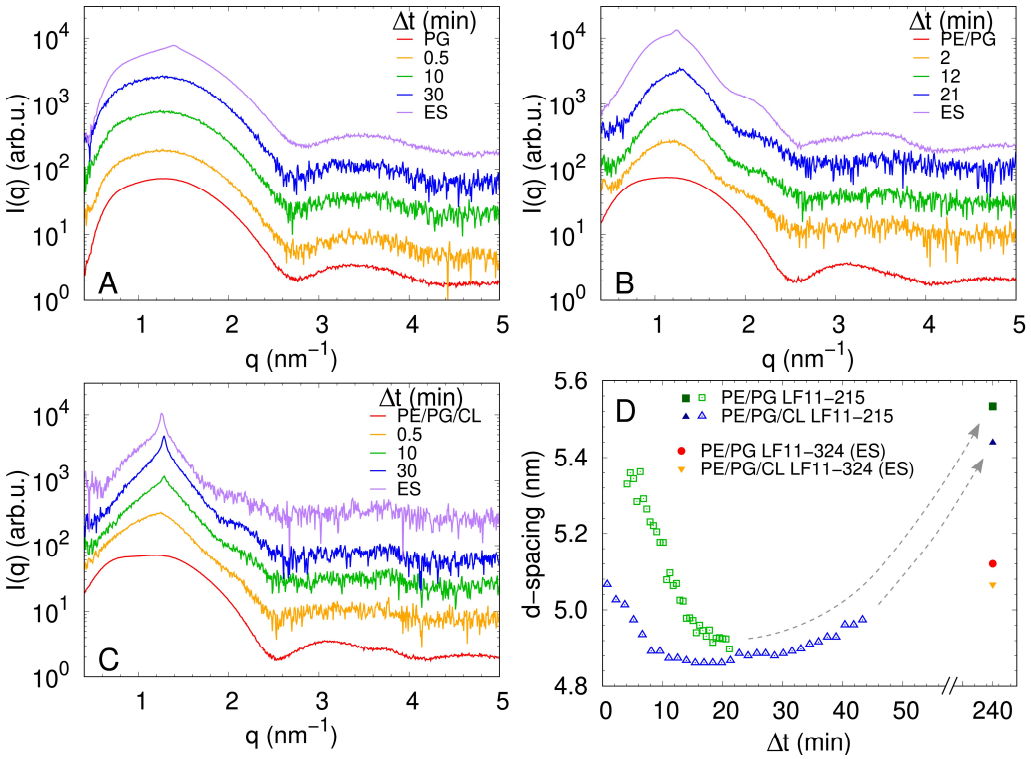

Figure 3.15: LF11-215 induced structural kinetics as observed in the evolution of SAXS patterns of **A)** PG, **B)** PE/PG and **C)** PE/PG/CL; $[P]/[L] = 1:25$, corresponding to $[L] = 24.5-27.9$ mM and $[P] \sim 1.1$ mM. Panel **D)** shows the changes in d-spacing over time for PE/PG and PE/PG/CL with LF11-215, as well as preliminary end-states (ES) for LF11-215 and LF11-324 measured after 4 h of system equilibration. Figure taken from [24]

For all investigated peptides and at high lipid and peptide concentrations used in SAXS experiments, especially for the equimolar mixture and hybrid peptide from the magainin family in combination with membrane mimics containing PE, particularly for PE/PG/CL LUVs, a major challenge proved to be the rapid, peptide-induced precipitation of the samples, causing increased noise levels in recorded data for longer measurement times, which can be explained due to a smaller fraction of the sample being hit by the X-ray beam. This

explains increased noise levels of scattering data at longer times.

3.1.5 Discussion of Studies with Symmetric Membrane Mimics

We investigated antimicrobial peptides from two different families regarding membrane partitioning and structural effects on different symmetric mimics of cytoplasmic membranes of Gram-negative bacteria.

Trp-measurements revealed complex partitioning interdependencies for different experimental parameters. Partitioning of L18W-PGLa in PE/PG mimics was shown to be dependend on the overall lipid concentration and the percentage of membrane associated AMPs more than doubled from ∼18% to ∼53% for an increase of $[L]$ =100 to 1000 μM (Fig. 3.1), higher investigated lipid concentrations, also led to faster partitioning kinetics (Fig. 3.2). Partitioning parameters derived from leakage studies of the same system at different [L]/[P] ratios for increasing lipid concentrations also showed concentration dependend behaviour. A comparison of partitioning studies derived from Trp-fluorescence and leakage experiments, revealed significantly higher partitioning values stemming from leakage measurements (up to a factor of 7). This is not necessarily contradictory and can be explained by how the partitioning parameters are actually determined for the two techniques. The equi-activity approach used to determine partitioning parameters in dye-leakage assays is an indirect method, since it measures the effect that a certain number of associated peptides have on the membrane, while Trp-fluorescence directly determines the number of partitioned AMPs and not their activity. It should be noted, that in the lipid concentration range used for L18W-PGLa partitioning studies, no structural changes of the investigated LUVs were detected in supplementary DLS measurements.

The equimolar peptide mixture of L18W-PGLa and MG2a is well known for its synergism and considerably boosts AMP activity, especially in Gram-negative bacterial strains. For the two magainins, it has recently been shown in a partitioning study derived from fluorescence experiments with NBD-labeled peptides in PE/PG 3:1 mimics investigating MG2a, L18W-PGLa, and their mixtures, that MG2a associates more strongly with the membrane than L18W-PGLa [19]. The membrane affinity of their mixture was shown to increase by an order of magnitude compared to individually added peptides. The data in this study were derived from a dilution assay, where both lipid and peptide concentrations were changing, therefore this method can be considered an indirect method, similar to the equi-activity approach used in dye-leakage assays [26], [27], [66]. We therefore also directly investigated the partitioned fraction of L18W-PGLa in the presence and absence of MG2a at a fixed $[L]$ with increasing $[P]$ using Trp-fluorescence measurements (Fig. 3.5). We likewise observed significantly increased partitioning of L18W-PGLa in the presence of MG2a, with an up to fourfold increase of the amount of L18W-PGLa incorporated into PE/PG mimics. Additional DLS measurements also revealed significant structural changes induced by the synergistic mixture even at the low investigated lipid and peptide concentrations, whereas no significant changes in size distribution were detected for separate addition of L18W-PGLa or MG2a (Fig. 3.6).

Investigations of peptide partitioning in dependence of lipid composition for the two lactoferricin-derived peptides LF11-215 and LF11-324 (Fig. 3.7) in PG, PE/PG and PE/PG/CL mimics, revealed the strongest partitioning for LF11-215 in PG membrane mimics, while, interestingly, it was shown to be the lowest for LF11-324. Due to electrostatic interactions between the anionic PG membranes and cationic AMPs, the preferential adsorption to more negatively charged membranes seems evident. However, this is not the only property driving peptide partitioning. The investigated AMPs also comprise a hydrophobic region, therefore the amphipathic moment of the peptides plays an

important role in membrane-peptide interactions. It has been shown (e.g. [23]) that lactoferricins insert into the membranes with their positively charged N-terminal part inside the hydrophobic region of the lipid bilayer, while their C-terminal part is partially interacting with the lipid head-groups and partially exposed to the solvent. The observed blue shift of recorded emission spectra in Trp-fluorescence data indicates, that Trp residues of the investigated peptides reside within an apolar environment, which also points toward their N-terminal lying within the same region for these short molecules. LF11-324 is the slightly larger peptide and is comprised of two additional Phe and Pro residues on the C-terminus, see Figure 2.5 for primary peptide sequences. Consequently this peptide needs to insert deeper into the membrane for the Trp residue to reside within the hydrophobic core of the bilayer. However, this means in turn that there is a larger distance between the N-terminus and the anionic lipid headgroups of the PG molecules, leading to less favorable electrostatic interactions for the LF11-324 peptide. This is corroborated by the fact, that the lower partitioning of LF11-324 was only observed in pure PG mimics and not for membrane mimics containing a significant amount of uncharged PE where electrostatic interactions have a decreasing influence on peptide-membrane affinity.
In membrane mimics containing cardiolipin, the highest partitioning was observed for both lactoferricin-derived peptides. This can be explained through peptide-induced domain formation, as previously observed for CL-containing mixtures in the presence of LF11 derivatives [22], [23] leading to packing defects at domain boundaries (see, e.g., [67]) which may make it easier for peptides to partition into membranes containing CL.
The interesting effect observed in ANTS/DPX leakage measurements has, to the best of our knowledge, not been reported before. As presented in Figure 3.9 B-C), in PE/PG and PE/PG/CL mimics at constant lipid concentration and increasing peptide concentration, LF11-215 induced increasing leakage values up to a certain AMP concentration and upon increasing peptide content even further, dye-efflux decreased

again and eventually reached seemingly stable values, never reaching 100% of leakage. Especially for LUVs consisting of PE/PG, recorded leakage values never exceeded ∼35%. Pure PG mimics show typical sigmoidal increase of leakage (Fig. 3.9), as reported above for L18W-PGLa and as previously established in e.g., [26], although elevated peptide concentrations were necessary, compared to concentrations used in PE-mimics. For all membrane mimics, significant leakage ($\geq$ 15%) always coincided with lipid aggregation as shown by dynamic light scattering for the 3 different mimics (Fig. 3.8) at 4 μM of LF11-215 and 10 mM PG vesicles with different concentrations of LF11-324. When compared to leakage induced by L18W-PGLa in PE/PG mimics (Fig. 3.3) the membrane activity of lactoferricins was very low even at highly elevated peptide concentrations. However, partitioning determined through Trp-fluorescence measurements revealed significantly higher membrane affinities of lactoferricins compared to magainins (for solely L18W-PGLa up to a factor of 4, indicating a completely different mode of action for the two peptide families.)

Structural kinetics induced by the peptides investigated through time-resolved SAXS were consistent with results discussed above and revealed much more pronounced membrane remodelling induced by magainins when compared to the lactoferricin derivatives, see Section 3.1.4.
For the magainins L18W-PGLa, MG2a, their equimolar mixture and the hybrid peptide, SAXS-pattern revealed distinctive Bragg-peaks already for short lipid-peptide incubation times. Comparable SAXS data was previously shown to stem from peptide-induced multibilayer systems with collapsed interbilayer distance for PE/PG (3:1 mol/mol) mimics [9]. For this specific lipid mixture, the steric bilayer thickness was shown to be $\sim$ 4.7 nm [21]. Multilamellar structures were observed for the individual L18W-PGLa and MG2a peptides (Fig. 3.11), in the case of their equimolar mixture an additional sponge phase was observed, which can essentially be described as a molten cubic phase consisting of a network of water channels throughout the multibilayer

system. Lipid-peptide mixtures with the hybrid peptide exhibited the collapsed multibilayer system, a sponge phase and an additional Pn3m cubic phase as described in [9]. The equimolar mixture, as well as the hybrid peptide therefore seem to induce high curvatures in the investigated mimic since the sponge phase and cubic phase consist of strongly curved membrane regions.

Although the first structural changes seem to be induced in the membrane mimics in a matter of seconds, recorded time-resolved SAXS data indicate that membrane fusion processes occur for all peptides on time-scales of 10 - 20 min after lipid-peptide mixing as revealed by a non-monotonic behaviour of the derived d-values. SAXS data of PE/PG mimics with all magainin systems except MG2a, already showed distinct Bragg-peaks for the first measurement 30s after lipid peptide mixing, growing more pronounced over the time-span of the measurement. The very weak Bragg-peaks and derived d-spacing values observed in SAXS measurements for lactoferricin peptides in PE/PG-mimetics point to the formation of a very small fraction of positionally well-correlated aggregates, but SAXS patterns also exhibited a large diffuse scattering fraction with an additional modulation at $q \sim 2$ nm^{-1} which was not observed for magainin peptides. This modulation could stem from an unequal distribution of peptides throughout the system by either preferentially locating in one leaflet of the lipid bilayer or through the formation of peptide-enriched domains.

A decrease and subsequent in increase in d-values determined from Bragg-peak positions was observed for all lipid-peptide systems (Fig. 3.10 and Fig. 3.15), corresponding to a convergence of membranes followed by swelling of the lamellar phase. The minimal derived d-values roughly corresponds to the steric thickness of the investigated PE/PG membranes.
The strongest membrane perturbations were observed for the equimolar mixture and the hybrid, for both of which the observed kinetics

were also shown to be the fastest. The addition of L18W-PGLa led to smaller *d*-values compared to MG2a, with the latter generally leading to significantly less pronounced structural changes. This can be explained by the position of the two peptides within the membrane. In membrane mimics with negative intrinsic curvature like PE/PG 3:1, L18W-PGLa and MG2a both were established to be aligned with the surface in solid-state NMR experiments [46] although the position of L18W-PGLa was shown to be slightly tilted. It was also previously demonstrated, that AMPs inserted into the membrane in a parallel orientation, do not form any pores and are preferentially located on the membrane surface within the region of the lipid headgroups [9]. The peptides thereby lead to a disorder of hydrocarbon chain packing and induce membrane thinning, which is especially pronounced for peptide aggregates. The slightly tilted angle of L18W-PGLa might lead to an even less ordered defect within the membrane, with the peptide not simply positioned nicely on the hydrocarbon chains of the opposing leaflets as suspected for the fully membrane-surface aligned MG2a, thereby exposing a larger hydrophobic fraction to the surroundings and favoring the formation of aggregates.

Partitioning data from leakage experiments with L18W-PGLa could be extrapolated to high lipid concentrations used in SAXS experiments (Fig. 1.1). Scattering experiments were conducted at lipid concentrations of $\sim$ 20 mM, while Trp-fluorescence and DLS measurements were performed with lipid concentrations as much as three orders of magnitude lower (50/100 μM). For experimental methods performed using high lipid concentrations like SAXS, this means that almost all L18W-PGLa peptides are partitioned into the membrane, regardless of the presence or absence of MG2a. In this lipid concentration regime, the observed multibilayer system with a coexisting sponge phase in membrane mimics induced by the equimolar L18W-PGLa:MG2a mixture, is not simply a consequence of increased peptide partitioning, but a unique structural impact of the synergistic mixture. It was previously shown [12] that L18W-PGLa and MG2a, when applied

separately to PE/PG 3:1 membrane mimics, did not induce significant dye-leakage (∼10%) at lipid concentrations conventionally used in membrane permeability assays (50 μM), while the equimolar mixture increased the induced dye efflux by approximately a factor of four. When comparing leakage results to SAXS data and not taking into account the increased lipid concentrations of the measurement technique only regarding the $[L]/[P]$ ratios, one could easily conclude that for the observed multibilayer systems induced by the single peptides, no leakage occurs and the multibilayer formation can take place without loss of dyes included in initial LUVs. It becomes evident (Fig. 1.1) that at the investigated $[P]/[L]$ ratios of 25:1 and a lipid concentration of 20 mM, 100% of leakage would be achieved also in the case of solely adding L18W-PGLa, therefore in this case the formation of collapsed multibilayers must be accompanied by significant dye-efflux.

Derived d-values from time-resolved SAXS measurements were higher for lipid-peptide mixtures containing MG2a than for mixtures with L18W-PGLa, signifying more condensed layer spacings for L18W-PGLa. d-values were even lower for the equimolar mixture and the hybrid ($d(\text{MG2a}) > d(\text{L18W-PGLa}) > d(\text{L18W-PGLa:MG2a}) > d(\text{hybrid})$) with minimal values ranging between d =4.98 nm for MG2a, down to as low as d =4.74 nm for the hybrid.
After the addition of LF11-215 and LF11-324 to PE/PG mimics, SAXS measurements revealed d-values of 5.53 nm and 5.12 nm, for the peptides respectively after one hour of lipid-peptide incubation (Fig. 3.15). In comparison to the thickness of the pure lipid system, this suggests also for lactoferricins that the recorded Bragg peaks stem from lamellar aggregates with almost completely collapsed bilayers that are probably only separated by the steric size of the peptides partitioned into the membranes. In case of LF11-324, the smaller d-values could be attributed to more pronounced membrane thinning due to the higher hydrophobicity of this peptide causing more disorder in the region of the fatty acid chains of the lipid bilayer.

In general, lower d-values were found for PE/PG/CL membrane mimics for all investigated AMPs. The steric membrane thickness of CL-containing membranes has not been published, therefore the lower d-spacing cannot be interpreted definitively. The hydrocarbon thickness is expected to be roughly the same for both PE-containing mimics, therefore the observed difference in d-values can most likely be attributed to an increased membrane perturbation induced by AMPs. Also, Trp-fluorescence and leakage measurements reported more pronounced effects of the peptides on the CL-containing mimic and related higher partitioning coefficients for lactoferricins (Fig. 3.7). Also, peptide kinetics appeared to be faster in membranes containing cardiolipin, revealed by both Trp-fluorescence and SAXS experiments. E.g. LF11-215, induced a Bragg peak in PE/PG/CL bilayer, 30 s after the addition of peptides, whereas the peak first appeared approximately 5 min after lipid-peptide mixing in PE/PG mimics. PE-mimics exhibited an initial increase in partitioning in Trp-fluorescence experiments during the first $10-20$ min which corresponds to the initial decrease in d-spacing observed in time-resolved SAXS measurements.

Mixtures of magainins with CL-containing mimics, also led to more inhomogeneous structures than in PE/PG systems. Derived d-values from mixtures of L18W-PGLa with either PE-mimic (Fig. 3.12), show corresponding temporal progression but significantly lower minimal d values of 4.92 nm in PE/PG and 4.69 nm in CL-containing membranes.
PE/PG/CL mixtures with MG2a showed more elaborate kinetics (Fig. 3.13), which can possibly explain how the collapsed lamellar structures, also observed for the other AMPs, are formed and where these kinetics were most likely to fast to be recorded. Approximately 10 min after mixing, a swollen lamellar phase appeared as indicated by corresponding d-values of 10.5 nm and 5.7 nm. After roughly 20 min, this swollen phase started to disappear simultaneously with the emergence of an additional lamellar peak with $d \sim 4.8$ nm. This could be explained through vesicle fusion processes of approaching mem-

branes, first leading to a swollen lamellar phase and then gradually changing into a system of fully collapsed multilayers.

The minimal d-values observed for LF11-215, approximately coincided for both PE-mimics at $\sim$ 4.9 nm, which roughly corresponds to the steric membrane thickness of PE/PG. This demonstrates that the bilayers within the sample come into very close contact, which can in turn be interpreted as the point in the peptide kinetics where the membranes fuse and form large aggregates. These findings also coincide with increased leakage reported for LF11-215 in CL-containing membranes, as discussed above (Fig. 3.9). Both PE [68] and CL [69] have been shown to be lipids with negative intrinsic curvature and are well-known for the formation of non-lamellar structures and membrane fusion events [70], [71], making this a likely explanation. Fusion of PE/PG membranes induced by magainin peptides has been previously shown in [9].

SAXS measurements of pure PG mimics in combination with lactoferricin-derived peptides only presented a weak Bragg peak in preliminary endstate measurements obtained after 7 h of lipid-peptide incubation (Fig. 3.15) with a derived $d \sim 4.5$ nm, which is even lower than the minimum values observed for PE-containing mimics. Unlike PE and CL, PG is a phospholipid with approximately zero intrinsic curvature [12], and is known to form unilamellar vesicles. In connection to dye leakage experiments, membrane fusion can also explain the decrease in dye-release in PE-containing membranes for increasing peptide concentrations shown in Figure 3.9, with ANTS/DPX staying trapped during the fusion process. Therefore we argue that the weak observed Bragg peak for PG mimics is not related to membrane fusion, but stems from adhesion of a few vesicles within the sample. This is supported by the fact that leakage measurements of PG vesicles did not show a drop in dye efflux with increasing AMP concentrations as was observed for PE-containing systems. To definitively identify all induced structures, further measurements would be required using

complementary techniques, which was out of the scope of this thesis.

Combining insights from all used techniques revealed that the shift of Bragg peak position over time observed in SAXS patterns can be related to an increasing accumulation of peptides on the membranes within roughly 20 min after lipid-peptide mixing and a subsequent peptide equilibration process by translocation throughout the multibilayers over hours. Concluding, overall higher peptide activities were observed for mimics containing lipids with negative intrinsic curvature, which can most likely be attributed to the stored elastic energy, making the membrane more vulnerable to the AMPs. Laggner and Lohner [72] proposed the 'balanced spring model' and suggested that membrane active compounds can relief this stored elastic energy when inserting into the membranes.
Lactoferricin derived peptides were revealed to generally induce significantly less pronounced structural changes compared to the investigated magainin peptides, although LF11-215 and LF11-324 have been demonstrated to be highly active against a broad range of Gram-positive and Gram-negative strains [22], [23], [49]. The observed effects of the lactoferricins were shown to strongly depend on the lipid composition of the used membrane mimics and the resulting collective membrane properties. However, in life Gram-negative bacteria the peptides do not only interact with the plasma membranes but also have other interaction partners. In order to shed some light on this issue, in a different study we also compared AMP partitioning studies in membrane mimics to studies of life *E.coli* bacteria as a representative strain of Gram-negative bacteria [24]. The comparison revealed that the majority of LF11-215 and LF11-324 pass through into inner bacterial compartments and solely $1-5\%$ stay bound on the surface. Neither the interaction with the bacterial cells outer membrane or other cellular components actually excludes the interaction of the peptides with the plasma membrane [73] and collective membrane properties play an important role in peptide translocation.

3.2 Peptide Kinetics of L18W-PGLa in Asymmetric Membrane Mimics

As shown in Section 3.1.3 the observed leakage rate induced by AMPs in ANTS/DPX filled LUVs and the peptides overall membrane affinity strongly depends on the lipid composition of the used membrane mimic (see also [12]). To obtain reference values of leakage percentages dependend on membrane composition, we performed time-resolved leakage measurements of dye-filled symmetric LUVs ($[L] = 50$ μM) composed of different PE/PG ratios shown (Fig. 3.16) after adding the AMP L18W-PGLa at a fixed concentration ($[P] = 0.125$ μM) in order to be able to observe leakage kinetics and to avoid rapid dye-release. Leakage kinetics show comparable progression, showing a fast initial increase within roughly the first 60 s and then a plateau or slow increase up to the end of the measurement time after 40 min. While leakage kinetics were comparable for all investigated systems, the final leakage values reached after 60 min of lipid-peptide incubation at 37°C, differed significantly for the different PE/PG mixtures. In PE rich systems only very little leakage was observed during the time-span of the measurement, while in pure PG vesicles 100% leakage was reached in a matter of minutes. Significant leakage values were only detected for systems containing a larger fraction of PG than PE, with final leakage values increasing gradually with increasing PG content.

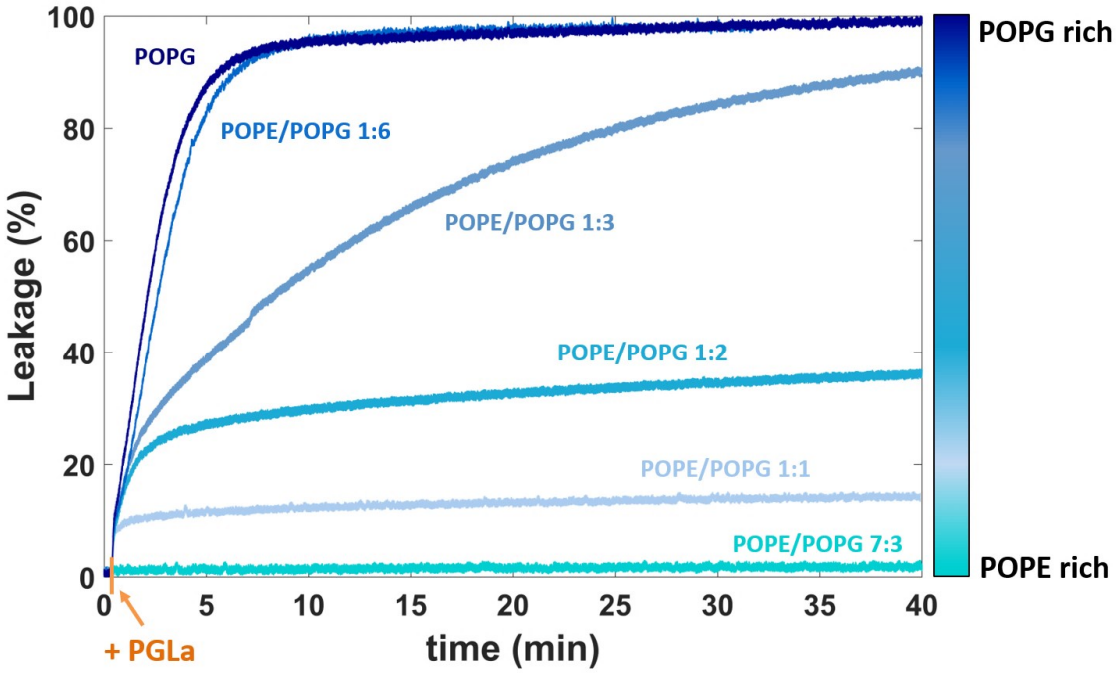

Figure 3.16: ANTS/DPX leakage kinetics induced by low concentrations of the AMP L18W-PGLa ($[P] = 0.125\ \mu$M) in membrane mimics consisting of different ratios of PE/PG (7:3-0:1) ($[L] = 50\ \mu$M) over the course of 40 min at 37°C.

The influence of membrane asymmetry on lipid-peptide interactions and membrane permeability was investigated using ANTS/DPX filled aLUVs, produced through CD mediated exchange, consisting of mostly PG in the inner leaflet and approximately 70 mol% PE in the outer leaflet. The observed leakage kinetics in this asymmetric membrane mimic show a different progression over time when compared to symmetric vesicles of the same composition or symmetric vesicles mimicking the outer leaflet of the membrane (Fig. 3.17). Leakage kinetics induced in aLUVs exhibit a two-step process, with the

first step, starting from lipid-peptide mixing to approximately 20 min after peptide addition and the second step from roughly 20-40 min when 100% of leakage is reached. Measurements of the symmetric system with the same overall lipid composition as the asymmetric sample and a symmetric system with the outer leaflet composition of the asymmetric sample did not exhibit this type of kinetic progression and overall much lower dye-efflux was recorded. We speculate that this different behaviour could originate from lipid flip-flop induced by the peptide in aLUVs over the course of 20-40 min thereby disturbing the integrity of the membrane and leading to dye-release.

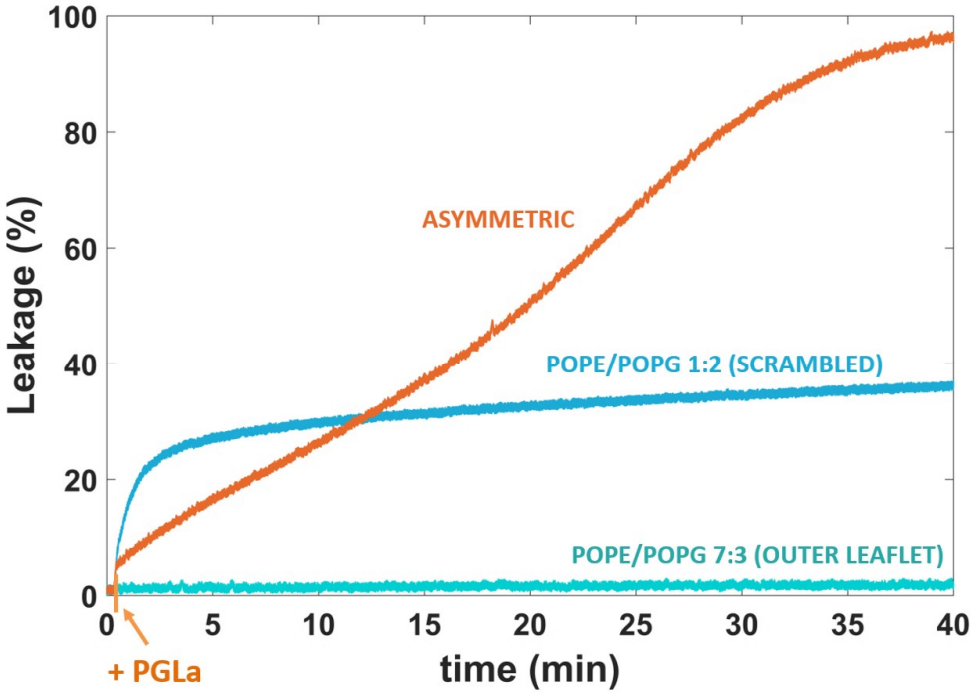

Figure 3.17: Time-resolved leakage measurements induced by L18W-PGLa ($[P] = 0.125\ \mu$M) in asymmetric membrane mimics consisting of PG on the inner and mostly PE on the outer leaflet. For comparison leakage from symmetric vesicles with the same lipid composition (scrambled) as well as outer leaflet composition are presented. Measurements were conducted over 40 min after lipid-peptide mixing at 37°C (manuscript in preparation).

To investigate the possibility of lipid flip-flop induced in asymmetric membranes by L18W-PGLa during the time-scales observed in leakage experiments, we performed small angle neutron scattering measurements, a technique that has a different sensitivity to the hydrogen isotopes protium and deuterium. Experiments were performed with aLUVs consisting of chain-deuterated PG on the inner leaflet and protiated PE on the outer leaflet, produced through cyclodextrin mediated exchange in 100% D_2O HBS buffer solution to

enhance contrast. SANS experiments were conducted at low $[P]/[L]$ ratios, where no formation of aggregates occurs. We first characterized aLUVs and symmetric (scrambled) control samples with the same overall lipid composition to ensure that their neutron scattering signal offered detectable differences, see Figure 2.6. We then tracked the influence of the AMP L18W-PGLa on lipid asymmetry through a decrease of the detected scattering signal over time, demonstrating lipid flip-flop and ultimately the transition into a symmetric, scrambled bilayer as previously shown by e.g. [6], [7]. SANS measurements were performed for mixtures of aLUVs with L18W-PGLa at three different $[L]/[P]$ ratios as well as MG2a, the equimolar mixture and LF11-215, to compare flip-flop rates induced by peptides of various structures. aLUV-PGLa mixtures at $[L]/[P]$ ratios of 400:1/100:1/800:1 are presented in Figure 3.18 A) C) and D), respectively. Presented data frames are measurements conducted at 37°C over 2 or 5 min, and then averaged over 10 or 20 min for better statistics in the case of sufficiently slow kinetics. For the fast kinetics of the 100:1 mixture, presented measurements recorded within 20 min of lipid peptide mixing, consist of only one recorded frame. At a $[L]/[P]$ ratio of 400:1, see Figure 3.18 A), a continuous intensity decrease in the q-range of the minimum is observed over the course of 60 min and full symmetry seems to be reached over night. At the lowest investigated lipid to peptide ratio, 800:1, see Figure 3.18 C), no significant changes were observed within 60 min after addition of L18W-PGLa, but relevant flip-flop seemed to occur during incubation over several hours. Figure 3.18 D) shows the highest $[L]/[P]$ ratio, where the membrane already seems to become significantly more symmetric within 1 min after peptide addition. Flip-flop rates k_f and flip-flop half-times $t_{1/2}$ could be determined according to Equations 2.6 from log-level regression fits of the normalized total intensity decay as shown in Figures 3.19 and 3.21. For all investigated peptides, L18W-PGLa exhibited the highest flip-flop rates and lowest corresponding flip-flop half-times which were shown to be highly concentration dependend Table 3.5. $t_{1/2}$ ranged from roughly 14 min at a $[L]/[P]$ =100:1 , 52 min at $[L]/[P]$ =400:1 down to

8 h at $[L]/[P]$ =800:1. Interestingly, the flip-flop halftime determined for MG2a, even at the highest investigated peptide concentration at $[L]/[P]$ =100:1, showed significantly slower lipid translocation with $t_{1/2}$ ~7 h. For lower concentrations of MG2a and for the LF11-215 peptide, no significant flip-flop was observed during the time-span of the measurement.

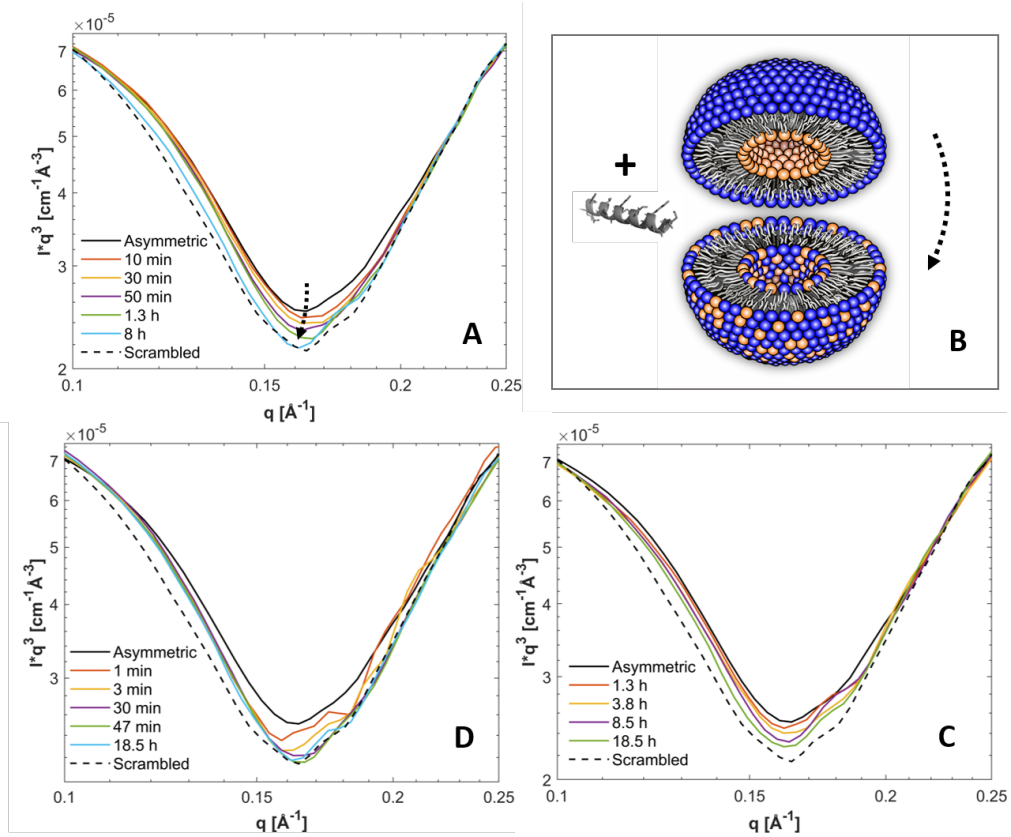

Figure 3.18: Time-resolved SANS measurements conducted at 37 °C showing flip-flop kinetics in asymmetric LUVs induced by L18W-PGLa at a $[L]/[P]$ ratio of **A)** 400:1, **C)** 800:1 and **D)** 100:1. The measurement of asymmetric vesicles without peptide is depicted in a continuous, black line. Scrambled references consisting of vesicles of the same lipid composition with symmetric lipid distribution are presented as dashed, black lines. Data are depicted with the scattering intensity (I) multiplied by the scattering vector q^3 plotted over q to highlight changes induced by the peptide. B) Shows a schematic of an asymmetric vesicle with different lipid composition in the two bilayer leaflets (top) and the same vesicle after the addition of the AMP L18W-PGLa (bottom), leading to a loss of lipid asymmetry (manuscript in preparation).

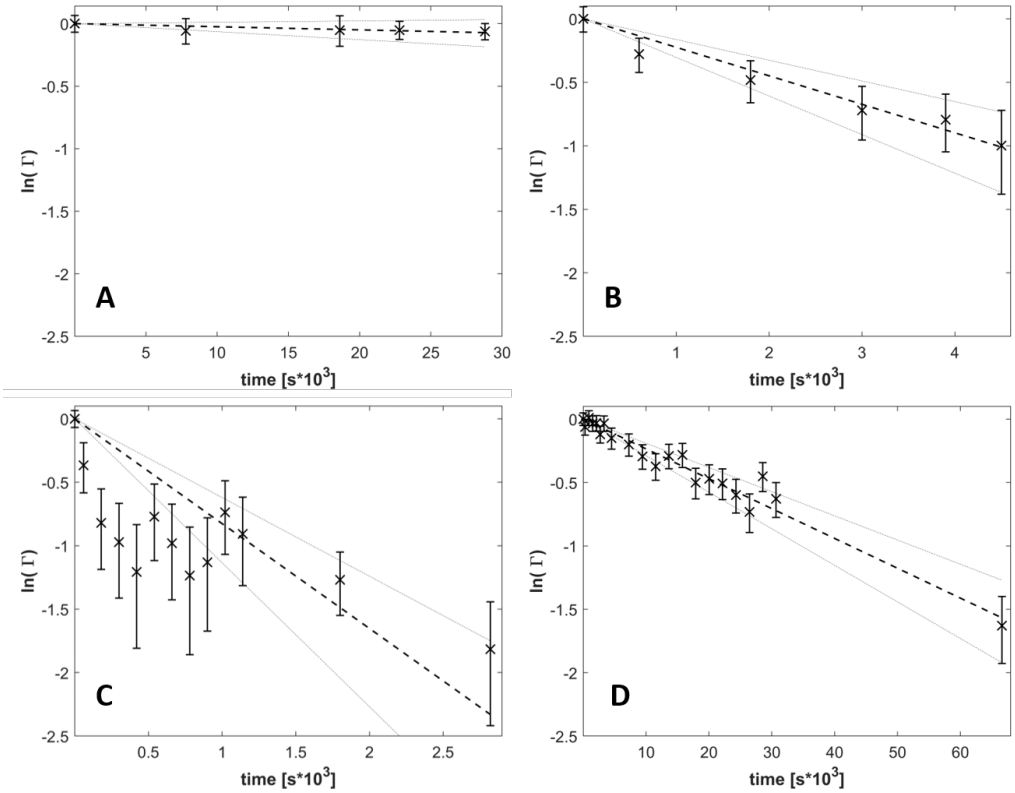

Figure 3.19: Log-level regression of the normalized total intensity decay of $\Gamma = \int_{0.1}^{0.25} I * q^3 \mathrm{dq}$ as a function of time in sec $*10^3$ in **A)** aLUVs without peptide, showing stable asymmetry over 8 h and after the addition of L18W-PGLa showing concentration dependend flip-flop at L/P ratios of **B)** 400:1, **C)** 100:1, and **D)** 800:1. Intensity decays stem from peptide-enhanced lipid flip-flop. Fastest lipid flip-flop was observed for the highest L18W-PGLa concentration at 100:1, and was significantly slowed down for lower AMP concentrations. Dashed lines represent best fits to the data and confidence interval from which the flip-flop rate (k_f) and flip-flop half-time ($t_{1/2}$) could be determined according to Equations 2.6. Derived values are presented in Table 3.5 (manuscript in preparation).

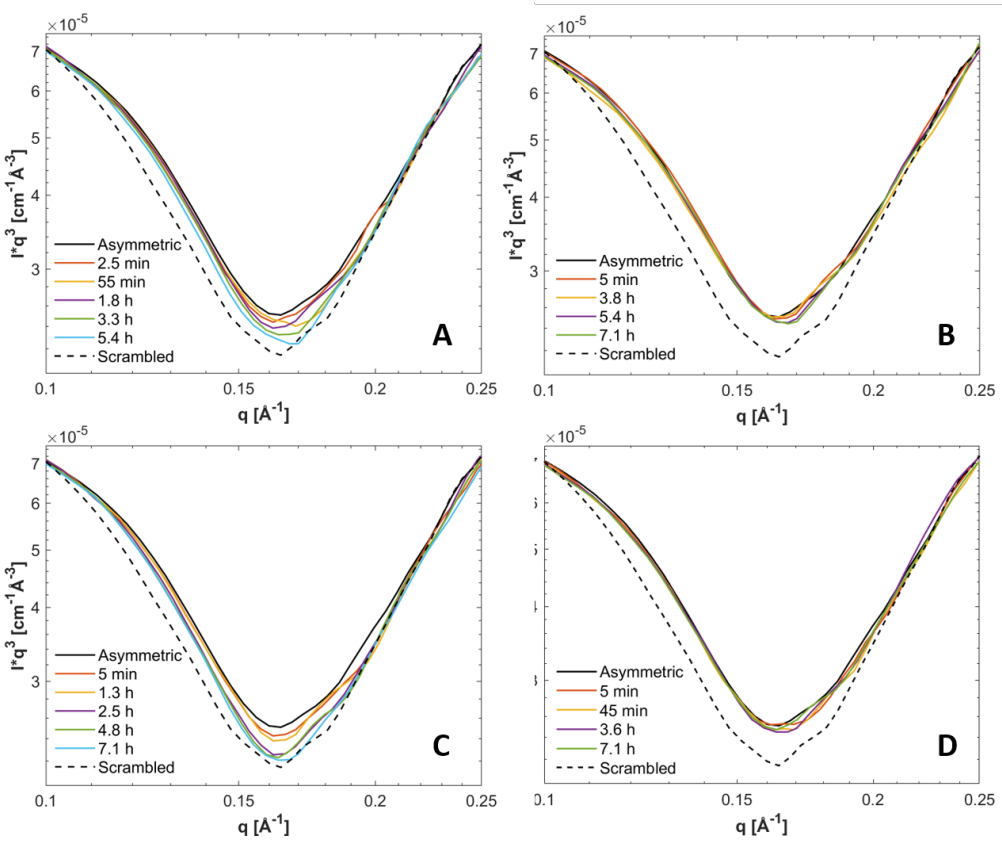

Figure 3.20: Flip-flop kinetics in asymmetric LUVs from SANS measurements, induced by the AMPS **A)** L18W-PGLa:MG2a 800:1, **B)** LF11-215 100:1, **C)** MG2a 100:1 and **D)** MG2a 200:1, at 37°C. Reference measurements of asymmetric vesicles and corresponding symmetric systems without peptide are depicted in a black, continuous and dashed lines, respectively. Data are depicted as $I * q^3$ over q to highlight changes induced by the peptide (manuscript in preparation).

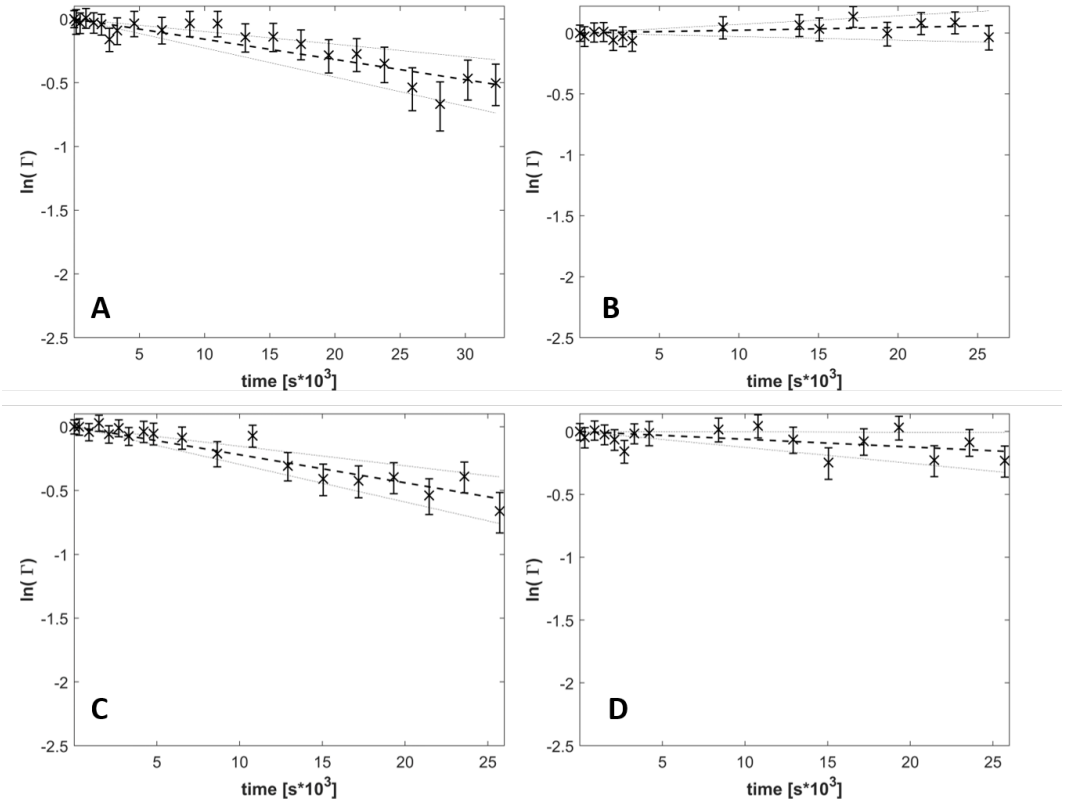

Figure 3.21: Log-level regression of the normalized total intensity decay of $\Gamma = \int_{0.1}^{0.25} I * q^3 \mathrm{dq}$ as a function of time in sec $*10^3$ indicating lipid flip-flop induced by **A)** L18W-PGLa:MG2a 800:1, **B)** LF11-215 100:1, **C)** MG2a 100:1 and **D)** MG2a 200:1. Dashed lines represent best fits to the data and confidence interval from which the the flip-flop rate (k_f) and flip-flop half-time ($t_{1/2}$) were determined according to equations 2.6, see Table 3.5 for derived values. No significant flip-flop was observed for LF11-215 100:1 and MG2a 200:1 during the time-span of this measurement (manuscript in preparation).

Table 3.5: Flip-flop rates k_f and flip-flop half-times $t_{1/2}$ for mixtures of asymmetric vesicles with L18W-PGLa, MG2a, their equimolar mixture at different L/P ratios, derived from SANS measurements presented in Figures 3.18 and 3.20 according to Equations 2.6 a-b, see Figures 3.19 and 3.21.

[L:P] AMP	$k_f\ [s^{-1}] * 10^{-5}$	$t_{1/2}\ [min]$
100:1 L18W-PGLa	41.3 ± 12.8	14 ± 4
400:1 L18W-PGLa	11.2 ± 3.5	52 ± 16
800:1 L18W-PGLa	1.2 ± 0.4	490 ± 200
100:1 MG2a	1.4 ± 0.5	420 ± 140
800:1 L18W-PGLa:MG2a	0.8 ± 0.3	730 ± 290

3.2.1 Discussion of Studies with Asymmetric Membrane Mimics

This discussion has so far concentrated on the interaction of AMPs with symmetric bacterial membranes mimics and the lion's share of available research investigating membrane-peptide interactions in the past was conducted using symmetric model membranes. However, membrane asymmetry has been shown to be a general feature of almost all biological membranes including plasma membranes and Gram-positive bacteria, see [14], [34], respectively and therefore make studying the influence of lipid asymmetry on membrane-peptide interactions the logical next step towards more realistic membrane mimics. In the course of this thesis, leakage studies with L18W-PGLa at low $[P]/[L]$ ratios where no formation of aggregates occurs, were conducted to compare asymmetric LUVs (PG_{in}/PE_{out}) with symmetric systems of the same lipid composition and highlighted the relevance of membrane asymmetry when studying interactions with antimicrobial peptides. These membrane permeability assays revealed significantly different leakage kinetics for aLUVs (Fig. 3.17), which could be connected to lipid flip-flop induced by the peptide. During

lipid translocation, the peptides see a changing membrane interface over time, with the outer vesicle leaflet changing from a PE-rich to a PG-rich system. Thus, lipid flip-flop is accompanied by changes in packing density and charge, leading to a fluctuating environment for the peptides over time and the formation of membrane defects with connected dye leakage.
Studies conducted on lipid flip-flop in the past have been performed using various techniques and membrane model mimics, although all studies were performed using isotopically distinct phosphocholines (PCs), which are not a part of bacterial membranes and therefore do not represent realistic mimetic systems of bacteria but offer experimental advantages. Previous studies include ^{1}H NMR measurements of DPPC-aLUVs at different sample temperatures and long time scales [56] as well as lipid flip-flop in asymmetric POPC/DMPC liposomes including gramicidin using differential scanning calorimetry [38] and investigations of intervesicular lipid exchange and flip-flop induced by AMPs using a strategic contrast matching scheme in two isotopically distinct DMPC vesicle populations as revealed by SANS [6], [7].
In very recent measurements, we could directly investigating peptide-induced lipid flip-flop in asymmetric LUVs (deuterated PG_{in}/protiated PE_{out}) using time-resolved neutron scattering measurements. SANS revealed stable asymmetric vesicles over the course of 8 h at 37°C in comparison to a scrambled, symmetric system of the same lipid composition (Fig. 2.6). Scattering data of aLUVs in a 400:1 $[L]/[P]$ ratio mixed with L18W-PGLa as investigated in dye-leakage experiments, showed significant translocation of lipids within the first 10-20 min after peptide addition with flip-flop halftimes of $t_{1/2}$ ∼50 min (Fig. 3.19, Tab. 3.5). When significant flip-flop is induced in aLUVs by any AMP, the outer leaflet sensed by the peptides becomes gradually more negatively charged and the packing density decreases with increasing PG-content. Therefore, electrostatic interactions become more and more crucial with progressing lipid translocation while curvature-mediated tension is lowered in the outer bilayer leaflet. The

determined flip-flop rate was shown to depend on the investigated peptide concentration, exhibiting significantly faster flip-flop halftimes of $t_{1/2}$ ∼14 min at a $[L]/[P]$ ratio of 100:1 as opposed to much slower lipid translocation at [L]/[P] 800:1 of $t_{1/2}$ ∼8 h. Interestingly, MG2a led to significantly lower flip-flop rates, at $[L]/[P]$ = 100:1 showing a flip-flop halftime of $t_{1/2}$ ∼7 h as opposed to only a few minutes for L18W-PGLa at the same $[L]/[P]$ ratio. A measurement of the L18W-PGLa:MG2a equimolar mixture at $[L]/[P]$ = 800:1 also revealed slower lipid flip-flop compared to L18W-PGLa applied on its own. This can be understood in the light of MG2a having only little effect on membrane asymmetry and with a decrease in induced flip-flop rates with decreasing L18W-PGLa concentration. For the mixture, only an effective lipid-to-PGLa ratio of 1600:1 is applied, leading to a low translocation rate for the otherwise highly active synergistic peptide mix. For lower MG2a concentrations ($[L]/[P]$ = 200:1), SANS measurements indicated no significant flip-flop, in case of LF11-215 no lipid translocation could be recorded during the time-span and within the error of the measurement even at a $[L]/[P] = 100{:}1$. This concurs with the differences in peptide activity measured for L18W-PGLa, MG2a and LF11-215 in PE/PG systems. Time-resolved SAXS measurements showed significantly less pronounced structural changes in PE/PG mimics induced by MG2a compared to L18W-PGLa during the time-span of flip-flop measurements (minutes up to 8 h). In this regard, the slightly tilted position of L18W-PGLa in the outer leaflet [46], might cause a less ordered defect within the membrane and lead to the observed increase in lipid translocation. The much shorter LF11-215 peptide also showed rather modest effects on model membranes in dye-leakage and kinetic SAXS measurements. It should be noted that compared to the aforementioned studies in PE/PG 3:1 mimics, the here investigated asymmetric systems consists of a significantly different overall PE/PG ratio of ∼1:2 but comparable outer leaflet composition of PE/PG ∼2:1 in the fully asymmetric system as described in Section 2.2.2.

3.3 Asymmetric Outer Membrane Mimics

Although partitioning data of antimicrobial peptides in mimics of the bacterial plasma membrane were shown to resemble the findings in *E. coli* [24], suggesting that these mimics are also first order proxies to peptide partitioning into outer membranes, despite the lack of LPS, the outer membrane of Gram-negative bacteria like *Escherichia coli* or *Salmonella Minnesota* acts as significant initial barrier for AMPs when interacting with bacterial cells. Realistic mimics of the highly asymmetric outer membrane of Gram-negative bacteria could be a means to further delineate the mode of action of AMPs and better understand their interaction with bacterial cells. Different experimental approaches have been used for the reconstitution of these highly asymmetric membranes, such as solid supported membranes prepared by the Langmuir-Blodgett technique, planar lipid bilayers prepared by the Montal-Mueller technique, and giant unilamellar vesicles (GUVs) prepared by the phase transfer method [40]. Following our investigations of the interaction of AMPs with LUVs mimicking the cytoplasmic membrane, it would be highly instructive to compare these findings with interactions with LUVs mimicking the outer membrane of Gram-negative bacteria. We therefore aspired to engineer asymmetric mimics of the OM consisting of aLUVs with LPS in the outer leaflet produced through cyclodextrin-mediated lipid exchange, following the protocol described in 2.2.2. Figure 3.22 shows DSC heating scans of A) PE/PG (3:/1 mol/mol), *Ra*-LPS from *Salmonella minnesota*, as well as asymmetric $(PE/PG)_{in}$/ *Ra*-LPS_{out} and scrambled PE/PG/*Ra*-LPS LUVs and B) PE/PG (4:1 mol/mol), *Re*-LPS from *Escherichia coli*, and asymmetric $(PE/PG)_{in}$/ *Re*-LPS_{out} and scrambled PE/PG/*Re*-LPS LUVs. Table 3.6 show the derived melting transitions, which indicate significant lipid exchange for the aLUVs containing *S. Minnesota*-LPS. The double peaked transition for aLUVs containing *E. coli*-LPS is shifted to significantly lower temperatures. The observed shifts of transition temperatures in aLUVs compared to PE/PG and LPS might originate from weak interleaflet coupling, see e.g. [64] or lipid flip-flop induced

by passing through the phase transition in the course of the DSC measurements [56]. We observed broadened transition peaks, as expected for an asymmetric membrane, where approximately, only half of the lipids melt cooperatively. A broadening of the phase transition could also result from an inhomogenous lipid composition throughout the vesicle population, tracing back to the CD-mediated exchange process. Presence of LPS after preparation of asymmetric vesicles was verified through phase transition peaks present at higher temperatures in DSC measurements.

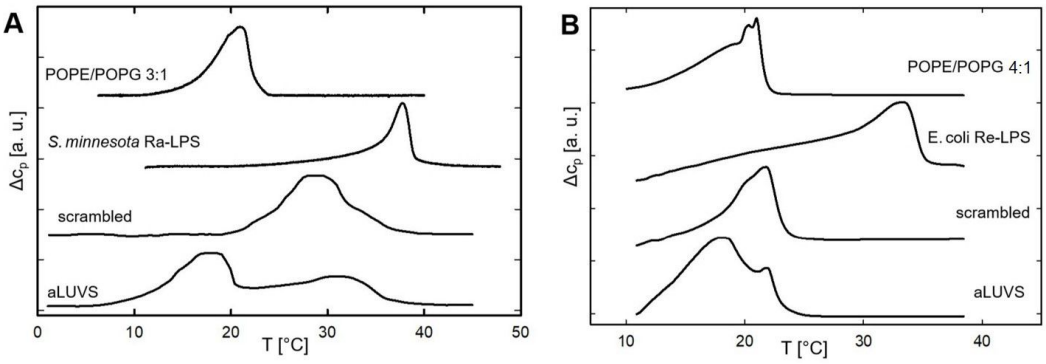

Figure 3.22: DSC heating scans (0.5°C/min) of **A)** PE/PG (3:1 mol/mol), Ra-LPS from *Salmonella minnesota*, as well as asymmetric $(PE/PG)_{in}$ / Ra-LPS_{out} and scrambled PE/PG/Ra-LPS LUVs and **B)** PE/PG (4:1 mol/mol), Ra-LPS from *Escherichia coli*, as well as asymmetric $(PE/PG)_{in}$ / Ra-LPS_{out} and scrambled PE/PG/Ra-LPS LUVs.

These first promising results could not be repeated in follow-up experiments using a freshly extracted batch of *E.coli-Re* LPS. As explained in Section 2.3, the LPS used for the measurements described above was stored prior to experiments at -20°C for extended periods of time. The discrepancy between initial and follow-up measurements could therefore be explained through insufficient LPS stability for longer storage periods, connected to hydrolysis of some of the double ester bonds of the studied LPS. This leads to a decreased number

Table 3.6: Derived melting transitions from DSC measurements (Figure3.22) of Ra-LPS from *Salmonella minnesota* and Re-LPS from *Escherichia coli*, as well as corresponding asymmetric and symmetric membrane mimics.

S.Minnesota	T_m^1 [°C]	T_m^2 [°C]
PE/PG 3:1	21	-
LPS	38	-
aLUV	18	31
scrambled	21	-
E.coli	T_m^1 [°C]	T_m^2 [°C]
PE/PG 4:1	20	21
LPS	33	-
aLUV	18	22
scrambled	22	-

of fatty acid chains attached to the lipid A moiety and therefore an impairment of LPS molecules. The lipopolysaccharides in their hydrolized state might be more easily accessible for cyclodextrin during the exchange process of the asymmetry assay (see Section 2.2.2), leading to partially deacylated LPS being more likely transferred into the phospholipid acceptor vesicles. The weak, additional transition peak observed in Figure 3.22 B) at 22°C, however, might also indicate a small amount of successfully exchanged LPS in aLUVs produced with *E. coli*-LPS.

4 Conclusion and Outlook

We investigated antimicrobial peptides from the magainin (L18W-PGLa, MG2a, their equimolar mixture and a hybrid peptide) and lactoferricin (LF11-215 and LF11-324) families regarding their membrane affinity and time-resolved structural effects on mimics of Gram-negative bacterial membranes of different complexity. In order to combine insights from diverse experimental methods, we applied a common thermodynamic framework to determine effective peptide partitioning for different lipid and peptide concentration regimes.

The data collected in the course of this thesis clearly demonstrates that for the investigation of antimicrobial peptide interactions with lipid membrane mimics, oversimplification in terms of the used model membranes and not carefully taking into account the investigated concentration ranges for different biophysical and biochemical techniques, can be highly misleading. E.g. by just looking at a simple delineation of leakage experiments, for the studied LF11-215 and LF11-324 peptides, the conclusion from leakage data could be drawn that pure PG vesicles suffice as mimics to investigate the membrane permeabilization of the lactoferricin-derived peptides, although the negative intrinsic curvature in PE/PG, and in the more realistic PE/PG/CL mixture was clearly connected to higher peptide activities and was shown to make the membrane more vulnerable to the peptides. This can most likely be attributed to the stored elastic energy within the PE-containing membranes.
Using a combination of different experimental techniques to investigate the effect of the magainins L18W-PGLa, MG2a, as well as their synergistic mixture, revealed complex interdependencies for different

lipid and peptide concentration regimes. At high lipid and peptide concentrations, topological changes in lipid vesicles were revealed, leading to the generation of multilamellar aggregates and even to the stabilization of a sponge phase, while in the lower lipid and peptide concentration regime, AMP partitioning also seems to play a key role in the synergistic activity of the two peptides.
Combining insights from all used investigation techniques revealed an increasing accumulation of peptides on the membranes during the first 20 min after lipid-peptide mixing and a subsequent peptide equilibration process by diffusion throughout the multibilayers over hours. Time-resolved SAXS measurements of PE/PG/CL mixtures with MG2a, provided further insight into how the collapsed lamellar structures are formed, while these kinetics were to fast to be recorded for other lipid-peptide systems. Observed MG2a kinetics indicate vesicle fusion processes of approaching membranes, first leading to a swollen lamellar phase within 10 minutes after lipid-peptide mixing and then gradually changing into a system of fully collapsed bilayers starting after approximately 20 min.

Lactoferricin-derived peptides comparably induced rather modest overall membrane effects, although they have been shown to be highly active against Gram-negative bacteria. This can be explained by the majority of LF11-215 and LF11-324 peptides passing through the membrane into inner bacterial compartments, with their efficacy arising from specific interactions with cytosolic components [24]. The stored elastic stress of the cell membranes in this case makes them more vulnerable to peptide translocation.

Investigations of the interaction of L18W-PGLa with asymmetric membrane mimics revealed a connection between enhanced membrane permeability of bilayers with asymmetric lipid distribution and peptide-induced lipid flip-flop on timescales of a few minutes, up to several hours depending on the used peptide concentration.

Concluding, achieving a full molecular understanding of membrane-peptide interactions requires not the only the use of realistic and specific membrane mimics and a combination of different experimental techniques to probe a large range of time and length scales, but also careful interpretation and delineation of the data in terms of actual number of peptides partitioned into the membrane at a specific lipid concentration.

Outlook

Resuming the direct investigation of partitioning using Trp-fluorescence of the peptide PGLa conducted in the course of this thesis, it would be highly instructive to also directly investigate the partitioning of solely MG2a or MG2a in the presence of PGLa. This could either be approached by exploiting the fluorescent nature of the amino acid Phenylalanin (F), already comprised in the investigated MG2a molecule which poses the challenge of fairly weak fluorescence signal compared to Trp, or alternatively using a variation of MG2a including the amino-acid Tryptophan and in turn, a PGLa-derivative without this intrinsic fluorescent probe. Thereby, a fuller picture of the partitioning of the magainin peptides and their synergistic mixture could be obtained, without resorting to an indirect measurement approach.

Further investigations on peptide-induced lipid flip-flop using Trp-fluorescence, could connect the different peptide activity observed in asymmetric LUVS, to the effective partitioning in symmetric and asymmetric membrane mimics. This will provide valuable information on the role of membrane asymmetry in the kinetics of peptide partitioning and in combination with SANS measurements conducted in the course of this thesis, could help to unveil the significance of lipid flip-flop induced by AMPs in their mode of action in live bacterial cells.

To investigate AMP interactions with the outer membrane of Gram-

negative bacteria, further efforts to engineer asymmetric outer membrane mimics consisting of LUVs containing LPS in the outer leaflet of the bilayer, could be a worthwhile objective. Following up on our approach, this could be tackled using cylcodextrin-mediated exchange but using different cyclodextrins (e.g. the smaller m-α-cylodextrin or larger m-γ-cyclodextrin) or use synthetically produced LPS alternatives that are more stable and more homogeneous than the LPS molecules used in the course of this work, extracted from bacteria in a complex and time-consuming process.

Bibliography

[1] World Health Organization, *Antimicrobial resistance: Global report on surveillance*, 2014.

[2] K. Lohner, "Membrane-active antimicrobial peptides as template structures for novel antibiotic agents," *Current Topics in Medicinal Chemistry*, no. 17, pp. 508–519, 2017. DOI: 10.2174/1568026616666160713122404.

[3] M. Zasloff, "Antimicrobial peptides of multicellular organisms," *Nature*, vol. 415, no. 6870, pp. 389–395, 2002. DOI: 10.1038/415389a.

[4] K. Lohner, "New strategies for novel antibiotics: Peptides targeting bacterial cell membranes," *General Physiology and Biophyiscs*, vol. 28, no. 2, pp. 105–116, 2009. DOI: 10.4149/gpb200902105.

[5] B. Findlay, G. G. Zhanel, and F. Schweizer, "Cationic amphiphiles, a new generation of antimicrobials inspired by the natural antimicrobial peptide scaffold," *Antimicrobial agents and chemotherapy*, vol. 54, no. 10, pp. 4049–4058, 2010, ISSN: 0066-4804. DOI: 10.1128/AAC.00530-10.

[6] M. H. L. Nguyen, M. DiPasquale, B. W. Rickeard, M. Doktorova, F. A. Heberle, H. L. Scott, F. N. Barrera, G. Taylor, C. P. Collier, C. B. Stanley, J. Katsaras, and D. Marquardt, "Peptide-induced lipid flip-flop in asymmetric liposomes measured by small angle neutron scattering," *Langmuir : the ACS journal of surfaces and colloids*, vol. 35, no. 36, pp. 11 735–11 744, 2019, ISSN: 0743-7463. DOI: 10.1021/acs.langmuir.9b01625.

[7] M. H. L. Nguyen, M. DiPasquale, B. W. Rickeard, C. G. Yip, K. N. Greco, E. G. Kelley, and D. Marquardt, "Time-resolved sans reveals pore-forming peptides cause rapid lipid reorganization," *New Journal of Chemistry*, vol. 45, no. 1, pp. 447–456, 2021, ISSN: 1144-0546. DOI: 10.1039/d0nj04717a.

[8] T. Salditt, C. Li, and A. Spaar, "Structure of antimicrobial peptides and lipid membranes probed by interface-sensitive x-ray scattering," *Biochimica et Biophysica Acta*, vol. 1758, no. 9, pp. 1483–1498, 2006, ISSN: 0006-3002. DOI: 10.1016/j.bbamem.2006.08.002.

[9] I. Kabelka, M. Pachler, S. Prévost, I. Letofsky-Papst, K. Lohner, G. Pabst, and R. Vácha, "Magainin 2 and pgla in bacterial membrane mimics ii: Membrane fusion and sponge phase formation," *Biophysical Journal*, vol. 118, no. 3, pp. 612–623, 2020, ISSN: 0006-3495. DOI: 10.1016/j.bpj.2019.12.019.

[10] E. Sevcsik, G. Pabst, A. Jilek, and K. Lohner, "How lipids influence the mode of action of membrane-active peptides," *Biochimica et Biophysica Acta*, vol. 1768, pp. 2568–2595, 2007, ISSN: 0006-3002. DOI: 10.1016/j.bbamem.2007.06.015.

[11] K. Lohner, "Membrane-active antimicrobial peptides as template structures for novel antibiotic agents," *Current Topics in Medicinal Chemistry*, vol. 17, no. 5, pp. 508–519, 2016, ISSN: 15680266. DOI: 10.2174/1568026616666160713122404.

[12] R. Leber, M. Pachler, I. Kabelka, I. Svoboda, D. Enkoller, R. Vácha, K. Lohner, and G. Pabst, "Synergism of antimicrobial frog peptides couples to membrane intrinsic curvature strain," *Biophysical Journal*, no. 8, pp. 1945–1954, 2018, ISSN: 0006-3495. DOI: 10.1016/j.bpj.2018.03.006.

[13] S. G. Wilkinson, "Gram-negative bacteria," in *Microbial Lipids*, C. Ratledge and S. Wilkinson, Eds., London: Academic Press, 1988, pp. 299–488.

[14] J. E. Rothman and E. P. Kennedy, "Asymmetrical distribution of phospholipids in the membrane of bacillus megaterium," *J Mol Biol*, vol. 110, no. 3, pp. 603–618, 1977. DOI: 10.1016/s0022-2836(77)80114-9.

[15] K. Matsuzaki, Y. Mitani, K. Y. Akada, O. Murase, S. Yoneyama, M. Zasloff, and K. Miyajima, "Mechanism of synergism between antimicrobial peptides magainin 2 and pgla," *Biochemistry*, vol. 37, no. 43, pp. 15 144–15 153, 1998. DOI: 10.1021/bi9811617.

[16] T. Hara, Y. Mitani, K. Tanaka, N. Uematsu, A. Takakura, T. Tachi, H. Kodama, M. Kondo, H. Mori, A. Otaka, F. Nobutaka, and K. Matsuzaki, "Heterodimer formation between the antimicrobial peptides magainin 2 and pgla in lipid bilayers: A cross-linking study," *Biochemistry*, vol. 40, no. 41, pp. 12 395–12 399, 2001. DOI: 10.1021/bi011413v.

[17] M. Nishida, Y. Imura, M. Yamamoto, S. Kobayashi, Y. Yano, and K. Matsuzaki, "Interaction of a magainin-pgla hybrid peptide with membranes: Insight into the mechanism of synergism," *Biochemistry*, vol. 46, no. 49, pp. 14 284–14 290, 2007. DOI: 10.1021/bi701850m.

[18] J. Zerweck, E. Strandberg, O. Kukharenko, J. Reichert, J. Bürck, P. Wadhwani, and A. S. Ulrich, "Molecular mechanism of synergy between the antimicrobial peptides pgla and magainin 2," *Scientific reports*, vol. 7, no. 1, p. 13 153, 2017. DOI: 10.1038/s41598-017-12599-7.

[19] C. Aisenbrey, M. Amaro, P. Pospíšil, M. Hof, and B. Bechinger, "Highly synergistic antimicrobial activity of magainin 2 and pgla peptides is rooted in the formation of supramolecular complexes with lipids," *Scientific reports*, vol. 10, no. 1, p. 11 652, 2020. DOI: 10.1038/s41598-020-68416-1.

[20] B. Bechinger, D. W. Juhl, E. Glattard, and C. Aisenbrey, "Revealing the mechanisms of synergistic action of two magainin

antimicrobial peptides," *Frontiers in Medical Technology*, vol. 2, 2020. DOI: 10.3389/fmedt.2020.615494.

[21] M. Pachler, I. Kabelka, M.-S. Appavou, K. Lohner, R. Vácha, and G. Pabst, "Magainin 2 and pgla in bacterial membrane mimics i: Peptide-peptide and lipid-peptide interactions," *Biophysical Journal*, vol. 117, no. 10, pp. 1858–1869, 2019, ISSN: 0006-3495. DOI: 10.1016/j.bpj.2019.10.022.

[22] D. Zweytick, G. Deutsch, J. Andrä, S. E. Blondelle, E. Vollmer, R. Jerala, and K. Lohner, "Studies on lactoferricin-derived escherichia coli membrane-active peptides reveal differences in the mechanism of n-acylated versus nonacylated peptides," *Journal of Biological Chemistry*, vol. 286, no. 24, pp. 21 266–21 276, 2011. DOI: 10.1074/jbc.M110.195412.

[23] D. Zweytick, B. Japelj, E. Mileykovskaya, M. Zorko, W. Dowhan, S. E. Blondelle, S. Riedl, R. Jerala, and K. Lohner, "N-acylated peptides derived from human lactoferricin perturb organization of cardiolipin and phosphatidylethanolamine in cell membranes and induce defects in escherichia coli cell division," *Plos One*, vol. 9, no. 3, 2014. DOI: 10.1371/journal.pone.0090228.

[24] L. Marx, E. F. Semeraro, J. Mandl, J. Kremser, M. P. Frewein, N. Malanovic, K. Lohner, and G. Pabst, "Bridging the antimicrobial activity of two lactoferricin derivatives in e. coli and lipid-only membranes," *Frontiers in Medical Technology*, vol. 3, 2021. DOI: 10.3389/fmedt.2021.625975.

[25] S. H. White and W. C. Wimley, "Membrane protein folding and stability: Physical principles," *Annu Rev Biophys Biomol Struct*, vol. 28, pp. 319–365, 1999.

[26] H. Heerklotz and J. Seelig, "Leakage and lysis of lipid membranes induced by the lipopeptide surfactin," *European biophysics journal : EBJ*, vol. 36, no. 4-5, pp. 305–314, 2007, ISSN: 1432-1017. DOI: 10.1007/s00249-006-0091-5.

[27] H. Y. Fan, M. Nazari, G. Raval, Z. Khan, H. Patel, and H. Heerklotz, "Utilizing zeta potential measurements to study the effective charge, membrane partitioning, and membrane permeation of the lipopeptide surfactin," *Biochimica et Biophysica Acta*, vol. 1838, no. 9, pp. 2306–2312, 2014, ISSN: 0006-3002. DOI: 10.1016/j.bbamem.2014.02.018.

[28] J. Knobloch, D. K. Suhendro, J. L. Zieleniecki, J. G. Shapter, and I. Köper, "Membrane-drug interactions studied using model membrane systems," *Saudi journal of biological sciences*, vol. 22, no. 6, pp. 714–718, 2015, ISSN: 1319-562X. DOI: 10.1016/j.sjbs.2015.03.007.

[29] K. Lohner, E. Sevcsik, and G. Pabst, Eds., *Chapter Five: Liposome-based biomembrane mimetic systems: Implications for lipid–peptide interactions*, 1st ed., ser. Advances in Planar Lipid Bilayers and Liposomes. Elsevier textbooks, 2007.

[30] N. Malanovic, L. Marx, S. E. Blondelle, G. Pabst, and E. F. Semeraro, "Experimental concepts for linking the biological activities of antimicrobial peptides to their molecular modes of action," *Biochimica et biophysica acta. Biomembranes*, vol. 1862, no. 8, p. 183 275, 2020. DOI: 10.1016/j.bbamem.2020.183275.

[31] M. M. Kozlov, "Determination of lipid spontaneous curvature from x-ray examinations of inverted hexagonal phases," in *Methods in Membrane Lipids*, A. M. Dopico, Ed., Totowa, NJ: Humana Press, 2007, pp. 355–366, ISBN: 978-1-59745-519-0. DOI: 10.1007/978-1-59745-519-0-24.

[32] H. W. Huang, "Molecular mechanism of antimicrobial peptides: The origin of cooperativity," *Biochimica et Biophysica Acta (BBA)*, vol. 1758, no. 9, pp. 1292–1302, 2006, ISSN: 0006-3002. DOI: 10.1016/j.bbamem.2006.02.001.

[33] G. R. Bartlett, "Phosphorus assay in column chromatography," *Journal of Biological Chemistry*, vol. 234, no. 3, pp. 466–468, 1959. DOI: 10.1016/S0021-9258(18)70226-3.

[34] J. M. Boon and B. D. Smith, "Chemical control of phospholipid distribution across bilayer membranes," *Medicinal research reviews*, vol. 22, no. 3, pp. 251–281, 2002, ISSN: 0198-6325. DOI: 10.1002/med.10009.

[35] L. I. Barsukov, V. I. Kulikov, and L. D. Bergelson, "Lipid transfer proteins as a tool in the study of membrane structure. inside-outside distribution of the phospholipids in the protoplasmic membrane of micrococcus lysodeikticus," *Biochem Biophys Res Commun*, vol. 71, no. 3, pp. 704–711, 1976. DOI: 10.1016/0006-291x(76)90888-3.

[36] F. A. Heberle, D. Marquardt, M. Doktorova, B. Eicher, R. F. Standaert, P. Heftberger, B. Kollmitzer, J. D. Nickels, R. A. Dick, G. W. Feigenson, J. Katsaras, E. London, and G. Pabst, "Subnanometer structure of an asymmetric model membrane: Interleaflet coupling influences domain properties," *Langmuir : the ACS journal of surfaces and colloids*, vol. 32, no. 20, pp. 5195–5200, 2016, ISSN: 0743-7463. DOI: 10.1021/acs.langmuir.5b04562.

[37] Q. Lin and E. London, "Ordered raft domains induced by outer leaflet sphingomyelin in cholesterol-rich asymmetric vesicles," *Biophysical Journal*, vol. 108, no. 9, pp. 2212–2222, 2015, ISSN: 0006-3495. DOI: 10.1016/j.bpj.2015.03.056.

[38] M. Doktorova, F. A. Heberle, D. Marquardt, R. Rusinova, R. L. Sanford, T. A. Peyear, J. Katsaras, G. W. Feigenson, H. Weinstein, and O. S. Andersen, "Gramicidin increases lipid flip-flop in symmetric and asymmetric lipid vesicles," *Biophysical Journal*, vol. 116, no. 5, pp. 860–873, 2019, ISSN: 0006-3495. DOI: 10.1016/j.bpj.2019.01.016.

[39] M. Doktorova, F. A. Heberle, B. Eicher, R. F. Standaert, J. Katsaras, E. London, G. Pabst, and D. Marquardt, "Preparation of asymmetric phospholipid vesicles for use as cell membrane models," *Nat Protoc*, vol. 13, pp. 2086–2101, 2018. DOI: 10.1038/s41596-018-0033-6.

[40] L. Paulowski, A. Donoghue, C. Nehls, S. Groth, M. Koistinen, S. O. Hagge, A. Böhling, M. Winterhalter, and T. Gutsmann, "The beauty of asymmetric membranes: Reconstitution of the outer membrane of gram-negative bacteria," *Frontiers in cell and developmental biology*, vol. 8, p. 586, 2020. DOI: 10.3389/fcell.2020.00586.

[41] S. Pautot, B. J. Frisken, and D. A. Weitz, "Engineering asymmetric vesicles," *Proceedings of the National Academy of Sciences of the United States of America*, vol. 100, no. 19, pp. 10 718–10 721, 2003. DOI: 10.1073/pnas.1931005100.

[42] M. Bagheri, S. Keller, and M. Dathe, "Interaction of w-substituted analogs of cyclo-rrrwfw with bacterial lipopolysaccharides: The role of the aromatic cluster in antimicrobial activity," *Antimicrobial agents and chemotherapy*, vol. 55, no. 2, pp. 788–797, 2011, ISSN: 0066-4804. DOI: 10.1128/AAC.01098-10.

[43] P. Garidel, M. Rappolt, A. B. Schromm, J. Howe, K. Lohner, J. Andra, M. H. Koch, and K. Brandenburg, "Divalent cations affect chain mobility and aggregate structure of lipopolysaccharide from salmonella minnesota reflected in a decrease of its biological activity," *Biochimica et Biophysica Acta*, vol. 1715, no. 2, pp. 122–131, 2005, ISSN: 0006-3002. DOI: 10.1016/j.bbamem.2005.07.013.

[44] G. Pabst, S. L. Grage, S. Danner-Pongratz, W. Jing, A. S. Ulrich, A. Watts, K. Lohner, and A. Hickel, "Membrane thickening by the antimicrobial peptide pgla," *Biophysical Journal*, vol. 95, no. 12, pp. 5779–5788, 2008, ISSN: 0006-3495. DOI: 10.1529/biophysj.108.141630.

[45] M. Zasloff, "Magainins, a class of antimicrobial peptides from xenopus skin: Isolation, characterization of two active forms, and partial cdna sequence of a precursor," *Proceedings of the National Academy of Sciences*, vol. 84, no. 15, pp. 5449–5453, 1987, ISSN: 0027-8424. DOI: 10.1073/pnas.84.15.5449.

[46] E. Strandberg, J. Zerweck, P. Wadhwani, and A. S. Ulrich, "Synergistic insertion of antimicrobial magainin-family peptides in membranes depends on the lipid spontaneous curvature," *Biophysical Journal*, vol. 104, no. 6, pp. L9–11, 2013, ISSN: 0006-3495. DOI: 10.1016/j.bpj.2013.01.047.

[47] N. Harmouche and B. Bechinger, "Lipid-mediated interactions between the antimicrobial peptides magainin 2 and pgla in bilayers," *Biophysical Journal*, vol. 115, no. 6, pp. 1033–1044, 2018, ISSN: 0006-3495. DOI: 10.1016/j.bpj.2018.08.009.

[48] D. Zweytick, G. Pabst, P. M. Abuja, A. Jilek, S. E. Blondelle, J. Andra, R. Jerala, D. Monreal, d. T. Martinez, and K. Lohner, "Influence of n-acylation of a peptide derived from human lactoferricin on membrane selectivity," *Biochimica et Biophysica Acta*, vol. 1758, no. 9, pp. 1426–1435, 2006, ISSN: 0006-3002. DOI: 10.1016/j.bbamem.2006.02.032.

[49] S. Sánchez-Gómez, M. Lamata, J. Leiva, S. E. Blondelle, R. Jerala, J. Andrä, K. Brandenburg, K. Lohner, I. Moriyón, and G. Martínez-de-Tejada, "Comparative analysis of selected methods for the assessment of antimicrobial and membrane-permeabilizing activity: A case study for lactoferricin derived peptides," *BMC microbiology*, vol. 8, p. 196, 2008. DOI: 10.1186/1471-2180-8-196.

[50] B. Gironi, Z. Kahveci, B. McGill, B.-D. Lechner, S. Pagliara, J. Metz, A. Morresi, F. Palombo, P. Sassi, and P. G. Petrov, "Effect of dmso on the mechanical and structural properties of model and biological membranes," *Biophysical Journal*, vol. 119, no. 2, pp. 274–286, 2020, ISSN: 0006-3495. DOI: 10.1016/j.bpj.2020.05.037.

[51] E. F. Semeraro, L. Marx, J. Mandl, M. P. K. Frewein, H. L. Scott, S. Prévost, H. Bergler, K. Lohner, and G. Pabst, "Evolution of the analytical scattering model of live escherichia coli," *bioRxiv*, 2020. DOI: 10.1101/2020.09.18.303305.

[52] M. Rappolt, "Chapter 9 the biologically relevant lipid mesophases as \textquotedblright by x-rays," in *Advances in Planar Lipid Bilayers and Liposomes*, A. Leitmannova Liu, Ed., vol. Volume 5, Academic Press, 2006, pp. 253–283, ISBN: 1554-4516.

[53] H. Amenitsch, M. Rappolt, M. Kriechbaum, H. Mio, P. Laggner, and S. Bernstorff, "First performance assessment of the small-angle x-ray scattering beamline at elettra," *J Synchrotron Rad*, vol. 5, pp. 506–508, 1998. DOI: 10.1107/S090904959800137X.

[54] A. P. Hammersley, S. O. Svensson, M. Hanfland, A. N. Fitch, and D. Hausermann, "Two-dimensional detector software: From real detector to idealised image or two-theta scan," *High Pressure Research*, vol. 14, no. 4-6, pp. 235–248, 1996, ISSN: 0895-7959. DOI: 10.1080/08957959608201408.

[55] R. Haider, B. Marmiroli, B. Sartori, A. Radeticchio, M. Wolf, S. Dal Zilio, and H. Amenitsch, *Nanodrop cell for x-ray and nanoanalytic applications*, NFFA, Ed., 2019. [Online]. Available: https://www.nffa.eu/media/225894/d69_nanodrop-cell-for-x-ray-and-nanoanalytic-applications.pdf.

[56] D. Marquardt, F. A. Heberle, T. Miti, B. Eicher, E. London, J. Katsaras, and G. Pabst, "1h nmr shows slow phospholipid flip-flop in gel and fluid bilayers," *Langmuir : the ACS journal of surfaces and colloids*, vol. 33, no. 15, pp. 3731–3741, 2017, ISSN: 0743-7463. DOI: 10.1021/acs.langmuir.6b04485.

[57] G. Bueldt, H. U. Gally, A. Seelig, J. Seelig, and G. Zaccai, "Neutron diffraction studies on selectively deuterated phospholipid bilayers," *Nature*, vol. 271, no. 5641, pp. 182–184, 1978. DOI: 10.1038/271182a0.

[58] G. Zaccai, G. Büldt, A. Seelig, and J. Seelig, "Neutron diffraction studies on phosphatidylcholine model membranes: Ii. chain conformation and segmental disorder," *J. Mol. Biol.*, vol. 134, no. 4, pp. 693–706, 1979, ISSN: 0022-2836. DOI: 10.1016/0022-2836(79)90480-7.

[59] G. Pabst, M. P. K. Frewein, Marx L., and Porcar L., *Peptide induced lipid flip-flop in asymmetric membrane mimics of gram-negative bacteria*, 2021. DOI: 10.5291/ILL-DATA.DIR-217.

[60] A. S. Ladokhin, S. Jayasinghe, and S. H. White, "How to measure and analyze tryptophan fluorescence in membranes properly, and why bother?" *Analytical Biochemistry*, vol. 285, no. 2, pp. 235–245, 2000, ISSN: 0003-2697. DOI: 10.1006/abio.2000.4773.

[61] S. H. White and W. C. Wimley, "Hydrophobic interactions of peptides with membrane interfaces," *Biochimica et Biophysica Acta*, vol. 1376, no. 3, pp. 339–352, 1998, ISSN: 0006-3002. DOI: 10.1016/s0304-4157(98)00021-5..

[62] W. C. Wimley, T. P. Creamer, and S. H. White, "Solvation energies of amino acid side chains and backbone in a family of host−guest pentapeptides," *Biochemistry*, vol. 35, no. 16, pp. 5109–5124, 1996. DOI: 10.1021/bi9600153.

[63] M.I. Worldwide, "Dynamic light scattering, common terms defined.," UK, 2011.

[64] B. Eicher, D. Marquardt, F. A. Heberle, I. Letofsky-Pabst, G. N. Rechberger, J. Katsaras, G. Pabst, I. Letofsky-Papst, M.-S. Appavou, J. Katsaras, and G. Pabst, "Intrinsic curvature-mediated transbilayer coupling in asymmetric lipid vesicles," *Biophysical Journal*, vol. 114, no. 114 // 1, pp. 146–157, 2018, ISSN: 0006-3495. DOI: 10.1016/j.bpj.2017.11.009.

[65] E. A. Burstein, N. S. Vedenkina, and M. N. Ivkova, "Fluorescence and the location of tryptophan residues in protein molecules," *Photochemistry and Photobiology*, vol. 18, no. 4, pp. 263–279, 1973, ISSN: 0031-8655. DOI: 10.1111/j.1751-1097.1973.tb06422.x.

[66] H. Patel, C. Tscheka, and H. Heerklotz, "Characterizing vesicle leakage by fluorescence lifetime measurements," *Soft Matter*, vol. 5, no. 15, p. 2849, 2009. DOI: 10.1039/B908524F.

[67] R. M. Epand and R. F. Epand, "Domains in bacterial membranes and the action of antimicrobial agents," *Molecular BioSystems*, vol. 5, no. 6, pp. 580–587, 2009. DOI: 10.1039/B900278M. [Online]. Available: https://pubs.rsc.org/en/content/articlepdf/2009/mb10.1039/b900278m.

[68] B. Kollmitzer, P. Heftberger, M. Rappolt, and G. Pabst, "Monolayer spontaneous curvature of raft-forming membrane lipids," *Soft Matter*, vol. 9, no. 45, pp. 10 877–10 884, 2013. DOI: 10.1039/C3SM51829A.

[69] Y.-F. Chen, K.-Y. Tsang, W.-F. Chang, and Z.-A. Fan, "Differential dependencies on ca2+ and temperature of the monolayer spontaneous curvatures of dope, dopa and cardiolipin: Effects of modulating the strength of the inter-headgroup repulsion," *Soft Matter*, vol. 11, no. 20, pp. 4041–4053, 2015. DOI: 10.1039/c5sm00577a.

[70] H. Ellens, D. P. Siegel, D. Alford, P. L. Yeagle, L. Boni, L. J. Lis, P. J. Quinn, and J. Bentz, "Membrane fusion and inverted phases," *Biochemistry*, vol. 28, no. 9, pp. 3692–3703, 1989. DOI: 10.1021/bi00435a011.

[71] D. P. Siegel, "The gaussian curvature elastic energy of intermediates in membrane fusion," *Biophysical Journal*, vol. 95, no. 11, pp. 5200–5215, 2008, ISSN: 0006-3495. DOI: 10.1529/biophysj.108.140152.

[72] P. Laggner and K. Lohner, "Liposome phase systems as membrane activity sensors for peptides," in *Lipid bilayers. Structure and interactions*, ser. Biological Physcis Series, J. Katsaras and T. Gutberlet, Eds., Berlin: Springer, 2000, pp. 233–264.

[73] C.-F. Le, C.-M. Fang, and S. D. Sekaran, "Intracellular targeting mechanisms by antimicrobial peptides," *Antimicrobial agents and chemotherapy*, vol. 61, no. 4, 2017, ISSN: 0066-4804. DOI: 10.1128/AAC.02340-16.

List of Publications

1. **Marx L.**, Semeraro E. F., Mandl J., Kremser J., Frewein M. P., Malanovic N., Lohner K., & Pabst G. (2021).

   Bridging the Antimicrobial Activity of Two Lactoferricin Derivatives in E. coli and Lipid-Only Membranes.

   Frontiers in Medical Technology 3:625975.
   DOI: 10.3389/fmedt.2021.625975

   Author contributions
   LM, ES, NM, GP, and KL conceptualized and designed the study.
   LM, ES, JM, JK, MF, and NM carried out the experiments.
   LM, ES, JM, and GP carried out the data analysis and interpretation.
   LM, ES, and GP wrote the manuscript.
   All authors provided critical feedback and helped to shape the research, analysis, and manuscript.

2. **Marx L.**, Frewein M., Semeraro E.F., Porcar L. & Pabst G.

   Antimicrobial peptide kinetics in asymmetric LUVs related to lipid flip-flop

   Manuscript in preparation

3. Semeraro E. F., **Marx L.**, Mandl J., Frewein M. P. K., Scott H. L., Prévost S., Bergler H., Lohner K., Pabst G. (2020)

Evolution of the Analytical Scattering Model of Live Escherichia Coli.

Journal of Applied Crystallography, 54(2).
DOI: 10.1101/2020.09.18.303305.

4. Malanovic N., **Marx L.**, Blondelle S. E., Pabst G., & Semeraro E. F. (2020)

Experimental concepts for linking the biological activities of antimicrobial peptides to their molecular modes of action

Biochimica et Biophysica Acta (BBA) - Biomembranes, Volume 1862, Issue 8
DOI: https://doi.org/10.1016/j.bbamem.2020.183275

5. Semeraro E. F., **Marx L.**, Frewein M. P., & Pabst G. (2021)

Increasing complexity in small-angle X-ray and neutron scattering experiments: from biological membrane mimics to live cells

Soft Matter, 17(2), 222-232. DOI: 10.1039/c9sm02352f

6. Kabelka I., **Marx L.**, Pajtinka P., Semeraro E.F., Leber R., Lohner K., Pabst G. Vácha R. (2021)

Magainin 2 and PGLa in a Bacterial Cytoplasmic Membrane Mimic: Part III – Membrane Partitioning and Curvature

Manuscript to be submitted to Biophysical Journal

7. Kabelka I., Georgiev V., **Marx L.**, Pajtinka P., Semeraro E.F., Leber R., Lohner K., Dimova R., Pabst G. & Vácha R. (2021)

Magainin 2 and PGLa in a Bacterial Cytoplasmic Membrane Mimic: Part IV – Synergism is Coupled to Both Membrane Fusion and Disruption

Manuscript to be submitted to Biophysical Journal

frontiers in Medical Technology

ORIGINAL RESEARCH
published: 24 February 2021
doi: 10.3389/fmedt.2021.625975

Bridging the Antimicrobial Activity of Two Lactoferricin Derivatives in *E. coli* and Lipid-Only Membranes

Lisa Marx[1,2,3†], *Enrico F. Semeraro*[1,2,3†], *Johannes Mandl*[1,2,3†], *Johannes Kremser*[1,2,3], *Moritz P. Frewein*[1,2,3,4], *Nermina Malanovic*[1,2,3], *Karl Lohner*[1,2,3] *and Georg Pabst*[1,2,3*]

[1] *Department of Biophysics, Institute of Molecular Biosciences, University of Graz, Graz, Austria,* [2] *BioTechMed Graz, Graz, Austria,* [3] *Field of Excellence BioHealth—University of Graz, Graz, Austria,* [4] *Soft Matter Science and Support Group, Institut Laue-Langevin, Grenoble, France*

OPEN ACCESS

Edited by:
Sattar Taheri-Araghi, California State University, Northridge, United States

Reviewed by:
Iolanda Cuccovia, University of São Paulo, Brazil
Miguel A. R. B. Castanho, University of Lisbon, Portugal

***Correspondence:**
Georg Pabst
georg.pabst@uni-graz.at

[†]*These authors have contributed equally to this work*

Specialty section:
This article was submitted to Pharmaceutical Innovation, a section of the journal Frontiers in Medical Technology

Received: *04 November 2020*
Accepted: *19 January 2021*
Published: *24 February 2021*

Citation:
Marx L, Semeraro EF, Mandl J, Kremser J, Frewein MP, Malanovic N, Lohner K and Pabst G (2021) Bridging the Antimicrobial Activity of Two Lactoferricin Derivatives in E. coli and Lipid-Only Membranes. Front. Med. Technol. 3:625975. doi: 10.3389/fmedt.2021.625975

We coupled the antimicrobial activity of two well-studied lactoferricin derivatives, LF11-215 and LF11-324, in *Escherichia coli* and different lipid-only mimics of its cytoplasmic membrane using a common thermodynamic framework for peptide partitioning. In particular, we combined an improved analysis of microdilution assays with ζ-potential measurements, which allowed us to discriminate between the maximum number of surface-adsorbed peptides and peptides fully partitioned into the bacteria. At the same time, we measured the partitioning of the peptides into vesicles composed of phosphatidylethanolamine (PE), phosphatidylglycerol (PG), and cardiolipin (CL) mixtures using tryptophan fluorescence and determined their membrane activity using a dye leakage assay and small-angle X-ray scattering. We found that the vast majority of LF11-215 and LF11-324 readily enter inner bacterial compartments, whereas only 1—5% remain surface bound. We observed comparable membrane binding of both peptides in membrane mimics containing PE and different molar ratios of PG and CL. The peptides' activity caused a concentration-dependent dye leakage in all studied membrane mimics; however, it also led to the formation of large aggregates, part of which contained collapsed multibilayers with sandwiched peptides in the interstitial space between membranes. This effect was least pronounced in pure PG vesicles, requiring also the highest peptide concentration to induce membrane permeabilization. In PE-containing systems, we additionally observed an effective shielding of the fluorescent dyes from leakage even at highest peptide concentrations, suggesting a coupling of the peptide activity to vesicle fusion, being mediated by the intrinsic lipid curvatures of PE and CL. Our results thus show that LF11-215 and LF11-324 effectively target inner bacterial components, while the stored elastic stress makes membranes more vulnerable to peptide translocation.

Keywords: antimicrobial peptides, lactoferricin, minimum inhibitory concentration, partitioning, zeta-potential, dye-leakage assay, tryptophan fluorescence, small-angle X-ray scattering

1. INTRODUCTION

The history of research on antimicrobial peptides (AMPs) as promising agents to combat infectious diseases is long and rich in diverse aspects. Studied for about four decades (1), AMPs continue to spur significant research efforts by their ability to discriminate the lipid architecture of cell envelopes, and evade classical resistance mechanisms based on direct molecular (key-lock) interactions, which increasingly limits medical treatments by conventional antibiotics [for review, see e.g., (2, 3)].

AMPs are typically composed of cationic and hydrophobic amino acids making them highly membrane active. Responses of their target membranes depend on the AMPs' physicochemical properties (primary structure, hydrophobic moment, length, etc.) and concentration (partitioning), as revealed from studies on membrane model systems, and include membrane thinning (4), or thickening (5), lipid flip/flop (6) or changes in membrane elasticity (7) at relatively low concentrations. Pore-formation (barrel-stave, toroidal/worm-hole) (8) or changes in membrane topology (9, 10) have been reported at elevated AMP concentrations, eventually leading to complete micellization (11) of the membrane, also known as the carpet model (12). It is increasingly becoming clear, however, that the observed effects strongly depend on the lipid composition of the used membrane mimics and the resulting collective membrane properties (13–15). At the same time, several studies also indicate that AMPs may have intracellular targets (16, 17), which might be coupled to highly specific interactions with cytosolic components and lead to the inhibition of different metabolic or biosynthesis pathways. Such multiple inhibitory processes, however, do not exclude any AMP activity within the bacterial membranes (17).

In order to shed some light on this issue, it would be highly instructive to compare AMP partitioning studies in microbes and artificial lipid-only membranes. However, and to the best of our knowledge, such data are currently not available. Instead, the peptide-to-lipid molar ratio commonly used in lipid-only systems, for example, dye leakage experiments, is about five orders of magnitude lower than in microbial killing assays (2, 18, 19). Estimates based on the surface/volume ratio of bacteria consequently indicate a large number of non-membrane bound peptides per cell (18). This may, however, be strongly biased by not considering cell-surface deformation, vesiculation processes, or extracellular peptide aggregation (16, 20). Reflecting on such controversies, Wimley and Hristova (2) formulated almost 10 years ago several unanswered questions relating to AMP activity studies in model membrane systems and microbes. Answering these questions is often challenged by the different experimental windows and sensitivities of the applied techniques (21). Here, focusing on the lactoferricin derivatives LF11-215 (H-FWRIRIRR-NH_2) and LF11-324 (H-PFFWRIRIRR-NH_2), we set out to address three of these questions: *(i) How are vesicle leakage and microbial killing correlated? (ii) Is membrane binding the sole basis for selectivity?* and *(iii) Is membrane translocation required for activity?*

Derived from human lactoferrin, the peptide lactoferricin and its 11 amino acids fragment LF11 are well-known for their affinity to lipid A and antimicrobial activity (22), with LF11-215 and LF11-324 being among the most promising LF11 derivatives with significantly improved activities against a broad range of Gram-positive and Gram-negative strains (20, 23–25). LF11-215 leads, for example, to a damage of the cell wall of Gram-negative bacteria, including an increased distance between cytoplasmic and outer membranes, membrane ruffling and formation of external blebs (20, 25). The somewhat increased hydrophobicity of LF11-324 was linked to a stronger efficacy in planktonic cultures, but at the same time led to a lower cell specificity (25). Interestingly, LF11-215 was instead reported to be more effective against bacterial biofilms (26), which is probably related to its lower hydrophobicity, facilitating the peptide diffusion within the matrix of microorganisms. Model membrane studies, using selected bacterial lipid species, suggest that both peptides interact preferentially with the negatively charged cardiolipin (CL), inducing a segregation into peptide-enriched and peptide-poor lipid domains (25). Further, LF11-215 and LF11-324 were shown to efficiently kill *Escherichia coli*, but exhibited at the same time only moderate membrane permeabilization in lipid vesicles consisting of *E. coli* total lipid extracts even at high peptide-to-lipid ratios, while N-acylated LF11 derivatives showed high activity both against bacteria and lipid-only membranes (20). Further, also effects of LF11-215 and LF11-324 on membranes, such as thinning or stored curvature stress, were rather modest (20). This suggests that the activity of both peptides in cytoplasmic membranes might not be the primary cause for their high efficiency in killing Gram-negative bacteria.

In order to gain some deeper insight in view of the three questions quoted above, we therefore correlated the partitioning of peptides in both bacterial cells and lipid-only systems with their effects on bacterial growth inhibition, membrane permeabilization, and structure, focusing on *E. coli* as representative strain of Gram-negative bacteria to demonstrate the feasibility of our approach. In particular, we exploited a thermodynamic framework that allowed us to relate the total number of AMPs located within bacteria at the minimum inhibitory concentration (MIC) to the membrane-bound fraction, combining a standard microbiological assay with ζ-potential measurements. The same theoretical framework was also applied to different lipid-only mimics of bacterial cytoplasmic membranes to determine the partitioning of the peptides and their membrane associated effects as a function of lipid composition, combining Trp fluorescence and dye leakage assays with small-angle X-ray scattering (SAXS). In agreement with previous studies, we find that LF11-324 is more active against *E. coli* than LF11-215 (20, 25). Performing our studies as a function of cell density, it has been further demonstrated that this difference in activity is enhanced at elevated cell concentrations, but also that the number of cell-associated AMPs at the MIC is about 4 times lower for LF11-324, while the number of surface-bound AMPs is about equal within the error of our experiments. At the same time, however, our results provide evidence that the vast majority of both peptides (up to 95—99%) are located in intracellular compartments. A slightly ($\sim$ 1.3 times) higher membrane partitioning of LF11-215 was observed in lipid mixtures of palmityol-oleoyl-phosphatidylethanolamine

(POPE), palmitoyl-oleoyl-phosphatidylglycerol (POPG), and tetra-oleoyl-cardiolipid (TOCL), which most closely mimic *E. coli* cytoplasmic membrane, while differences in peptide partitioning into POPE/POPG membrane mimics were negligible. The overall partition process of AMPs into these systems plateaued after 10–20 min. Pure POPG bilayers instead showed instantaneous uptake of the peptides, but disparate partitioning for LF11-215 and LF11-324. Dye leakage experiments in turn showed intriguing effects. While pure POPG membranes followed typical permeabilization behavior [see, e.g., (27)] and showed the highest peptide partitioning coefficient, POPE/POPG and POPE/POPG/TOCL vesicles exhibited a maximum leakage at low peptide concentration, followed by a decrease of permeabilization upon further addition of peptide. Using dynamic light scattering (DLS) and SAXS, we were able to attribute this effect to the formation of large aggregate structures containing collapsed lipid membranes, sandwiching the peptides, and capable of encapsulating the dyes. No aggregates with collapsed lipid bilayers were formed for POPG. While the initial formation of the collapsed bilayers was most rapid for TOCL-containing membranes (within 30 s), the overall process including a relaxation was slower and occurred over the course of $\sim$ 2 h.

2. MATERIALS AND METHODS

2.1. Samples

2.1.1. Lipids, Peptides, and Chemicals

POPE, POPG, and TOCL were purchased from Avanti Polar Lipids (Alabaster, AL) as powder (purity >99%), and freeze-dried LF11-215 and LF11-324 (purity >95%) were obtained from PolyPeptide Laboratories (San Diego, CA). ANTS (8-aminonaphthalene-1,3,6-trisulfonic acid, disodium salt) and DPX (*p*-xylene-bis-pyridinium bromide) were purchased from Molecular Probes (Eugene, OR) and dimethyl sulfoxide (DMSO) from Sigma-Aldrich (Vienna, Austria). HEPES (purity >99.5%) and LB-agar and LB-medium (Luria/Miller) powders were purchased from Carl Roth (Karlsruhe, Germany). All other chemicals were obtained from Sigma-Aldrich (Vienna, Austria) in *pro analysis* quality.

2.1.2. Bacterial Suspensions

Colonies of *E. coli* K12 5K (courtesy of Günther Koraimann, University of Graz) were grown in LB-agar plates at 37°C. Overnight cultures (ONCs) were prepared by inoculating a single colony in 3 ml LB-medium in sterile polypropylene conical tubes (15 ml), enabling bacterial growth under aerobic conditions for 12–16 h in a shaking incubator at 37°C. Main cultures were prepared by suspending an aliquot of the ONCs in 10 ml LB-medium in sterile polypropylene conical tubes (50 ml) and harvested in the middle of the exponential growth phase. Bacteria were then immediately washed twice and re-suspended in nutrient-free and isotonic phosphate-buffered saline (PBS) solution (phosphate buffer 20 mM, NaCl 130 mM) at pH 7.4. Bacterial concentration was measured via turbidity measurements. The optical density at $\lambda = 600$ nm (OD_{600}) was acquired with the spectrophotometer Thermo Spectronic Genesys 20 (Thermo Fisher Scientific, Waltham, MA), where $OD_{600} = 1$ corresponds approximately to 8×10^8 CFU/ml (where CFU is colony forming units).

2.1.3. Lipid Vesicles

Lipid stock solutions for sample preparation were prepared in organic solvent chloroform/methanol (9:1, vol/vol) and phosphate assayed for quantification of lipid content (28). Lipid thin films for SAXS measurements were prepared by mixing appropriate amounts of lipid stock solutions to obtain samples composed of POPE/POPG (3:1, mol/mol) and POPE/POPG/TOCL (82:6:12, mol/mol) followed by solvent evaporation under a nitrogen stream at 35°C and overnight storage in a vacuum chamber. Dry lipid films were hydrated in HEPES-buffered saline (HBS) solution (10 mM HEPES, 140 mM NaCl, pH 7.4).

All hydrated samples were equilibrated for 1 h at 40°C followed by 5 freeze-and-thaw cycles using liquid N_2 and intermittent vortex-mixing. Large unilamellar vesicles (LUVs) were obtained by 31 extrusions with a handheld mini extruder (Avanti Polar Lipids, Alabaster, AL) using a 100 nm pore diameter polycarbonate filter. Vesicle size and polydispersity were determined via DLS using a Zetasizer NANO ZSP (Malvern Panalytical, Malvern, UK). ANTS/DPX-containing vesicles were separated from free ANTS/DPX by exclusion chromatography using a column filled with SephadexTM G-75 (Amersham Biosciences, Little Chalfont, UK) fine gel swollen in iso-osmotic HBS. Phospholipid concentrations for all samples were determined by phosphate analysis.

2.1.4. Peptides

Peptide stock solutions of LF11-215 and LF11-324 were prepared in PBS solution for bacteria and HBS solution for lipid vesicles. Due to the weak solubility of LF11-324 in buffer, AMP stock solutions were prepared by adding acetic acid and DMSO, up to 0.3% and 3% vol/vol, respectively. Prior to each measurement, the concentrations of such compounds were systematically lowered down to 0.01% acetic acid and 0.1% vol/vol DMSO (final pH 7.2), in order to minimize, or even remove, any effect on the membrane structure (29). AMP concentrations of the stock solutions were determined by comparing against the absorption band of the aromatic amino acids with the spectrophotometer NanoDrop ND-1000 (Thermo Fisher Scientific, Waltham, MA). Peptide stock solutions were stored in silanized glass tubes until use.

2.2. Methods

2.2.1. Microdilution Assay

The antimicrobial activity of the AMPs on *E. coli* was tested using a modified susceptibility microdilution assay (30) in the bacterial concentration range of 5×10^5 to 10^9 CFU/ml. Bacterial suspensions were incubated at a given AMP concentration for 2 h at 37°C (control samples were incubated in buffer only). Then, cell growth was monitored upon addition of double concentrated LB-medium for about 20 h using a Bioscreen C MBR (Oy Growth Curves Ab, Helsinki, Finland).

Data were analyzed assuming that the AMP-induced delayed bacterial growth is entirely due to a lower number density of survived cells, which is supported by the observation that the growth rate in the exponential phase does not depend on peptide concentration (**Supplementary Figure 1A**), i.e., the growth of the viable fraction of cells is similar to bacterial growth in absence of AMPs. This allowed us to quantify the number density of surviving bacteria from the onset of the exponential growth via the relation $\Delta t_{\mathrm{exp}} = a + b\log(n_{\mathrm{cell}})$, where a and b were obtained from a calibration curve in absence of AMPs (**Supplementary Figure 1B**). Then, the inhibited bacterial fraction $\mathrm{IF} = 1 - n_{\mathrm{cell}}([P])/n^0_{\mathrm{cell}}$ was calculated for different values of peptide concentration, $[P]$, and of bacterial number density of the control sample, n^0_{cell}. Following the so-called "equi-activity" analysis (27, 31), we further interpolated IF using a Gompertz function, which enabled us to derive inhibitory peptide concentrations IC_x, where x is the corresponding inhibited bacterial fraction (**Supplementary Figure 1C**). By convention, the standard MIC is defined at inhibition levels of 99.9%, i.e., $\mathrm{IC}_{99.9} \equiv$ MIC. Additional control experiments were performed in order to test whether DMSO and acetic acid, used in buffer solutions of both peptides (see above), affect bacterial growth. In particular, the microdilution assays were repeated with LF11-215 dissolved in pure PBS, yielding equivalently delayed onsets of bacterial growth. This suggests that DMSO and acetic acid at low concentrations used in this study do not significantly affect our derived MIC and IC_x-values.

2.2.2. Size and ζ-Potential Measurements

DLS and ζ-potential measurements were carried out with a Zetasizer Nano ZSP (Malvern Panalytical, Malvern, UK). *E. coli* suspensions were incubated with a given AMP concentration at 37°C for 1 h prior to each measurement. The used AMP concentrations were centered at the MIC values, and ranged from about 0.2× to 2.5×MIC. Control samples (no AMPs) were suspended and incubated in buffer alone. A concentration of 10^7 CFU/ml was found to provide the optimal compromise between high signal-to-noise ratio and low multiple-scattering bias. Because of the high conductivity of PBS, the electrode voltage was set to 4 V for ζ-potential measurements to keep currents below 1 mA. Further, measurements were paused for 180 s between individual runs. This prevented Joule heating leading to sample denaturation and electrode blackening. Experiments were repeated three times on different preparations, each consisting of at least six measurements. Reported ζ-potential values are given by the median of the corresponding measurements (i.e., from at least 18 values) and errors were derived using the median absolute deviations.

2.2.3. Leakage

Dye leakage experiments were performed combining previously reported protocols (20, 27). In brief, the dependencies of ANTS/DPX leakage on lipid and peptide concentration were determined by first incubating lipid vesicles ($[L] = 1$, 4, 10, and 20 mM) with peptides ($[P] = (0.025 - 2)$ mM] at 37°C for 1 h using a gently rocking shaker (Eppendorf Thermomixer C, Hamburg, Germany). Similar time protocols were applied previously (27) and are justified here based on separate time-resolved leakage experiments (**Supplementary Figure 3**) and Trp-fluorescence measurements (**Figure 3**), showing that a quasi steady state has been reached after 1 h. Before measurements, lipid/peptide solutions were diluted with HBS to a lipid concentration of 50 μM, and every measurement was repeated at least twice. Vesicle size was checked after each incubation period using DLS. Samples were excited at $\lambda = 360$ nm, and the intensity of the fluorescence emission peak at $\lambda = 530$ nm, I_p, was recorded with a slit width of 10 nm for both excitation and emission monochromators. Measurements were performed in quartz cuvettes in 2 ml of the iso-osmotic buffer on a Cary Eclipse Fluorescence Spectrophotometer (Varian/Agilent Technologies, Palo Alto, CA). The percentage of leakage, $E_{\%}$, was calculated according to the relation

$$E_{\%} = \frac{I_p - I_{min}}{I_{max} - I_{min}}, \tag{1}$$

where I_{min} is the initial fluorescence without peptide, and I_{max} is the fluorescence corresponding to 100% leakage determined through the addition of a 1 vol% solution of Triton X-100. The initial, monotonic increase of $E_{\%}$ values with increasing [P] was interpolated with a sigmoidal function. This enabled us to obtain peptide and lipid concentrations leading to a specific $E_{\%}$ value, which can in turn be used to calculate the partitioning parameters (see section 2.3.1).

2.2.4. Tryptophan Fluorescence

Fluorescence emission from Trp, present in both peptides, was measured with the Cary Eclipse Fluorescence Spectrophotometer, setting the excitation wavelength to $\lambda = 280$ nm, which corresponds to the maximum intensity of the Trp absorption/excitation band. Intensities of exciting and emitting light were adjusted by setting the slit widths of both incident and outgoing beam to 5 or 10 nm, depending on the emission intensity, in order to optimize the signal-to-noise ratio. Emission spectra were background-subtracted to remove contributions originating from the instrument's baseline and scattered light from vesicles. All samples were measured in HBS at 37°C using a quartz cuvette, with a magnetic stirrer to prevent sample sedimentation in the case of aggregation. LUVs ($[L] = 100$ μM) were mixed with peptides ($[P] = 2$ and 4 μM), recording fluorescence spectra at various post-mixing time intervals ranging from 0.5 to 60 min. Peptide solutions were measured at concentrations of 2, 3, and 4 μM in order to calibrate their intensity dependence in buffer.

The fluorescence emission band was fitted with the log-normal-like function (32, 33)

$$I(I_0, \lambda, \Gamma) = \begin{cases} I_0 \exp\left[-\frac{\ln 2}{\ln^2 \alpha} \ln^2\left(1 + \frac{(\lambda - \lambda_{\max})}{y\Gamma}\right)\right], & \lambda > \left(\lambda_{\max} - y\Gamma\right) \\ 0, & \lambda \leq \left(\lambda_{\max} - y\Gamma\right) \end{cases} \tag{2}$$

where $\lambda_{\max}$ and I_0 are, respectively, wavelength and intensity of the emission peak; Γ is the full-width-at-half-maximum

(FWHM) of the band; α is a skewness parameter (fixed at an optimum values 1.36 after testing); and $y = \alpha/(\alpha^2 - 1)$. Spectra from mixtures of LUVs and peptides were analyzed with a linear combination of two independent bands I^W and I^B, referring to AMPs in bulk (W) and partitioned into the lipid bilayer (B). λ^W and Γ^W were fixed to the reference values obtained by analyzing spectra from pure AMPs. Instead, I_0^W, I_0^B, λ^B, and Γ^B were adjustable parameters. The so obtained set of I_0^W values was converted to the concentration of dissociated peptides $[P]_W$ and further analyzed for peptide partitioning as detailed in section 2.3.1.

2.2.5. Small-Angle X-ray Scattering (SAXS)

SAXS experiments were performed at the highflux Austrian beamline at Elettra Synchrotron in Trieste, Italy (34) using a photon energy of 8 keV. SAXS patterns were recorded using a Pilatus 1 M detector (Dectris, Baden-Daettwil, Switzerland) in the q-range from 0.1 to 5 nm^{-1}, and further processed with FIT2D (35). A custom-build cell, termed "nanodrop," was used, allowing for precise measurements of very small volumes (10 μl) (36). Measurements were performed at a lipid concentration of 20 mg/ml (24.5–27.9 mM depending on the used membrane mimic) at 37°C. Lipids and peptides were mixed using an automatic sample changer and automatically injected into the nanodrop cell immediately after mixing. Peptide kinetics were measured starting 30 s after lipid-peptide mixing with an acquisition time of 1 s and a rest time of 10 s.

For the end-states, lipids mixed with peptides were incubated at 37°C for at least 4 h. These samples were measured using 12 frames of 10 s exposure each and a rest time of 12 s. Data were analyzed based on Bragg peak positions only. Using Bragg's law, the reported d-spacing values are simply given by $d = 2\pi/q_h$, where q_h is the peak position.

2.3. Data Analysis

2.3.1. Partitioning Equations for Lipid and Bacterial Systems

Following a previously reported thermodynamic formalism for the partitioning of peptides into lipid bilayers (37), based on the free energy of transfer of molecules from water into octanol (38), we define the mole fraction partitioning coefficient, K, as

$$K = \frac{[P]_B/([P]_B + [L])}{[P]_W/([P]_W + [W])} \simeq \frac{[P]_B[W]}{[P]_W[L]}, \tag{3}$$

where $[P]_B$ is the molar concentration of peptides partitioned into the lipid phase; $[P]_W$ is the peptide concentration in the water phase; and $[L]$ and $[W]$ are, respectively, the molar concentrations of lipids and bulk water (55.5 M at 25°C and 55.3 M at 37°C). The approximation for K (Equation 3) is obtained applying $[W] \gg [P_W]$ and $[L] \gg [P_B]$ (similarly, the concentration of ions in water, i.e., buffer solutions, is negligible compared to $[W]$). By definition, the total concentration of peptides is $[P] = [P]_W + [P]_B$, thus leading to

$$[P] = \underbrace{\frac{R_B[W]}{K}}_{[P]_W} + \underbrace{R_B[L]}_{[P]_B} = R_B\left(\frac{[W]}{K} + [L]\right), \tag{4}$$

where $R_B = [P]_B/[L]$.

An analogous approach can be applied to cells (39), replacing the lipid membrane with a so-called "cell phase," i.e., treating bacteria as a homogeneous medium consisting of all cell compartments accessible to the peptides. Then, similarly to Equation (3), the mole fraction partitioning coefficient, K_C, of peptides in bacterial cells is defined as

$$K_C \simeq \frac{[P]_B[W]}{[P]_W[X]}, \tag{5}$$

where $[X]$ is the total molar concentrations of all molecular species within the cell phase, including cytoplasmic water. This leads to

$$[P] = [P]_B\left(1 + \frac{[W]}{K_C[X]}\right). \tag{6}$$

Furthermore, $[P]_B$ and $[X]$ can be expressed as a function of the cell number density n_{cell}:

$$[P]_B = \frac{N_B\, n_{\text{cell}}}{N_A} \quad \text{and} \quad [X] = \frac{N_X\, n_{\text{cell}}}{N_A}, \tag{7}$$

where N_B is the absolute number of partitioned peptides per single cell, N_A is Avogadro's constant, and N_X, in analogy to $[X]$, represents the *number of molecules that constitute the accessible compartments of a single cell*. The combination of Equations (6) and (7) gives:

$$[P](n_{\text{cell}}) = \underbrace{\frac{N_B[W]}{N_X K_C}}_{[P]_W} + \underbrace{\frac{N_B}{N_A} n_{\text{cell}}}_{[P]_B} = \frac{N_B}{N_A}\left(\frac{N_A[W]}{N_X K_C} + n_{\text{cell}}\right) \tag{8}$$

Since N_X is inaccessible, we thus define the *effective partitioning coefficient* $K^{eff} = N_X K_C$ as measurable quantity.

2.3.2. Estimating the Maximum Number of AMPs Adsorbed to the Bacterial Surface

Remembering that ζ-potential values are sensitive only to the charges exposed to the outside of any particle, including bacteria, we can obtain upper boundaries for the number of surface adsorbed peptides. Given the high abundance of lipopolysaccharides (LPS) in the outer leaflet (about 70–90 vol%) of Gram-negative bacteria, as compared to other charged lipid species such as PG and CL (<2 vol%) and membrane proteins (7–20 vol%) (40), it is justified to assume that LPS dominates the surface potential of *E. coli*. Then, following considerations put forth for peptides partitioning in liposomes (31, 41), the ratio of ζ-potential values in the presence and absence of AMPs is

$$\frac{\zeta}{\zeta_0} \approx \frac{\sigma}{\sigma_0} \simeq \left(\frac{S_0}{S}\right)\frac{\sum_i N_i z_i + N_P z_P}{N_{\text{LPS}}^0 z_{\text{LPS}}}, \tag{9}$$

where (σ, σ_0) and (S, S_0) are the corresponding surface charge densities and cell surface areas, respectively. Further, N_{LPS}^0 is the initial number of LPS molecules in the outer leaflet, with a nominal charge $z_{\text{LPS}} \simeq -6$ (42); N_P is the number of surface adsorbed AMPs of nominal charge $z_P \simeq +5$ (20); and $\sum_i N_i z_i =$

$N_{\mathrm{LPS}}z_{\mathrm{LPS}} + N_{\mathrm{PG}}z_{\mathrm{PG}} + N_{\mathrm{CL}}z_{\mathrm{CL}}$ considers anionic lipids that translocate into the outer leaflet due to AMP activity (3, 6, 18). This term also accounts for a possible loss of LPS molecules in the outer leaflet due to vesiculation processes (25). Note that Equation (9) is only valid for $|\zeta| \leq 25$ mV, in which range $\zeta \propto \sigma$ (43). Equation (9) also assumes that the position of the slipping plane is not significantly altered upon the addition of peptides. Rearranging Equation (9) leads to

$$\frac{N_P}{N^0_{\mathrm{LPS}}} \simeq \left(\frac{z_{\mathrm{LPS}}}{z_P}\right)\left(\frac{\zeta}{\zeta_0}\frac{S}{S_0} - \frac{\sum_i N_i z_i}{N^0_{\mathrm{LPS}} z_{\mathrm{LPS}}}\right), \tag{10}$$

which is physically meaningful only if

$$\frac{\zeta}{\zeta_0}\frac{S}{S_0} \leq \frac{\sum_i N_i z_i}{N^0_{\mathrm{LPS}} z_{\mathrm{LPS}}} \leq 1. \tag{11}$$

This leads to two extreme cases, the first one being the maximum "charge scrambling"

$$\frac{\zeta}{\zeta_0}\frac{S}{S_0} = \frac{\sum_i N_i z_i}{N^0_{\mathrm{LPS}} z_{\mathrm{LPS}}}, \tag{12}$$

leading to $N_P/N^0_{\mathrm{LPS}} = 0$, i.e., complete dissociation of peptides from the bacteria, which is physically not realistic. The second limiting scenario is given by $\sum_i N_i z_i = N^0_{\mathrm{LPS}} z_{\mathrm{LPS}}$, i.e., bacteria retain their original surface exposure of LPS, which yields, upon insertion into Equation (10),

$$\frac{N^{\max}_P}{N^0_{\mathrm{LPS}}} \approx \left(\frac{z_{\mathrm{LPS}}}{z_P}\right)\left(\frac{\zeta}{\zeta_0} - 1\right), \tag{13}$$

where $N^{\max}_P$ is the upper boundary of surface adsorbed peptides. Moreover, this assumes $S/S_0 \sim 1$, which may be contradictory to previously observed bacterial cell shrinking in the presence of AMPs [see, e.g., (44)]. However, it can be justified in view of our goal to obtain an estimate the upper boundary values for N^{max}_P. N^0_{LPS} can be estimated using $N^0_{\mathrm{LPS}} \approx 0.9S_0/A_{\mathrm{LPS}}$, where $A_{\mathrm{LPS}} \simeq 1.6$ nm^2 (45, 46) is the lateral area per LPS molecule and S_0 is supplied by size measurements. The prefactor originates from considering a maximum surface coverage of 90% by LPS molecules (40). For example, using DLS, we measured a hydrodynamic diameter of *E. coli* K12 $2R_H = 980\pm30$ nm, from which we calculate $S_0 \simeq 4.5 \times 10^6$ nm^2, approximating the bacteria's shape with a cylinder of radius r and length l using $R^2_H \simeq r^2/2 + l^2/12$ and $r \sim 400$ nm (47). This yields $N^0_{\mathrm{LPS}} \approx 3 \times 10^6$.

3. RESULTS

3.1. Antimicrobial Activity and Partitioning in Bacterial Systems

3.1.1. Efficacy and Partitioning

We started our analysis of peptide activity in *E. coli* with measuring a range of inhibitory concentrations, including the MIC, by means of a slightly modified susceptibility assay, and for different bacterial concentrations. An example using LF11-324 is reported in **Figure 1A**, showing different IC_x values as a function of n_{cell} (note that in these bacterial suspensions 1 CFU corresponds to one single cell).

The partitioning formalism, described in section 2.3.1, was used to fit the linear increase of IC_x with cell concentration (**Figure 1A**) (LF11-215 data not shown). Also the MIC values increased linearly with cell concentration (**Figure 1B**), but more rapidly for LF11-215; results at $n \simeq 5 \times 10^5$ CFU/ml are consistent with previous reports (20, 25). At low concentrations, $n_{\mathrm{cell}} \ll N_A[W]/K^{eff} \sim 2 \times 10^8$ ml^{-1}, $[P] \approx [P]_W$, explaining the apparent plateau in the semi-log plot at low bacterial densities (see inset in **Figure 1B**). In this regime, the number of peptides dispersed in buffer dominates the total AMP amount. At high concentrations, instead, i.e., $n_{\mathrm{cell}} \gg N_A[W]/K^{eff}$, most of AMPs partition into the cell volume; thus $[P] \approx [P]_B$.

Finally, results for N_B and K^{eff} from our thermodynamic analysis are shown in **Figures 2A,B**. About four times less LF11-324 is needed to bind to the cells compared to LF11-215 in order to induce full growth inhibition (**Figure 2A**). Interestingly, this is not related to the affinity of the AMPs to the cell (see **Figure 2B**), as LF11-215 exhibits ~2-fold higher K^{eff} values over the whole range of inhibited fractions. Further, K^{eff} slightly decreases as a function of inhibited fraction for both AMPs, suggesting that the likelihood of interactions with cells becomes lower the more AMPs are added to the system.

3.1.2. Outer Leaflet Distribution of AMPs

The distribution of charged AMPs on the outer leaflet of the outer cell membrane was interrogated by analyzing ζ-potential data. Unfortunately, the "equi-activity" approach (31) was not applicable, because ζ-potential differences from the control systems were weak in magnitude and constant over a wide range of $[P]$ around the MIC values (**Figure 2C**). Nevertheless, the maximum number of peptides partitioned in the outer bacterial surface, $N^{\max}_P$, can be estimated to be in the order of 10^6 AMPs for both LF11 molecules. $N^{\max}_P$ (corresponding to about one peptide over 2–3 LPS molecules) is rather constant in the concentration range of 0.3× to 2.5×[MIC], suggesting that the cellular surface is already saturated with peptides in the sub-MIC range. In addition, $N^{\max}_P$ can be compared with the total number of peptides per cell, N_B. The ratio $N^{\max}_P/N_B$ as a function of the inhibited fraction, and hence of the peptide concentration, is displayed in **Figure 2D**. We found $N^{\max}_P/N_B \leq 25\%$ at the lowest measured inhibited fraction, followed by a decrease of about 1 and 5% at the MIC of LF11-215 and LF11-324, respectively.

3.2. Effects in Cytoplasmic Membrane Mimics

In order to compare the growth inhibition of *E. coli* by LF11-215 and LF11-324 with their membrane activity, we prepared 100 nm sized LUVs of three different cytoplasmic membrane mimics, pure POPG, POPE/POPG (3:1 mol/mol), and POPE/POPG/TOCL/ (82:6:12 mol/mol/mol), all of which are frequently used in biophysical studies on the mode of action of AMPs [see e.g., (15, 48–50)]. Out of these

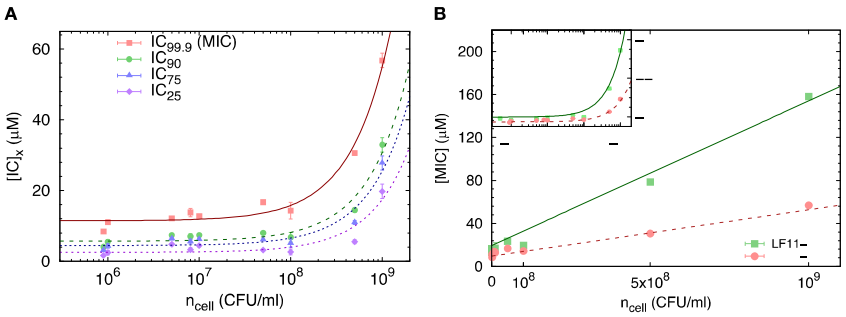

FIGURE 1 | (A) Selected IC_x-values of LF11-324 related to different inhibited fractions (see legend) as a function of n_{cell}. Lines represent best fits using Equation (8). **(B)** Dependence of minimum inhibitory concentration (MIC) on the cell number density for LF11-215 and LF11-324, including best fits using Equation (8) (straight lines). The inset displays the same data on logarithmic scale.

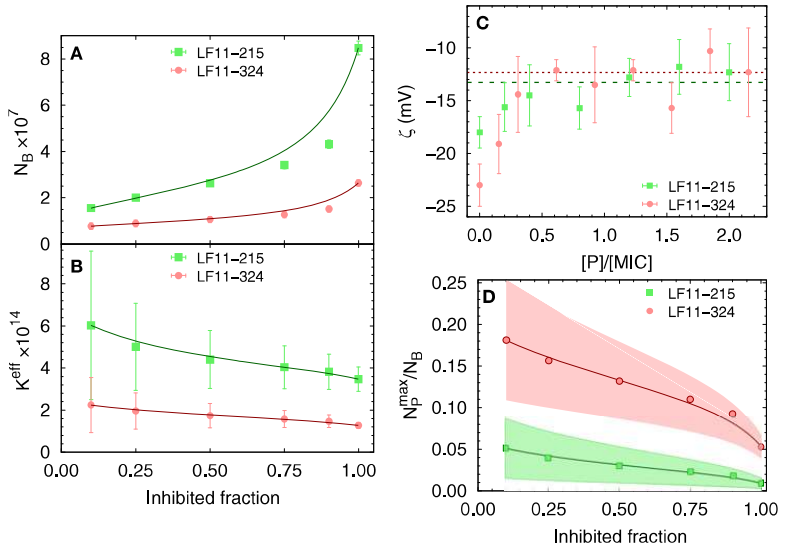

FIGURE 2 | Dependence of the total number of antimicrobial peptides (AMPs) partitioned into *E. coli* **(A)**, as well as the effective partitioning coefficient **(B)** on the inhibited bacterial fraction; lines are a guide to the eyes. **(C)** Variation of ζ-potential with peptide concentration [normalized by the respective minimum inhibitory concentrations (MICs)]. The lines mark the average, constant ζ-values from $[P] = 0.3 \times$ MIC to $2.5 \times$ MIC for LF11-215 (green dashed line) and LF11-324 (red dotted line). **(D)** Upper boundaries of the ratio of surface-adsorbed to cell-partitioned AMPs as a function of inhibited fraction. Color-shaded areas represent confidence intervals; lines are guides to the eyes.

systems, POPE/POPG/TOCL/ (82:6:12 mol/mol/mol) most closely resembles the natural lipid composition of *E. coli* inner membranes (51).

3.2.1. Tryptophan Fluorescence

We first measured the partitioning of the two peptides using Trp fluorescence. The emission spectra of the single Trp residue of LF11-215 and LF11-324 exhibited in buffer a band with $\lambda^W \simeq 354$ nm and $\Gamma^W \simeq 65$ nm [see e.g., **Figure 3A**]. This is in agreement with the emission maximum of Trp exposed to a polar environment (52). When peptides were added to the LUVs, the Trp emission bands exhibited a blue-shift regardless of lipid composition and peptide type (example in **Figure 3A**). The analysis of the spectra (see example in **Figure 3B** and details in section 2.2.4) enabled us to derive the kinetics of AMPs partitioning into the different bilayers. For all membranes, the fluorescence signal from the partitioned AMPs exhibited values of $\lambda^B \simeq (331 - 335)$ nm and $\Gamma^B \simeq (49 - 54)$ nm, indicating an average location of the Trp residues within the hydrophobic region of the lipid bilayer (52).

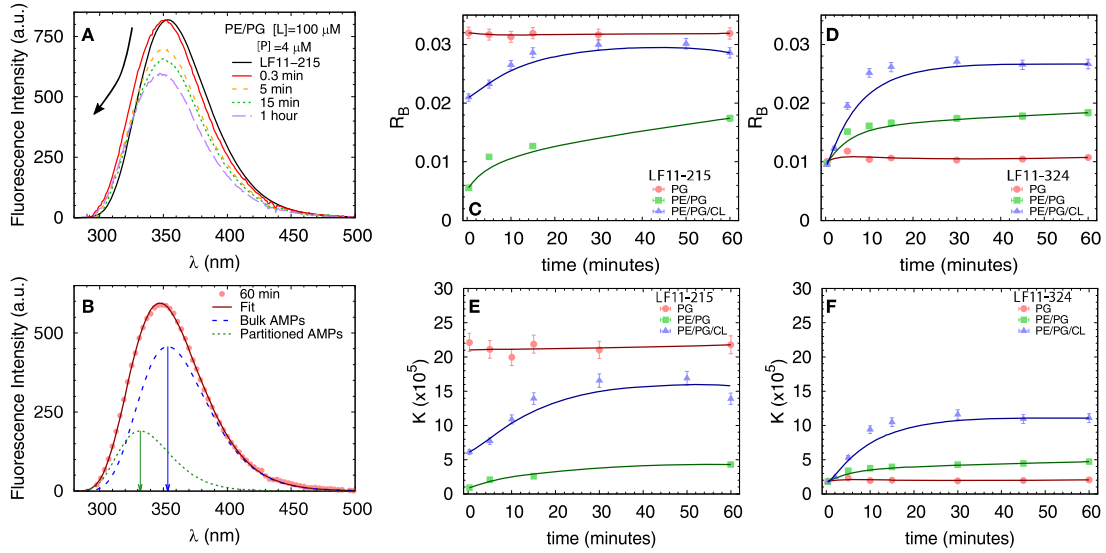

FIGURE 3 | Peptide partitioning from Trp fluorescence experiments. **(A)** Example of Trp emission-band kinetics. The arrow indicates the decrease in intensity and blue-shift as a function of time. **(B)** Example of spectral analysis (POPE/POPG [L] = 100 μM, LF11-215 [P] = 4 μM); red line: best fit; blue dashed line: emission from antimicrobial peptides (AMPs) in suspension; green dotted line: emission from AMPs partitioned into the membrane. The arrows mark the different λ_{max} values. **(C,D)** Adsorption kinetics for LF11-215 and LF11-324, respectively, for three different membrane mimics. **(E,F)** Kinetics of the partitioning coefficient K for LF11-215 and LF11-324, respectively, for three different membrane mimics.

CL-containing systems displayed broader bands, $\Gamma^B \approx 65$ nm, after 20—30 min of incubation, probably due to a heterogeneous distribution of Trp locations within the bilayers (33). Speculating that this might be related to supramolecular structural changes, we performed DLS after 60 min of incubation. Indeed, we observed large aggregate structures, for POPE/POPG/TOCL samples, but also for POPE/POPG in presence of 4 μM LF11-324 (see **Supplementary Figure 2A** and **Table 1**). We note, however, that the derived AMP partitioning data are not directly linked to such morphological changes. Overall, CL and LF11-324-containing samples showed the highest propensity to form aggregates, whereas POPG LUVs remained intact under present conditions.

Table 1 reports results of the AMP partitioning analysis (see section 2.1) after 60 min of incubation with the peptides, and the temporal evolution of these parameters for [P] = 4 μM is shown in **Figures 3C–F**. Both peptides quickly achieve stationary R_B and K values in POPG LUVs (within 30 s), but the amount of adsorbed LF11-215 is three times higher than for LF11-324. In PE-containing bilayers both peptides instead exhibited similar adsorption and partitioning kinetics, with an increase over the first 10-20 min before reaching stable values. Both peptides showed, however, a higher affinity to POPE/POPG/TOCL membranes than to POPE/POPG. In contrast, at lower peptide concentration (2 μM), this effect was not observed (**Table 1**). In this case, the parameters derived from the partitioning analysis including POPG did not depend on whether LF11-215 or LF11-324 was added.

3.2.2. Leakage

To test the permeability of the three membrane mimics, we investigated the dye efflux from LUVs after incubation with LF11-215 at various lipid-to-peptide ratios. This allowed us to pursue the effect of peptides at a physiological temperature, where all lipid systems are in the fluid phase, up to very high lipid concentrations typically used in small angle scattering experiments ([L] ~20 mM). **Figures 4A–C** display leakage percentages as a function of [P] for different concentrations of POPG, POPE/POPG, and POPE/POPG/TOCL systems. In all three systems, substantial leakage seemed to coincide with the formation of larger structures, as corroborated with DLS measurements (see example in **Supplementary Figure 2B**). Indeed, the transformation from unilamellar vesicles to larger aggregates (marked as a gray, shaded areas in **Figures 4A–C**) depends on the overall lipid and peptide concentrations, and coincides with a leakage of 15—20%, and [P] $\leq$ 1 mM for POPG and [P] $\leq$ 0.25 mM for PE-containing systems. Interestingly, while POPG LUVs showed a sharp, sigmoidal increase of leakage up to 100%, PE-containing systems exhibited a maximum at a certain peptide-to-lipid ratio, followed by a leakage decrease and, most likely, a stabilization at higher [P] values. POPE/POPG vesicles, in particular, resulted in a relatively low total efflux $\leq$ 40%. In analogy with the equi-activity analysis used for the susceptibility assay, leakage curves where exploited to calculate the partitioning parameters (27). The peptide concentrations needed to induce leakage $E_{\%}$ at a given [L] were all fitted with Equation (4), demonstrating that

TABLE 1 | Partitioning parameters calculated from the spectral analysis of the Trp emission band for LF11-215 and LF11-324.

LF11-215 (2 μM / 4 μM)	$R_B \times 10^{-3}$	$K \times 10^4$	$[P]_W$ (μM)
POPG	14.9 ± 0.3 / 31.9 ± 0.4	161 ± 6 / 217 ± 8	0.513 ± 0.015 / 0.81 ± 0.04
POPE/POPG	11.2 ± 0.3 / 17.5 ± 0.7	70 ± 4 / 43 ± 3	0.88 ± 0.03 / 2.25 ± 0.07
POPE/POPG/TOCL*	11.9 ± 0.2 / 28.6 ± 0.3	82 ± 4 / 139 ± 6	0.81 ± 0.02 / 1.14 ± 0.03
LF11-324 (2 μM / 4 μM)	$R_B \times 10^{-3}$	$K \times 10^4$	$[P]_W$ (μM)
POPG	10.5 ± 0.3 / 10.7 ± 0.9	61 ± 4 / 20 ± 20	0.95 ± 0.03 / 2.93 ± 0.09
POPE/POPG*	11.0 ± 0.3 / 18.4 ± 0.6	67 ± 4 / 47 ± 3	0.90 ± 0.02 / 2.16 ± 0.06
POPE/POPG/TOCL**	10.6 ± 0.3 / 26.7 ± 0.4	63 ± 4 / 111 ± 5	0.95 ± 0.03 / 1.33 ± 0.04

*Data refer to systems after 1 h of incubation with peptides (see **Figure 3**), and [L] = 100 μM. *Samples showing aggregation at [P] = 4 μM; **Samples showing aggregation at [P] = 2 and 4 μM.*

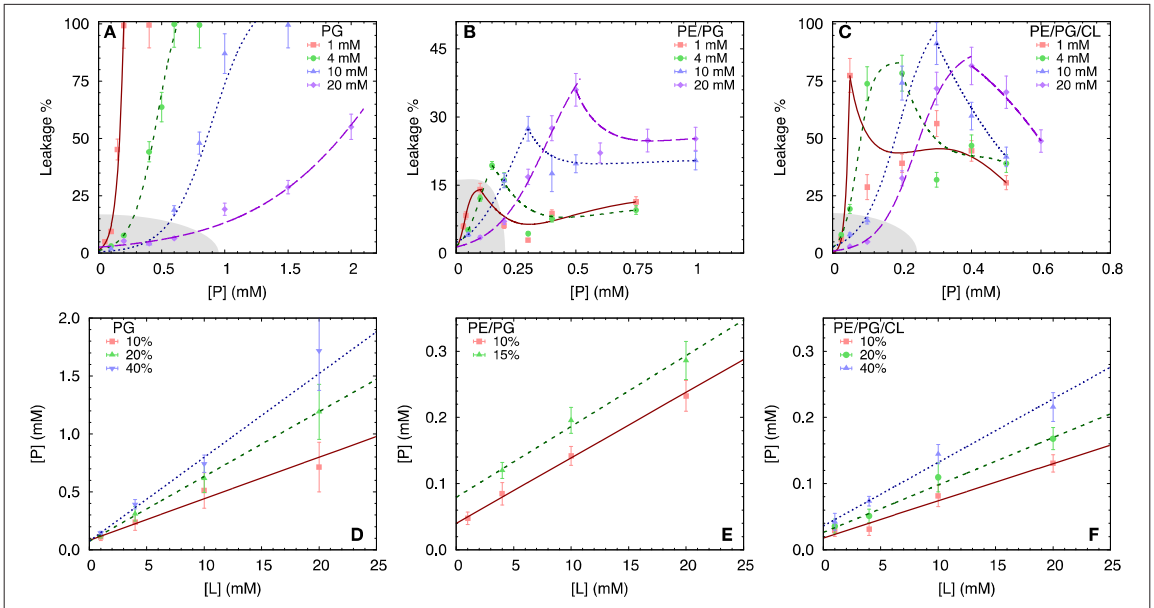

FIGURE 4 | LF11-215 induced permeabilization of LUVs composed of POPG **(A)**, POPE/POPG **(B)**, and POPE/POPG/TOCL **(C)** at different lipid concentrations (see legend). A sigmoidal function was used to interpolate the initial leakage increase, whereas lines describing the following decrease **(B,C)** are just guides to the eyes. Gray-shaded areas indicate regimes where the formation of large aggregates was not detected. **(D–F)** Analysis of peptide induced ANTS/DPX leakage (see legend) in terms of Equation (4) (straight lines) for the different membrane mimics. For result, see **Table 2**.

in these ranges of $[P]$ and $[L]$, the partitioning characteristic are alike, regardless of transitions from a unilamellar system to more complex lipid aggregates. Fitting results are shown in **Table 2**. POPG samples seem to require a high number of LF11-215 per lipid in order to achieve leakage, showing the highest R_B and K values, which increase along with higher leakage, and with a rather constant $[P]_W$. This means that at $[L] \simeq 20$ mM, $>$ 90% of peptides are partitioned into the lipid phase. Leakage from PE-containing systems instead needs less AMPs per lipid (see **Table 2**), with a maximum amount of partitioned AMPs of $<$ 80% for $[L] \simeq 20$ mM.

3.2.3. SAXS

We performed SAXS experiments to investigate structural changes in membrane mimics induced by the peptides. Vesicles composed of POPG, POPE/POPG, and POPE/POPG/TOCL without AMPs (reference systems) as well as end-states at a lipid-to-peptide ratio of 1:25 measured 4 h after lipid-peptide mixing are shown in **Figures 5A,B** for LF11-215 and LF11-324, respectively. All reference systems showed purely diffuse scattering patterns originating from positionally uncorrelated lipid bilayers, as expected for LUVs. In the case of POPG liposomes, after addition of either peptide, a shift of the first

TABLE 2 | Partitioning parameters for LF11-215, resulting from the leakage assay analysis of three differently composed LUVs (see also **Figure 4**).

Leakage	$R_B \times 10^{-3}$	$K \times 10^4$	$[P]_W$ (mM)
POPG 10%	36 ± 4	2.4 ± 0.7	0.08 ± 0.03
POPG 20%	55.9 ± 1.6	4.2 ± 0.4	0.073 ± 0.009
POPG 40%	72 ± 6	5.4 ± 1.4	0.08 ± 0.03
POPE/POPG 10%	9.8 ± 0.4	1.37 ± 0.16	0.040 ± 0.006
POPE/POPG 15%	10.7 ± 1.0	0.75 ± 0.15	0.08 ± 0.02
POPE/POPG/TOCL 10%	5.6 ± 0.7	1.7 ± 0.8	0.018 ± 0.010
POPE/POPG/TOCL 20%	7.2 ± 0.5	1.5 ± 0.3	0.026 ± 0.007
POPE/POPG/TOCL 40%	9.6 ± 0.9	1.5 ± 0.4	0.036 ± 0.012

Concentration ranges: $[L] = (1 - 20)$ *mM,* $[P] = (0.05 - 2)$ *mM.*

minimum at $q \sim 2.8$ nm^{-1} can be observed, which could originate from a thinning of the membrane. Most pronounced for PE-containing mimics, the measurements after peptide mixing showed a small, but clearly discernible positional correlation peak at $q \sim 1.1 - 1.3$ nm^{-1} in addition to a significant diffuse scattering pattern; a similar feature—but much less expressed—was also observed for POPG in the presence of LF11-215. The diffuse scattering of POPE/POPG and POPE/POPG/TOCL mixtures in the presence of both peptides showed an additional modulation at $q \sim 2$ nm^{-1}. This feature might originate from a preferential enrichment of AMPs in one leaflet or the formation of thin peptide-enriched domains. Clarification of the underlying structures would require dedicated experiments using neutron scattering combined with contrast variation and computational modeling [see e.g., (49)]. This is, however, beyond the scope of the present study. Instead, we focused on the evolution of the correlation peak in case of LF11-215 using time-resolved SAXS (**Figure 6**). For the PE-containing samples, especially in the case of POPE/POPG/TOCL, addition of peptides led to a rapid precipitation of the sample, which reduced the amount of sample being hit by the X-ray beam. This explains the increased noise of scattering data at longer times. For liposomes consisting of pure POPG, only the final pattern contained a weak feature of a positional correlation peak. In turn, TOCL-containing membrane mimics showed the onset of peak formation already 30 s after mixing, while this was slightly delayed to about 5 min in POPE/POPG. The d-value, derived directly from the peak position, exhibited a non-monotonic behavior over time in both POPE/POPG and POPE/POPG/TOCL mimics (**Figure 6D**), showing first a decrease and subsequent increase over several minutes after peptide addition. During this equilibration process, the d-values of POPE/POPG were always larger than those of POPE/POPG/TOCL mixtures, with a difference of $\sim$ 0.1 nm in the end-states. Interestingly, final d-values of both PE-containing mixtures were even lower in the presence of LF11-324 (POPE/POPG: $d = 5.12$ nm and POPE/POPG/TOCL: $d = 5.07$ nm). This could stem either from a pronounced membrane thinning or/and different penetration depths of the peptides within the bilayer (see section 4). Notably, the time scale of the related equilibration process is much longer (hours) than peptide adsorption (minutes) (see **Figure 3**).

4. DISCUSSION

We exploited a common thermodynamic framework for the partitioning of antimicrobial peptides to bridge the activities of LF11-215 and LF11-324 in *E. coli* and different lipid-only mimics of their cytoplasmic membranes. In the case of bacteria, this was achieved by evolving a susceptibility microdilution assay for the antimicrobial activity of the two AMPs. This yielded more accurate results (confidence $< 3\%$) than standard MIC evaluations over a broad range of cell concentrations. In particular, we found $\text{MIC}_{\text{LF11-215}} = (13.7 \pm 0.4)\ \mu$M and $\text{MIC}_{\text{LF11-324}} = (11.1 \pm 0.6)\ \mu$M at $n_{\text{cell}} = 10^6$ CFU/ml [in agreement with (20, 25)] increasing linearly up to $\text{MIC}_{\text{LF11-215}} = (158 \pm 2)\ \mu$M and $\text{MIC}_{\text{LF11-324}} = (57 \pm 2)\ \mu$M at $n_{\text{cell}} = 10^9$ CFU/ml. The higher antimicrobial efficacy of LF11-324 was conserved for all measured cell concentrations and extended also to lower growth-inhibited fractions at decreased AMP concentrations. Intriguingly, LF11-324 showed a lower partitioning coefficient than LF11-215, suggesting energetically less-favored interaction with cells, despite its higher efficacy. Combing these data with ζ-potential measurements further allowed us to obtain an upper boundary for the surface adsorbed AMP fraction. Strikingly, we found that both lactoferricin derivatives bind about equally to the microbial envelope, but constitute only a minor fraction of the total number of AMPs interacting with the bacteria. That is, at the MIC only 1—5% of AMPs are surface bound, and even at bacteria inhibition levels of 10% only $\sim$ 5% (LF11-215) to $\sim$ 18% (LF11-324) of the cell associated peptides do not enter inner compartments (**Figure 2**). Consequently, both peptides target mainly inner bacterial components.

Partitioning of LF11-215 and LF11-324 in lipid membrane mimics was instead investigated using Trp fluorescence and ANTS/DPX leakage. While the first technique quantifies the actual number of partitioned peptides per lipid, the second provides the number of adsorbed AMPs leading to a specific dye-efflux. Trp fluorescence revealed a faster and stronger partitioning into POPG membranes than into PE systems in the case of LF11-215, whereas LF11-324 showed the lowest adsorption and partitioning into POPG. Based on pure electrostatic interactions of anionic POPG and cationic residues, which are identical for both peptides, this appears counterintuitive. It can be understood, however, considering that the amphipathic moment of both LF11 peptides is normal to the membrane plane, with the aromatic amino acids of the N-terminal inserted into the hydrophobic core of the membrane, and the Arg-rich section of the amidated C-terminal interacting with the lipid head-groups and exposed to the solvent as reported from previous studies on this family of peptides (25, 53). Indeed, our fluorescence data show that the Trp side chain is segregated into the apolar environment of the bilayer, hence suggesting that the protonated amino group of the N-terminal lies in the same region. Consequently, the positively charged N-terminus of

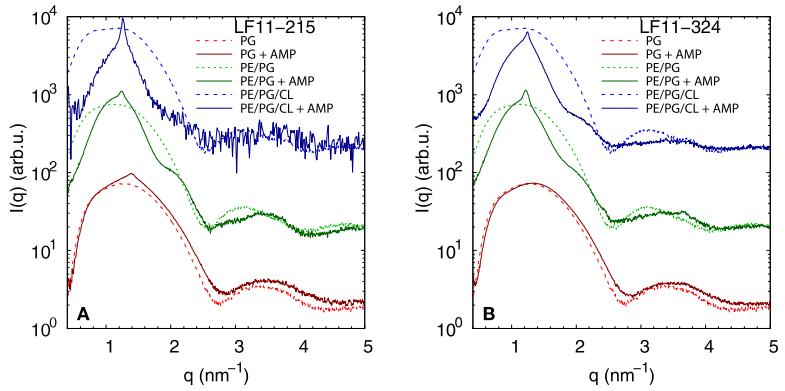

FIGURE 5 | SAXS patterns of POPG, POPE/POPG, and POPE/POPG/TOCL before and after 4 h after incubation with **(A)** LF11-215 and **(B)** LF11-324 (end-states) at $[P]/[L] = 1:25$, corresponding to $[L] = (24.5–27.9$ mM) and $[P] \sim 1.1$ mM.

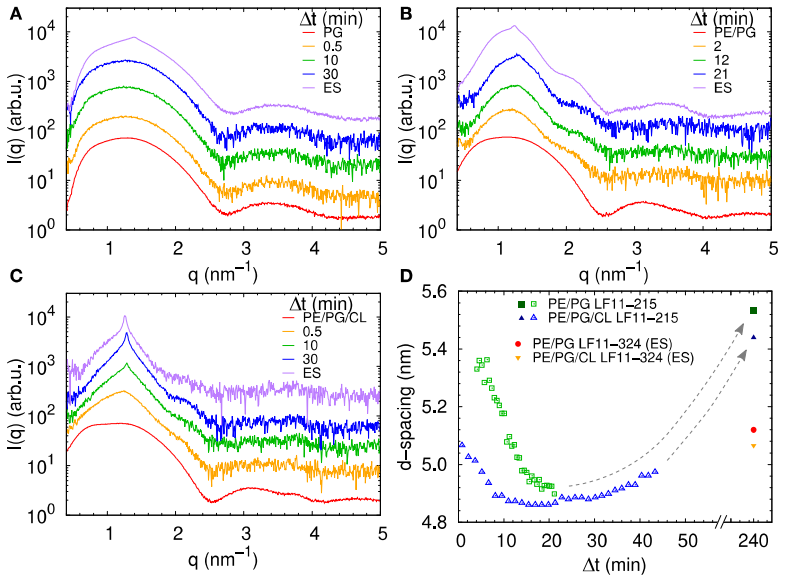

FIGURE 6 | LF11-215-induced structural kinetics as observed in the evolution of SAXS patterns of **(A)** POPG, **(B)** POPE/POPG, and **(C)** POPE/POPG/TOCL; $[P]/[L] = 1:25$, corresponding to $[L] = (24.5–27.9$ mM) and $[P] \sim 1.1$ mM. Panel **(D)** shows the changes in *d*-spacing over time for POPE/POPG and POPE/POPG/TOCL with LF11-215, as well as end-states (ES) for LF11-215 and LF11-324 measured after 4 h of system equilibration.

LF11-324 needs, because of the additional Phe and Pro residues, to insert deeper into the hydrophobic core of the bilayer and thus further away from the anionic PG than in the case of LF11-215, leading to an unfavorable configuration. In the case of PE-containing mixtures, such electrostatic interactions are less pronounced; moreover, peptide-induced domain formation, as previously observed for CL-containing mixtures in the presence of LF11 derivatives (20, 25), may facilitate peptide insertion due to packing defects at domain boundaries [see e.g., (54)]. Hence, POPE/POPG and POPE/POPG/TOCL mixtures are thus more reliable mimics of *E. coli* inner membranes than pure POPG. Moreover, the approximate similar adsorption of both peptides (**Figures 3C,D**) resembles roughly the findings in *E. coli* (**Figure 2D**), thus suggesting that these mimics are also first-order proxies to peptide partitioning into outer membranes, despite the lack of LPS.

Dye leakage experiments for PE-containing mimics showed an effect that, to the best of our knowledge, has not been reported before. Upon raising peptide concentration, we observed an initial increase of dye-efflux, peaking at relatively low peptide concentrations, followed by a subsequent decrease of permeabilization upon further addition of peptide (**Figures 4A–C**). POPG vesicles in contrast showed a typical pure sigmoidal increase of permeabilization [see e.g., (27)], but required significantly higher peptide concentrations than in other mixtures, which aligns with our above discussion on competing electrostatic interactions of the charged N-terminus with PG headgroups. Moreover, DLS experiments revealed that significant leakage was always associated with the formation of large aggregates, independent of the lipid membrane mimic (i.e., also for pure POPG). The intricate entrapment of dyes in POPE/POPG and POPE/POPG/TOCL membranes at increased levels of AMP concentration can be rationalized considering our SAXS data. Here all three lipid mixtures, with the exception of POPG in the presence of LF11-324, showed the formation of a weak Bragg peak (**Figure 5**), signifying the presence of a minor fraction of positionally well-correlated aggregates.

While a sole correlation peak does not enable a conclusion about the specific supramolecular structure, it is still possible to derive *d*-spacing values from the peak positions, which can be connected to previous studies on peptide-induced multibilayer systems with collapsed interbilayer distance (10). Consider first POPE/POPG (3:1 mol/mol) and its steric bilayer thickness, which has been previously determined with high accuracy to be $\sim$ 4.7 nm (49). The final *d*-values for this system after addition of LF11-215 and LF11-324 were 5.53 and 5.12 nm. This suggests that the Bragg peaks originate from lamellar aggregates with almost completely collapsed bilayers, most likely only separated by the steric size of peptides partially inserted into the membranes. Thus, the lower *d*-value observed for LF11-324 suggests pronounced membrane thinning as a result of a stronger perturbation of the membrane, which could be due to the bigger size of the peptides' hydrophobic patch, leading to stronger disordering effects within the hydrocarbon chain region.

For TOCL containing mixtures, we found slightly lower final *d*-values for both peptides, but again more pronounced for LF11-324 (**Figure 6D**). Since we do not have any reference data on the steric thickness of POPE/POPG/TOCL (82:6:12 mol/mol/mol) bilayers, this might be due to either differences in membrane thickness in the absence of peptide or peptide-induced membrane perturbation. However, given that the hydrocarbon thickness of TOCL is expected to be about equal to POPG and POPE, we speculate that the smaller *d*-values for POPE/POPG/TOCL are due to an increased membrane perturbation by the peptides. Indeed, a more pronounced effect of peptides for TOCL containing mixtures, as compared to POPE/POPG, was also observed in Trp fluorescence experiments, where these mixtures exhibited the higher partitioning coefficients, as well as faster kinetics (**Figure 3**). Faster kinetics were also observed for the formation of the collapsed lamellar phase in the presence of LF11-215, where the weak Bragg peak was present in POPE/POPG/TOCL 30 s after the addition of peptides, but needed about 5 min to form in POPE/POPG (**Figure 6D**). The initial decrease in *d*-spacing observed for the first 10—20 min interestingly correlates with the Trp fluorescence kinetics. This suggests that the shift of the peak position over time is related to an initial accumulation of peptides on the membranes during approximately 20 min, followed by a slow equilibration over the course of the next few hours, where peptides diffuse into the newly formed aggregates, most of which are not forming collapsed multibilayers.

Interestingly, the lowest *d*-values of both membranes are $\sim$ 4.9 nm (**Figure 6D**), which is about equal to the steric membrane thickness of POPE/POPG (49). This provides evidence that the membranes come in close contact. The negative intrinsic curvatures of POPE (55) and TOCL (56) and their well-known propensity to form non-lamellar structures [see e.g., (57)] make them highly prone to induce membrane fusion (58, 59). We thus propose that the *d* value minima indicate time points of membrane fusion. Note that peptide-induced fusion of membranes was reported previously (10). Membrane fusion would also explain why some of the dyes are not released by the peptides activity, but remain trapped within some aggregates (**Figure 4**). Interestingly, however, also POPG showed in the presence of LF11-215 a weak signature of collapsed bilayers after extended equilibration times (**Figure 5A**), with a $d \sim 4.5$ nm that is even lower than the smallest values observed for POPE/POPG and POPE/POPG/TOCL (**Figure 5D**). Note that POPG has an intrinsic curvature close to zero (15), and is well-known as a lamellar-phase forming lipid. The collapsed lamellar structure formed in POPG is thus unlikely to be related to membrane fusion, but merely the result of possibly disintegrated membrane patches, forming a stack of bilayers. This notion is supported by the high permeability of POPG vesicles and the absence of a drop of dye leakage at increased peptide concentrations (**Figure 4A**).

The overall higher peptide activity in PE and PE/CL-containing mixtures (as observed, for example, by the lower amounts of peptide needed to induce dye leakage) further suggests that the intrinsic lipid curvatures of these lipids and the resulting stored elastic energy stress (60) makes the bilayers more vulnerable to the peptides. A similar view has been previously proposed as the "balanced spring model for membrane interactions" (61), where membrane active compounds can relief the stored elastic stress in bilayers upon insertion. Finally, we note that also LPS is known for their propensity to form non-lamellar structures (62, 63). We thus expect analogous driving forces occurring in the bacterial outer membrane, although details of membrane composition and in particular asymmetry certainly cannot be neglected. *Nota bene*, we do not necessarily expect that both peptides induce membrane fusion in live bacterial systems, as the complex architecture of the cell envelope or the presence of a densely packed cytosol provides additional constrains. The occurrence of fusion events in lipid-only systems is a mere indication for elastic curvature stress stored within the membranes, which upon relaxation in the presence of peptides will assist their translocation into the cytosol.

In conclusion, our results show that bridging peptide activities in live bacteria and lipid membrane mimics is intricate and that a simple delineation of common leakage experiments can be

highly misleading. In particular, for the here studied LF11-215 and LF11-324, one might have concluded based on leakage data that pure POPG would be sufficient to explain the membrane permeabilizing potential of both peptides. Yet, detailing the partitioning of the peptides in different membrane mimics and microbes allowed us to arrive at a completely different picture. Instead, LF11-215 and LF11-324 both target mainly intracellular components, presumably DNA due to its highly negative charge, reaching local concentrations of up to $\sim$ 100 mM at the MIC. Moreover, the elastic curvature stress stored in POPE/POPG, and to an even greater extent in the more realistic POPE/POPG/TOCL mixture, bestows the membranes with an increased potential for peptide translocation, which might in general be exploited by surface adsorbed wedge-like AMPs. Thus, at least for the presently studied peptides we may answer the initially posed questions as follows: *(ad i)* Vesicle leakage and microbial killing are not directly correlated, but some valuable insight can be obtained upon coupling leakage data to peptide partitioning and studies of membrane structural changes. *(ad ii)* Both peptides bind about equally well to membranes, so for this part, their selectivity indeed seems determined by membrane binding. The difference in their efficacy, however, is due to specific interactions with cytosolic components, and most likely DNA. *(ad iii)* Our partitioning studies provide strong evidence that membrane translocation is definitely required for LF11-215 and LF11-324. Additional studies using different bacteria and AMPs need to be performed to verify whether it is possible to generalize these findings. In general, and although we restricted our study to two AMPs and a single bacterial strain, the developed framework provides a path and guidelines for future studies intending to get deep insight on AMP activity by coupling *in vitro* cell studies with lipid membrane mimics.

DATA AVAILABILITY STATEMENT

The original contributions presented in the study are included in the article/**Supplementary Materials**, further inquiries can be directed to the corresponding author/s.

AUTHOR CONTRIBUTIONS

LM, ES, NM, GP, and KL conceptualized and designed the study. LM, ES, JM, JK, MF, and NM carried out the experiments. LM, ES, JM, and GP carried out the data analysis and interpretation. LM, ES, and GP wrote the manuscript. All authors provided critical feedback and helped to shape the research, analysis, and manuscript.

FUNDING

This project was supported by the Austrian Science Funds (FWF), project no. P 30921 (to KL).

ACKNOWLEDGMENTS

We thank Heinz Amenitsch for technical assistance at the SAXS beamline.

SUPPLEMENTARY MATERIAL

The Supplementary Material for this article can be found online at: https://www.frontiersin.org/articles/10.3389/fmedt.2021.625975/full#supplementary-material

REFERENCES

1. Steiner H, Hultmark D, Engström Å, Bennich H, Boman HG. Sequence and specificity of two antibacterial proteins involved in insect immunity. *Nature*. (1981) 292:246–48. doi: 10.1038/292246a0
2. Wimley WC, Hristova K. Antimicrobial peptides: Successes, challenges and unanswered questions. *J Membr Biol*. (2011) 239:27–34. doi: 10.1007/s00232-011-9343-0
3. Lohner K. Membrane-active antimicrobial peptides as template structures for novel antibiotic agents. *Curr Top Med Chem*. (2017) 17:508–19. doi: 10.2174/1568026616666160713122404
4. Heller WT, Waring AJ, Lehrer RI, Harroun TA, Weiss TM, Yang L, et al. Membrane thinning effect of the beta-sheet antimicrobial protegrin. *Biochemistry*. (2000) 39:139–45. doi: 10.1021/bi991892m
5. Pabst G, Grage SL, Danner-Pongratz S, Jing W, Ulrich AS, Watts A, et al. Membrane thickening by the antimicrobial peptide PGLa. *Biophys J*. (2008) 95:5779–88. doi: 10.1529/biophysj.108.141630
6. Nguyen MHL, DiPasquale M, Rickeard BW, Doktorova M, Heberle FA, Scott HL, et al. Peptide-induced lipid flip-flop in asymmetric liposomes measured by small angle neutron scattering. *Langmuir*. (2019) 35:11735–44. doi: 10.1021/acs.langmuir.9b01625
7. Kumagai A, Dupuy FG, Arsov Z, Elhady Y, Moody D, Ernst RK, et al. Elastic behavior of model membranes with antimicrobial peptides depends on lipid specificity and d-enantiomers. *Soft Matter*. (2019) 15:1860–8. doi: 10.1039/C8SM02180E
8. Salditt T, Li C, Spaar A. Structure of antimicrobial peptides and lipid membranes probed by interface-sensitive X-ray scattering. *Biochim Biophys Acta*. (2006) 1758:1483–98. doi: 10.1016/j.bbamem.2006.08.002
9. Hickel A, Danner-Pongratz S, Amenitsch H, Degovics G, Rappolt M, Lohner K, et al. Influence of antimicrobial peptides on the formation of nonlamellar lipid mesophases. *Biochim Biophys Acta*. (2008) 1778:2325–33. doi: 10.1016/j.bbamem.2008.05.014
10. Kabelka I, Pachler M, Prévost S, Letofsky-Papst I, Lohner K, Pabst G, et al. Magainin 2 and PGLa in bacterial membrane mimics II: membrane fusion and sponge phase formation. *Biophys J*. (2020) 118:612–23. doi: 10.1016/j.bpj.2019.12.019
11. Bechinger B, Lohner K. Detergent-like actions of linear amphipathic cationic antimicrobial peptides. *Biochim Biophys Acta*. (2006) 1758:1529–39. doi: 10.1016/j.bbamem.2006.07.001
12. Shai Y. Mechanism of the binding, insertion and destabilization of phospholipid bilayer membranes by alpha-helical antimicrobial and cell non-selective membrane-lytic peptides. *Biochim Biophys Acta*. (1999) 1462:55–70. doi: 10.1016/S0005-2736(99)00200-X
13. Sevcsik E, Pabst G, Jilek A, Lohner K. How lipids influence the mode of action of membrane-active peptides. *Biochim Biophys Acta*. (2007) 1768:2568–95. doi: 10.1016/j.bbamem.2007.06.015
14. Lohner K, Sevcsik E, Pabst G. Liposome-based biomembrane mimetic systems: implications for lipid-peptide interactions. In: Leitmannova-Liu A, editor. *Advances in Planar Lipid Bilayers and Liposomes*. Vol. 6. Amsterdam: Elsevier (2008). p. 103–37. doi: 10.1016/S1554-4516(07)06005-X

15. Leber R, Pachler M, Kabelka I, Svoboda I, Enkoller D, Vácha R, et al. Synergism of antimicrobial frog peptides couples to membrane intrinsic curvature strain. *Biophys J.* (2018) 114:1945–54. doi: 10.1016/j.bpj.2018.03.006
16. Brogden KA. Antimicrobial peptides: pore formers or metabolic inhibitors in bacteria? *Nat Rev Microbiol.* (2005) 3:238–50. doi: 10.1038/nrmicro1098
17. Le CF, Fang CM, Sekaran SD. Intracellular targeting mechanisms by antimicrobial peptides. *Antimicrob Agents Chemother.* (2017) 61:1–16. doi: 10.1128/AAC.02340-16
18. Wimley WC. Describing the mechanism of antimicrobial peptide action with the interfacial activity model. *ACS Chem Biol.* (2010) 5:905–17. doi: 10.1021/cb1001558
19. Snoussi M, Talledo JP, Del Rosario NA, Mohammadi S, Ha BY, Košmrlj A, et al. Heterogeneous absorption of antimicrobial peptide LL37 in *Escherichia coli* cells enhances population survivability. *eLife.* (2018) 7:1–21. doi: 10.7554/eLife.38174
20. Zweytick D, Deutsch G, Andrä J, Blondelle SE, Vollmer E, Jerala R, et al. Studies on Lactoferricin-derived *Escherichia coli* membrane-active peptides reveal differences in the mechanism of N-acylated versus nonacylated peptides. *J Biol Chem.* (2011) 286:21266–76. doi: 10.1074/jbc.M110.195412
21. Malanovic N, Marx L, Blondelle SE, Pabst G, Semeraro EF. Experimental concepts for linking the biological activities of antimicrobial peptides to their molecular modes of action. *Biochim Biophys Acta.* (2020) 1862:183275. doi: 10.1016/j.bbamem.2020.183275
22. Zweytick D, Pabst G, Abuja PM, Jilek A, Blondelle SE, Andra J, et al. Influence of N-acylation of a peptide derived from human lactoferricin on membrane selectivity. *Biochim Biophys Acta.* (2006) 1758:1426–35. doi: 10.1016/j.bbamem.2006.02.032
23. Sánchez-Gómez S, Lamata M, Leiva J, Blondelle SE, Jerala R, Andrä J, et al. Comparative analysis of selected methods for the assessment of antimicrobial and membrane-permeabilizing activity: a case study for lactoferricin derived peptides. *BMC Microbiol.* (2008) 8:196. doi: 10.1186/1471-2180-8-196
24. Blondelle SE, Jerala R, Pristovšek P, Majerle A, Zorko M, Japelj B, et al. *Antimicrobial Peptides: International Patent Publication WO 2008/006125 A1.* (2008). Available online at: https://books.google.at/books?id=-dHcOAAACAAJ
25. Zweytick D, Japelj B, Mileykovskaya E, Zorko M, Dowhan W, Blondelle SE, et al. N-acylated peptides derived from human lactoferricin perturb organization of cardiolipin and phosphatidylethanolamine in cell membranes and induce defects in *Escherichia coli* cell division. *PLos ONE.* (2014) 9:e90228. doi: 10.1371/journal.pone.0090228
26. Sánchez-Gómez S, Ferrer-Espada R, Stewart PS, Pitts B, Lohner K, Martínez de Tejada G. Antimicrobial activity of synthetic cationic peptides and lipopeptides derived from human lactoferricin against *Pseudomonas aeruginosa* planktonic cultures and biofilms. *BMC Microbiol.* (2015) 15:137. doi: 10.1186/s12866-015-0473-x
27. Heerklotz H, Seelig J. Leakage and lysis of lipid membranes induced by the lipopeptide surfactin. *Eur Biophys J.* (2007) 36:305–14. doi: 10.1007/s00249-006-0091-5
28. Bartlett GR. Colorimetric assay in methods for free and phosphorylated glyceric acids. *J Biol Chem.* (1959) 234:469–71. doi: 10.1016/S0021-9258(18)70227-5
29. Gironi B, Kahveci Z, McGill B, Lechner BD, Pagliara S, Metz J, et al. Effect of DMSO on the mechanical and structural properties of model and biological membranes. *Biophys J.* (2020) 119:274–86. doi: 10.1016/j.bpj.2020.05.037
30. Jorgensen JH, Ferraro MJ. Antimicrobial susceptibility testing: a review of general principles and contemporary practices. *Clin Infect Dis.* (2009) 49:1749–55. doi: 10.1086/647952
31. Fan HY, Nazari M, Raval G, Khan Z, Patel H, Heerklotz H. Utilizing zeta potential measurements to study the effective charge, membrane partitioning, and membrane permeation of the lipopeptide surfactin. *Biochim Biophys Acta.* (2014) 1838:2306–12. doi: 10.1016/j.bbamem.2014.02.018
32. Burstein EA, Emelyanenko VI. Log-normal description of fluorescence spectra of organic fluorophores. *Photochem Photobiol.* (1996) 64:316–20. doi: 10.1111/j.1751-1097.1996.tb02464.x
33. Ladokhin AS, Jayasinghe S, White SH. How to measure and analyze tryptophan fluorescence in membranes properly, and why bother? *Anal Biochem.* (2000) 285:235–45. doi: 10.1006/abio.2000.4773
34. Amenitsch H, Rappolt M, Kriechbaum M, Mio H, Laggner P, Bernstorff S. First performance assessment of the small-angle X-ray scattering beamline at ELETTRA. *J Synchrotron Rad.* (1998) 5:506–8. doi: 10.1107/S090904959800137X
35. Hammersley AP, Svensson SO, Hanfland M, Fitch AN, Hausermann D. Two-dimensional detector software: from real detector to idealised image or two-theta scan. *High Press Res.* (1996) 14:235–48. doi: 10.1080/08957959608201408
36. Haider R, Marmiroli B, Sartori B, Radeticchio A, Wolf M, Dal Zilio S, et al. *Nanodrop Cell for X-Ray and Nanoanalytic Applications.* (2019). Available online at: https://www.nffa.eu/media/225894/d69_nanodrop-cell-for-x-ray-and-nanoanalytic-applications.pdf
37. White SH, Wimley WC, Ladokhin AS, Hristova K. Protein folding in membranes: determining energetics of peptide-bilayer interactions. In: Ackers GK, Johnson ML, editors. *Energetics of Biological Macromolecules, Part B. Vol. 295 of Methods in Enzymology.* San Diego, CA; London: Academic Press (1998). p. 62–87. doi: 10.1016/S0076-6879(98)95035-2
38. Wimley WC, Creamer TP, White SH. Solvation energies of amino acid side chains and backbone in a family of host–guest pentapeptides. *Biochemistry.* (1996) 35:5109–24. doi: 10.1021/bi9600153
39. Savini F, Luca V, Bocedi A, Massoud R, Park Y, Mangoni ML, et al. Cell-density dependence of host-defense peptide activity and selectivity in the presence of host cells. *ACS Chem Biol.* (2017) 12:52–6. doi: 10.1021/acschembio.6b00910
40. Seltmann G, Holst O. *The Bacterial Cell Wall.* Berlin; Heidelberg: Springer (2002). doi: 10.1007/978-3-662-04878-8
41. Freire JM, Domingues MM, Matos J, Melo MN, Veiga AS, Santos NC, et al. Using zeta-potential measurements to quantify peptide partition to lipid membranes. *Eur Biophys J.* (2011) 40:481–7. doi: 10.1007/s00249-010-0661-4
42. Wiese A, Münstermann M, Gutsmann T, Lindner B, Kawahara K, Zähringer U, et al. Molecular mechanisms of polymyxin B-membrane interactions: direct correlation between surface charge density and self-promoted transport. *J Membr Biol.* (1998) 162:127–38. doi: 10.1007/s002329900350
43. Adamson AW, Gast AP. *Physical Chemistry of Surfaces.* 6th ed. New York, NY; Chichester: Wiley (1997).
44. Sochacki KA, Barns KJ, Bucki R, Weisshaar JC. Real-time attack on single *Escherichia coli* cells by the human antimicrobial peptide LL-37. *Proc Natl Acad Sci USA.* (2011) 108:E77–81. doi: 10.1073/pnas.1101130108
45. Kim S, Patel DS, Park S, Slusky J, Klauda JB, Widmalm G, et al. Bilayer properties of lipid A from various gram-negative bacteria. *Biophys J.* (2016) 111:1750–60. doi: 10.1016/j.bpj.2016.09.001
46. Micciulla S, Gerelli Y, Schneck E. Structure and conformation of wild-type bacterial lipopolysaccharide layers at air-water interfaces. *Biophys J.* (2019) 116:1259–69. doi: 10.1016/j.bpj.2019.02.020
47. Semeraro EF, Marx L, Mandl J, Frewein MPK, Scott HL, Prévost S, et al. Evolution of the analytical scattering model of live *Escherichia coli. J. Appl. Cryst.* (2020) 54. doi: 10.1107/S1600576721000169
48. Malanovic N, Leber R, Schmuck M, Kriechbaum M, Cordfunke RA, Drijfhout JW, et al. Phospholipid-driven differences determine the action of the synthetic antimicrobial peptide OP-145 on gram-positive bacterial and mammalian membrane model systems. *Biochim Biophys Acta.* (2015) 1848(10 Pt A):2437–47. doi: 10.1016/j.bbamem.2015.07.010
49. Pachler M, Kabelka I, Appavou MS, Lohner K, Vácha R, Pabst G. Magainin 2 and PGLa in bacterial membrane mimics I: peptide-peptide and lipid-peptide interactions. *Biophys J.* (2019) 117:1858–69. doi: 10.1016/j.bpj.2019.10.022
50. Swain J, El Khoury M, Kempf J, Briée F, van der Smissen P, Décout JL, et al. Effect of cardiolipin on the antimicrobial activity of a new amphiphilic aminoglycoside derivative on *Pseudomonas aeruginosa. PLos ONE.* (2018) 13:e0201752. doi: 10.1371/journal.pone.0201752
51. Wilkinson SG. Gram-negative bacteria. In: Ratledge C, Wilkinson SG, editors. *Microbial Lipids.* London: Academic Press (1988). p. 299–488.
52. Burstein EA, Vedenkina NS, Ivkova MN. Fluorescence and the location of tryptophan residues in protein molecules. *Photochem Photobiol.* (1973) 18:263–79. doi: 10.1111/j.1751-1097.1973.tb06422.x
53. Zorko M, Japelj B, Hafner-Bratkovic I, Jerala R. Expression, purification and structural studies of a short antimicrobial peptide. *Biochim Biophys Acta.* (2009) 1788:314–23. doi: 10.1016/j.bbamem.2008.10.015

54. Epand RM, Epand RF. Domains in bacterial membranes and the action of antimicrobial agents. *Mol Biosyst*. (2009) 5:580–7. doi: 10.1039/b900278m
55. Kollmitzer B, Heftberger P, Rappolt M, Pabst G. Monolayer spontaneous curvature of raft-forming membrane lipids. *Soft Matter*. (2013) 9:10877–84. doi: 10.1039/c3sm51829a
56. Chen YF, Tsang KY, Chang WF, Fan ZA. Differential dependencies on Ca2+ and temperature of the monolayer spontaneous curvatures of DOPE, DOPA and cardiolipin: effects of modulating the strength of the inter-headgroup repulsion. *Soft Matter*. (2015) 11:4041–53. doi: 10.1039/C5SM00577A
57. Koller D, Lohner K. The role of spontaneous lipid curvature in the interaction of interfacially active peptides with membranes. *Biochim Biophys Acta*. (2014) 1838:2250–9. doi: 10.1016/j.bbamem.2014.05.013
58. Ellens H, Siegel DP, Alford D, Yeagle PL, Boni L, Lis LJ, et al. Membrane fusion and inverted phases. *Biochemistry*. (1989) 28:3692–703. doi: 10.1021/bi00435a011
59. Siegel DP. The Gaussian curvature elastic energy of intermediates in membrane fusion. *Biophys J*. (2008) 95:5200–15. doi: 10.1529/biophysj.108.140152
60. Marsh D. Lateral pressure profile, spontaneous curvature frustration, and the incorporation and conformation of proteins in membranes. *Biophys J*. (2007) 93:3884–99. doi: 10.1529/biophysj.107.107938
61. Laggner P, Lohner K. Liposome phase systems as membrane activity sensors for peptides. In: Katsaras J, Gutberlet T, editors. *Lipid Bilayers. Structure and Interactions*. Berlin: Springer (2000). p. 233–64. doi: 10.1007/978-3-662-04496-4_11
62. Seydel U, Koch MHJ, Brandenburg K. Structural polymorphisms of rough mutant lipopolysaccharides Rd to Ra from *Salmonella minnesota*. (1993). 110:232–43. doi: 10.1006/jsbi.1993.1026
63. Rappolt M, Rössle M, Kaconis Y, Howe J, Andrä J, Gutsmann T, et al. X-ray scattering of bacterial cell wall compounds and their neutralization. In: Bauwens CM, editor. *X-Ray Scattering. Materials Science and Technologies*. Hauppauge, NY: Nova Science Publishers (2011) p. 133–48.

Conflict of Interest: The authors declare that the research was conducted in the absence of any commercial or financial relationships that could be construed as a potential conflict of interest.

frontiers

Supplementary Material

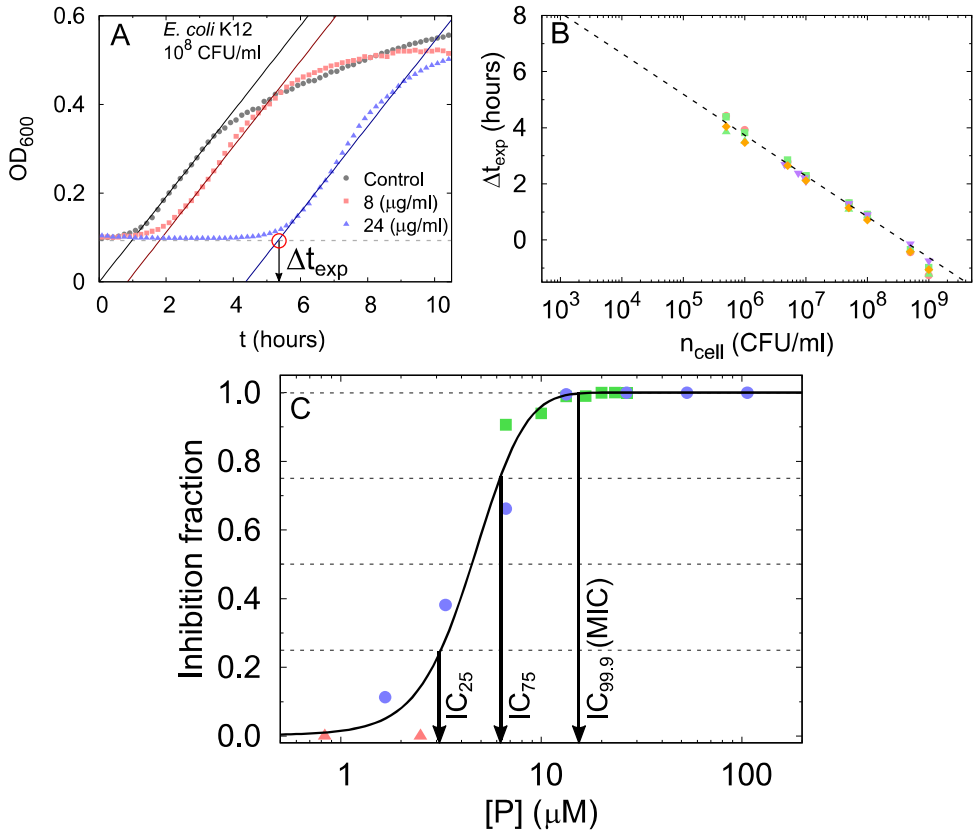

Figure S1. **(A)** Example of delayed growth as a function of AMP concentration, and extraction of t_{exp} values. **(B)** Calibration: logarithmic description of t_{exp} as a function of n_{cell}. **(C)** Sigmoidal interpolation of the inhibition fraction data as a function of AMP concentration (different colors represent independent experiments). As an example, arrows highlight the calculated IC_x in the case of inhibition fraction 0.25, 0.5 and 0.999 (MIC).

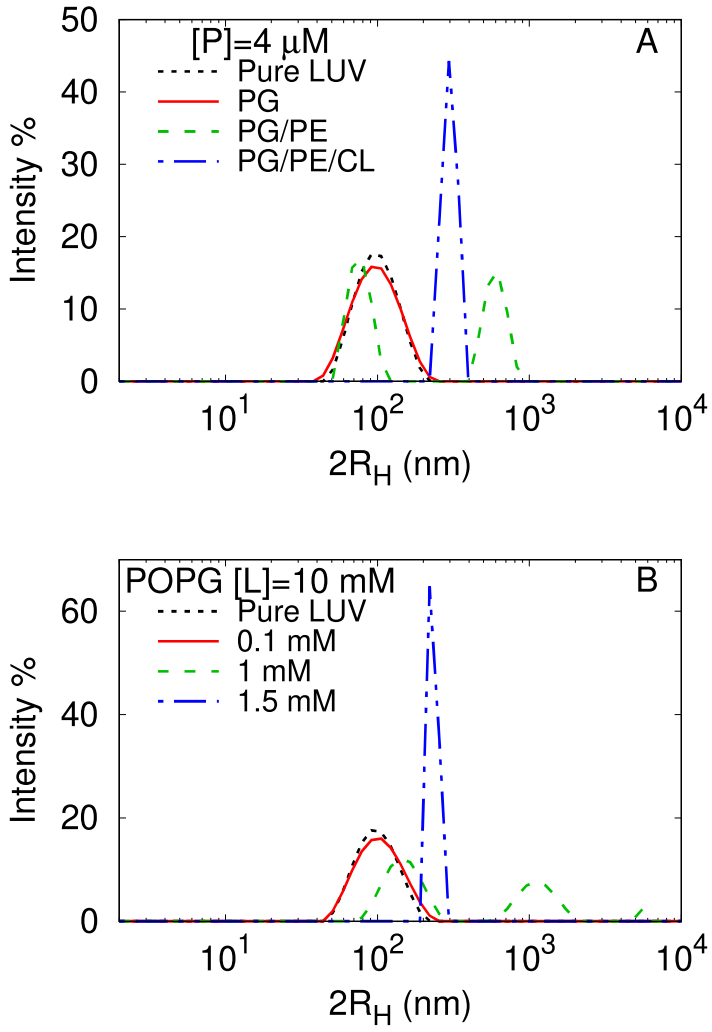

Figure S2. **(A-B)** Representative size distribution functions (intensity-weighed) after incubation with peptides for one hour at 37 °C. **(A)** Different lipid systems ($[L] = 100$ μM) after incubation with LF11-215 ($[P] = 4$ μM). **(B)** Different LF11-324 concentrations and mixing with POPG LUVs ($[L] = 10$ mM).

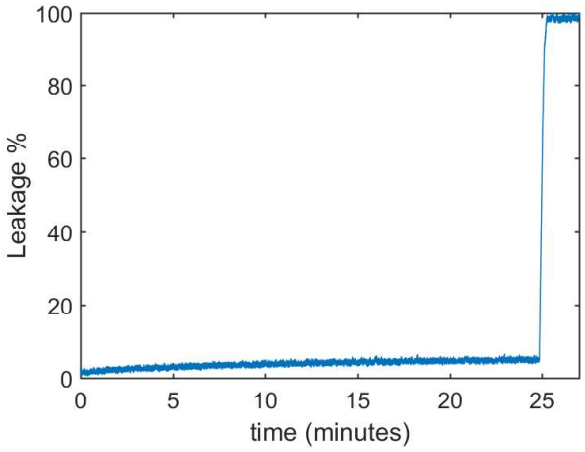

Figure S3. Time-resolved measurement of LF11-215($[P] = 0.5$ μM) induced permeabilization of LUVs composed of POPE/POPG ($[L] = 50$ μM), showing peptide induced ANTS/DPX leakage kinetics after peptide addition converging to ~ 5 % dye efflux after 25 min. The jump to 100% leakage is induced by addition of Triton X-100.